Award Number: W81XWH-20-1-0117

TITLE: The Use of High-Quality Chemical Tools to Rescue TBK1 Function and Identify Novel ATP-Competitive Targets in ALS

PRINCIPAL INVESTIGATOR: Dr. Alison Axtman, Ph.D.

CONTRACTING ORGANIZATION: University of North Carolina at Chapel Hill

REPORT DATE: May 2021

TYPE OF REPORT: Annual

PREPARED FOR: U.S. Army Medical Research and Materiel Command
                         Fort Detrick, Maryland 21702-5012

DISTRIBUTION STATEMENT: Approved for Public Release;
                         Distribution Unlimited

REPORT DOCUMENTATION PAGE

1. REPORT DATE	2. REPORT TYPE	3. DATES COVERED
May 2021	Annual	1 April 2020 – 31 March 2021

4. TITLE AND SUBTITLE

The Use of High-Quality Chemical Tools to Rescue TBK1 Function and Identify Novel ATP-Competitive Targets in ALS

5a. CONTRACT NUMBER

5b. GRANT NUMBER
W81XWH-20-1-0117

5c. PROGRAM ELEMENT NUMBER

6. AUTHOR(S)
Alison Axtman, Carrow Wells, Thomas Durcan, Lenore Beitel, Mathilde Marie Ĉhaineau, Sarah Lépine

E-Mail: alison.axtman@unc.edu

5d. PROJECT NUMBER

5e. TASK NUMBER

5f. WORK UNIT NUMBER

7. PERFORMING ORGANIZATION NAME(S) AND ADDRESS(ES)

University of North Carolina at Chapel Hill
Chapel Hill, NC 27599-5023

McGill University
Montreal, Quebec, Canada H3A 0G4

8. PERFORMING ORGANIZATION REPORT NUMBER

9. SPONSORING / MONITORING AGENCY NAME(S) AND ADDRESS(ES)
U.S. Army Medical Research and Materiel Command
Fort Detrick, Maryland 21702-5012

10. SPONSOR/MONITOR'S ACRONYM(S)

11. SPONSOR/MONITOR'S REPORT NUMBER(S)

12. DISTRIBUTION / AVAILABILITY STATEMENT
Approved for Public Release; Distribution Unlimited

13. SUPPLEMENTARY NOTES

14. ABSTRACT

We are developing chemical tools and biological reagents to interrogate the regulation of kinase-mediated biological pathways as new avenues to combat the accumulation of toxic protein and RNA aggregates in ALS. TDP-43 is an example of the most commonly misfolded and deposited protein in ALS. Failure of the autophagy system is one mechanism that allows protein aggregates accrue. TBK1 is a human protein kinase that plays an essential role in autophagy and which, through multiple genetic studies, has surfaced as a protein that suffers from inactivating mutations in ALS patients. We have identified linkable compounds that potently engage TBK1 in cells and a putative TRAF3-recruiting warhead. These will be covalently linked to produce the first TBK1-activating activation-targeting chimera. As an alternative approach, we have identified the best available chemical probe targeting casein kinase 2 (CK2), which indirectly activates TBK1. We have and will continue to improve the physical properties of this scaffold to make it suitable for *in vivo* use. We have also selected a potent, cell-active back-up compound from the CK2-targeting naphthyridine series for further optimization. Furthermore, through development of a novel TDP-43 aggregation assay in motor neurons derived from stem cells, we aim to identify additional protein kinases that, when modulated, reduce the deposition of misfolded proteins. We have generated motor neurons harboring ALS-relevant TDP-43 and characterized expression of mutant versus wild-type (WT) TDP-43 during differentiation. We have confirmed that ethacrynic acid elicits mutant and WT TDP-43 translocation and have developed a methodology to quantify this movement.

15. SUBJECT TERMS

ALS, TDP-43, iPSC, TRAF3, TBK1, ATTAC, CK2, SGC-CK2-1, chemical probe, CX-4945, pyrazolopyrimidine, naphthyridine

16. SECURITY CLASSIFICATION OF:			17. LIMITATION OF ABSTRACT	18. NUMBER OF PAGES	19a. NAME OF RESPONSIBLE PERSON USAMRMC
a. REPORT U	**b. ABSTRACT** U	**c. THIS PAGE** U	UU	79	**19b. TELEPHONE NUMBER** *(include area code)*

Table of Contents

Introduction

Accumulation of protein and RNA aggregates is a hallmark in the pathology of amyotrophic lateral sclerosis (ALS). Misfolded wild-type (WT) and mutant proteins deposit and form inclusions that are toxic to motor neurons (MNs) in ALS patients. The most common protein inclusion found in the cytoplasm of MNs from ALS patients is transactive response DNA-binding protein 43 (TDP-43).[1] Although only 2% of familial ALS cases are linked to mutations in the TDP-43 gene, TDP-43 positive inclusions have been demonstrated in nearly 97% of ALS patients, irrespective of whether they have familial or sporadic disease.[2] Protein aggregation is exacerbated in ALS due to failure of the autophagy system, allowing aggregates to accumulate rather than be cleared. The severe impact of impaired autophagy on ALS progression supports that identification of target proteins that regulate autophagy would be therapeutically beneficial. Loss-of function mutations in TANK-binding kinase (TBK1) have been genetically linked with ALS.[1, 3] TBK1, which is highly expressed in neurons, plays important roles in both innate immunity and autophagy pathways. Studies related to TBK1 function, pathological findings and known pathogenic mechanisms in ALS emphasize autophagy as the major pathway impacted by TBK1 mutations and that targeting this kinase could modify the pathology of ALS.[3] Chemical tools capable of rescuing or enhancing TBK1 function, either through directly modifying TBK1 or acting indirectly via modulation of casein kinase 2 (CK2), could therefore serve as novel ALS therapeutics. Via a more unbiased strategy, any small molecule that reduces translocation and/or seeding of TDP-43 in MNs could accelerate the identification of key regulators of aggregation. Targeting protein aggregation and/or autophagy is a novel approach to ALS therapy that holds promise for altering the course of disease and slowing its progression.
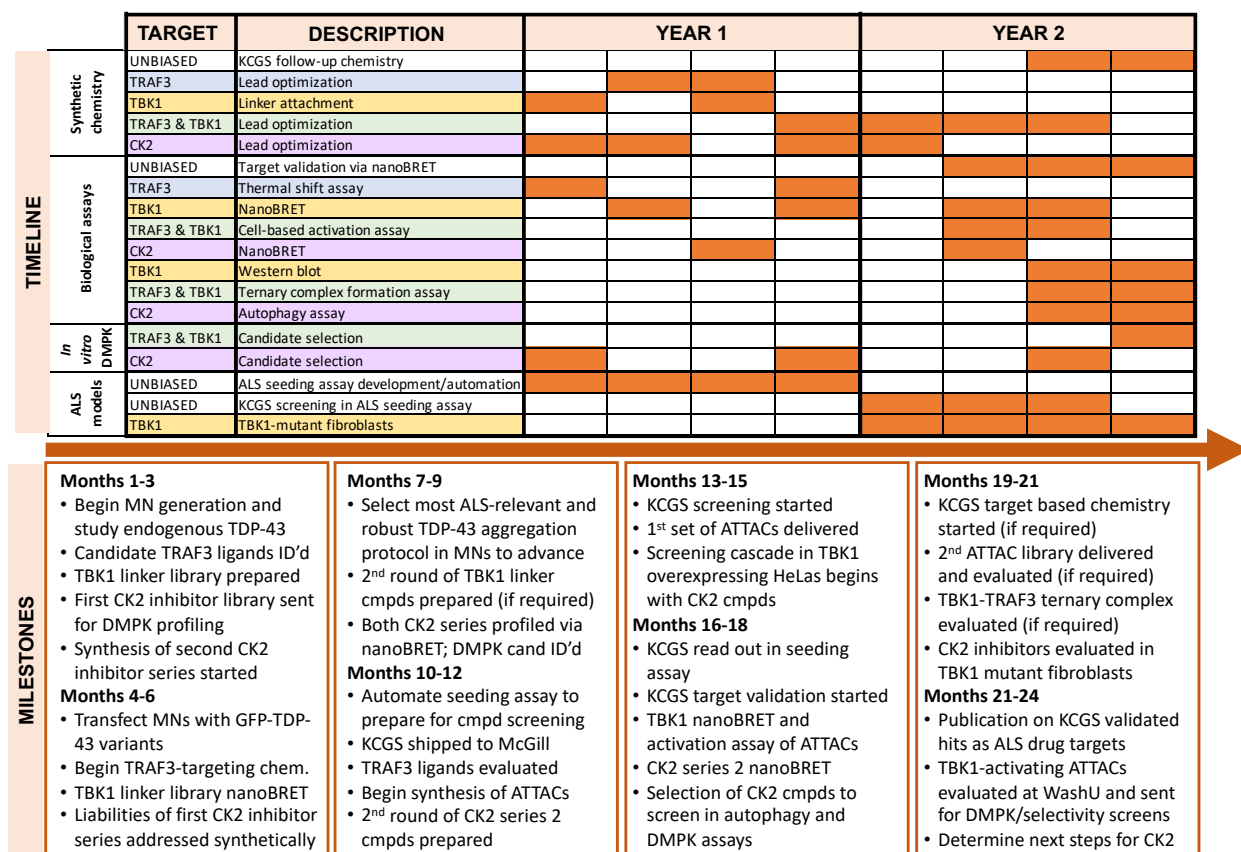
TIMELINE

	TARGET	DESCRIPTION	YEAR 1	YEAR 2
Synthetic chemistry	UNBIASED	KCGS follow-up chemistry		
	TRAF3	Lead optimization		
	TBK1	Linker attachment		
	TRAF3 & TBK1	Lead optimization		
	CK2	Lead optimization		
Biological assays	UNBIASED	Target validation via nanoBRET		
	TRAF3	Thermal shift assay		
	TBK1	NanoBRET		
	TRAF3 & TBK1	Cell-based activation assay		
	CK2	NanoBRET		
	TBK1	Western blot		
	TRAF3 & TBK1	Ternary complex formation assay		
	CK2	Autophagy assay		
In vitro DMPK	TRAF3 & TBK1	Candidate selection		
	CK2	Candidate selection		
ALS models	UNBIASED	ALS seeding assay development/automation		
	UNBIASED	KCGS screening in ALS seeding assay		
	TBK1	TBK1-mutant fibroblasts		

MILESTONES

Months 1-3
- Begin MN generation and study endogenous TDP-43
- Candidate TRAF3 ligands ID'd
- TBK1 linker library prepared
- First CK2 inhibitor library sent for DMPK profiling
- Synthesis of second CK2 inhibitor series started

Months 4-6
- Transfect MNs with GFP-TDP-43 variants
- Begin TRAF3-targeting chem.
- TBK1 linker library nanoBRET
- Liabilities of first CK2 inhibitor series addressed synthetically

Months 7-9
- Select most ALS-relevant and robust TDP-43 aggregation protocol in MNs to advance
- 2nd round of TBK1 linker cmpds prepared (if required)
- Both CK2 series profiled via nanoBRET; DMPK cand ID'd

Months 10-12
- Automate seeding assay to prepare for cmpd screening
- KCGS shipped to McGill
- TRAF3 ligands evaluated
- Begin synthesis of ATTACs
- 2nd round of CK2 series 2 cmpds prepared

Months 13-15
- KCGS screening started
- 1st set of ATTACs delivered
- Screening cascade in TBK1 overexpressing HeLas begins with CK2 cmpds

Months 16-18
- KCGS read out in seeding assay
- KCGS target validation started
- TBK1 nanoBRET and activation assay of ATTACs
- CK2 series 2 nanoBRET
- Selection of CK2 cmpds to screen in autophagy and DMPK assays

Months 19-21
- KCGS target based chemistry started (if required)
- 2nd ATTAC library delivered and evaluated (if required)
- TBK1-TRAF3 ternary complex evaluated (if required)
- CK2 inhibitors evaluated in TBK1 mutant fibroblasts

Months 21-24
- Publication on KCGS validated hits as ALS drug targets
- TBK1-activating ATTACs evaluated at WashU and sent for DMPK/selectivity screens
- Determine next steps for CK2

Figure 1. Timelines and milestones for entire award period.

Body

In our grant proposal we set out to accomplish the following **Hypothesis or Objective:** *Successful completion of this project will yield several key compounds and biological assays that target essential proteins in ALS-propagating pathways. Discovery of previously untapped biological targets as well as pre-clinical candidates that reduce protein aggregation provide potential to offer new ALS treatment options.* We defined specific aims to enable delivery of the chemical and biological reagents. Our progress can be framed in terms of these aims as well as a defined timeline/milestone Gantt chart provided in the grant proposal (Figure 1).

Aim 1. Screen kinase chemogenomic set (KCGS) to identify new ATP-binding protein targets that reduce seeding of protein aggregates. In addition to the design and screening of targeted SMs in Aims **2** and **3**, we will perform an unbiased screening of our newest curated set of 188 narrowly selective and potent kinase inhibitors known as KCGS (Kinase Chemogenomic Set). Details related to the development and kinome coverage of KCGS were published earlier this year (pre-print ahead of peer-reviewed publication).[4, 5] We will screen KCGS in a newly developed assay that examines whether TDP-43 translocation and/or aggregation is impacted by these small molecule kinase inhibitors. Development of this assay has been one focus of the first year of the award period.

As shown in Figure 2, we have worked toward establishment of this TDP-43 aggregation assay and modified a few steps along the way. Instead of working with artificial GFP-labeled wild-type (WT) or mutant TDP-43, we have opted to use antibodies to visualize TDP-43 and avoided introduction of GFP. Thus, we have knocked-in mutant TDP-43 (two ALS-relevant mutants: G348C and A382T) into human induced pluripotent stem cells (hiPSCs) and differentiated them into spinal motor neurons (MNs), alongside WT hiPSCs. In parallel, WT and mutant MNs were differentiated, stained and analyzed via qPCR for markers of differentiation, and imaged for their ability to form neuronal networks. TDP-43 transcript and protein levels were analyzed during differentiation and in the resultant MNs, blotting to look for differences, including in the soluble and insoluble fractions. No differences in WT and mutant TDP-43 expression were noted across genotypes and developmental stages.
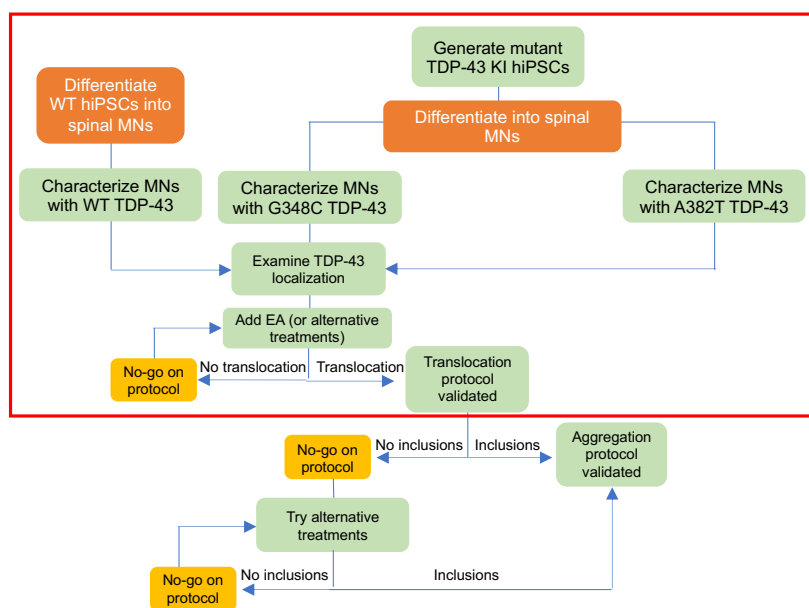

Figure 2. Aim 2 decision tree with current progress boxed in red, edits to the original workflow in light green boxes

Next, we monitored localization of TDP-43 in these MNs. TDP-43 is a widely expressed protein that predominantly resides within the nucleus, where it binds both DNA and RNA, with implicated roles in RNA stabilization, splicing and translational regulation.[6] Intriguingly, TDP-43 was observed to translocate from the nucleus into the cytoplasm where it is a predominant component of ubiquitinated inclusions in diseases like ALS.[7, 8] Since TDP-43 mutations are rare, other mechanisms, including oxidative stress, have been suggested to drive this nuclear to cytoplasmic translocation.[9] Using both N- and C-terminal
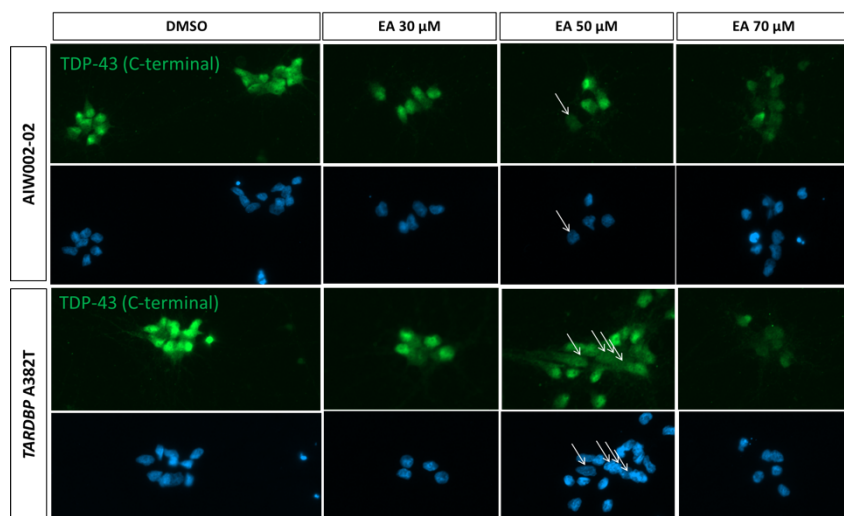
	DMSO	EA 30 µM	EA 50 µM	EA 70 µM

Figure 3. Dose-response of EA treatment.

antibodies, we imaged the localization of WT and mutant TDP-43, finding both to reside almost exclusively in the nucleus. Treatment of MNs with ethacrynic acid (EA) induced TDP-43 translocation (also referred to as mislocalization). Figure 3 shows the dose-response of 5-hour EA treatment specifically for the mutant TDP-43-containing MNs (G348C= AIW002-02 and A382T = *TARDBP* A382T). Similar results were observed when MNs containing WT TDP-43 were treated and when the N-terminal TDP-43 antibody was used to image. MNs could be dosed up to 70 µM without resultant toxicity. In general, the bright staining that was observed when MNs were treated with DMSO became less bright with EA treatment. Interpretation of this observation was that concentrated nuclear staining of untreated MNs became more diffuse staining when TDP-43 moved into the cytoplasm.

While we have qualitatively identified TDP-43 translocation, we are currently validating a method to quantify this translocation. Using CellProfiler, we have developed a pipeline to be able to input an image, identify the TDP-43 staining within the image, subtract out the nucleus (stained with Hoescht), and allow us to quantify both cytoplasmic and nuclear TDP-43 (Figure 4). This
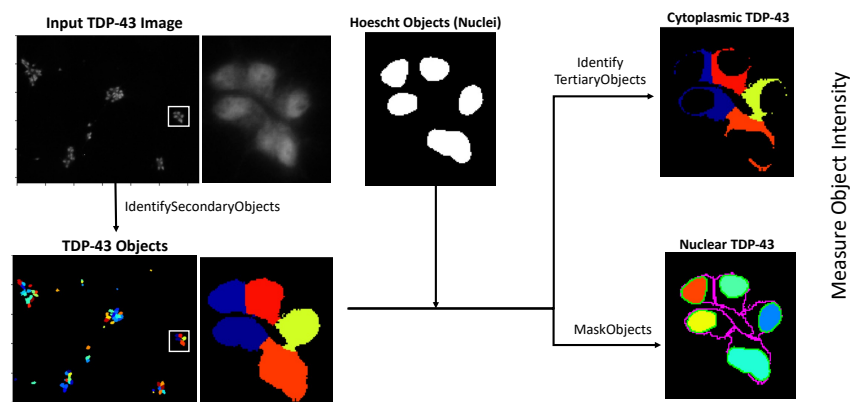
Figure 4. Pipeline to quantify TDP-43 translocation.

pipeline is being used to quantify any differences observed between WT and mutant TDP-43 as well as in MNs that have been in culture for a different number of weeks. Initial results indicate that translocation is subtle, as only minor differences have been observed. In addition, we are testing other oxidative/ER stressors either alone (glutamate or cyclopiazonic acid, for example) or in combination with EA to determine if TDP-43 relocalization can be further increased. Finally, we are probing whether any stressors will promote mutant and not WT TDP-43 translocation.

In parallel, efforts are centered around the identification of chemical agents that elicit cytoplasmic TDP-43 aggregation. We are blotting for the presence of p-TDP43 aggregates following the treatment with EA using a p-TDP-43 antibody that specifically identifies phosphorylation at Ser409/410. Phosphorylation of TDP-43 has been proposed to promote its aggregation.[10-12] In addition, we are investigating whether reintroducing EA after TDP-43 translocation can promote TDP-43 aggregation. Once the assay is validated, we propose to look at the impact of KCGS on both the translocation of TDP-43 and clearance of aggregated TDP-43 in motor neurons.

Relative to our initial proposed timeline and milestones, the delays posed by COVID-19 have set us back slightly. While we intended to complete assay development in year 1 and begin KCGS screening in Q1 of year 2, we are not yet prepared for compound screening. We have pivoted our strategy along the way and made improvements to the original proposed workflow. We will deliver a more relevant and robust assay as a result of these modifications.

Aim 2. Develop a TBK1-activating activation-targeting chimera (ATTAC). As a departure from customary kinase inhibitor campaigns that screen for small molecules that *inhibit* substrate phosphorylation, we are developing compounds that *promote* phosphorylation of TBK1 substrates. Phosphorylated TBK1 is the active form of the kinase. Different types of ubiquitination have been described to activate (UbK63) and degrade (UbK48) protein kinases.[13-15] As UbK63 is a known activation step for TBK1, we hypothesize that a heterobifunctional molecule can be designed to activate rather than degrade TBK1. To further explore this hypothesis, novel ATTACs that link a potent and selective TBK1-targeting SM and a ligand for an E3 ligase responsible for UbK63 of TBK1 (TRAF3) are being prepared.
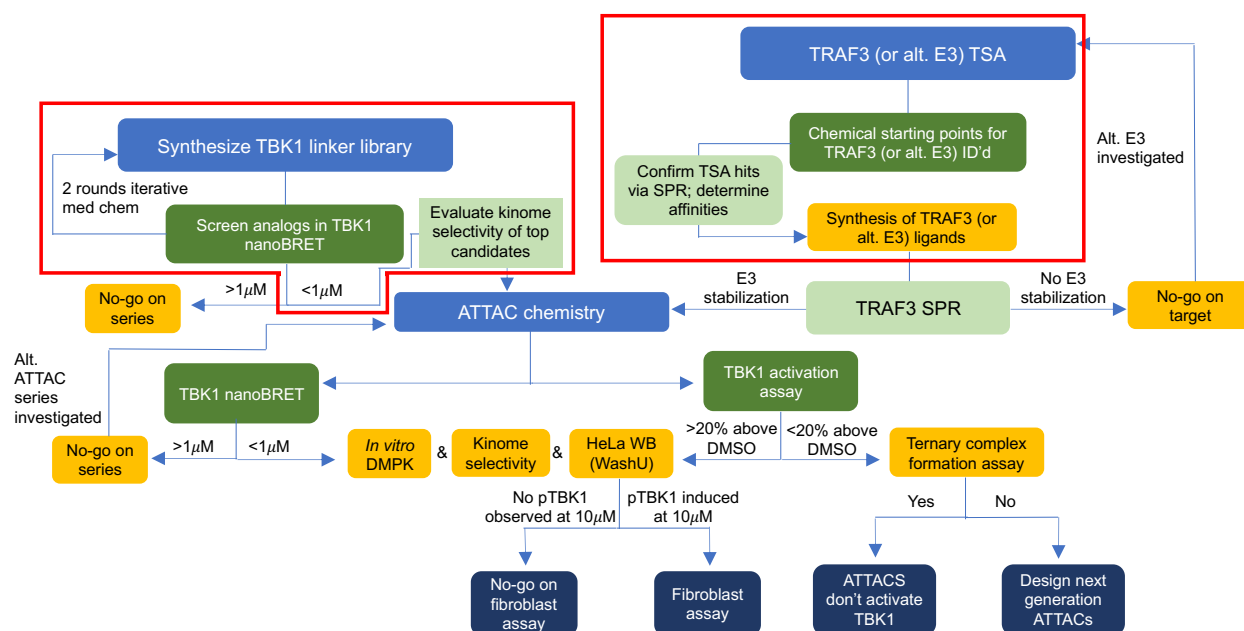
Figure 5. Aim 2 decision tree with current progress boxed in red, edits to the original workflow in light green boxes

As shown in Figure 5, assembly of ATTACs relies on development of the warhead that recruits TBK1 and a ligand for TRAF3. We started by modifying 3 cell-active, pyrimidine-based inhibitors of TBK1 that we developed and have recently published as a pre-print (in revision stage at *J Med Chem*): AA-CS-1-005, AA-CS-1-007, AA-CS-017.[16] Data associated with these lead TBK1 inhibitors is included in blue in Figure 6. Analogs were designed specifically to probe where a linker could be attached without compromising cellular target engagement of TBK1. Based on recently published bifunctional TBK1-targeting molecules,[17] modification of the aryl ring attached to the 2-position of the pyrimidine core with a linker is tolerated. With this design strategy in mind, we modified the pyrazole ring of AA-CS-1-005 and AA-CS-1-007 with alkyl, alkoxy, or alkylamino groups projecting into different parts of the binding pocket. The pyrazole was also converted to an imidazole and modified in a similar way. Similarly, the aryl ring of AA-CS-1-017 was substituted with either a 3- or 4-position alkyl, alkoxy, or alkylamino group. These groups were selected to include diversity in the linker and, in some cases, with a group that could be further functionalized.

For the first TBK1 linker library, 22 compounds were synthesized in total. The TBK1 linker library was tested using the TBK1 cellular target engagement assay (NanoBRET) in triplicate. We found that the switching the pyrazole to an imidazole was not well tolerated and that AA-CS-1-

005 could not be modified with a linker without modest losses in TBK1 affinity. AA-CS-6-003 was identified as a promising lead compound in need of additional selectivity profiling within the AA-CS-1-005 series. AA-CS-6-004, as a direct comparison to AA-CS-6-003 but with R_1 = methyl, was also selected for selectivity profiling. In addition, it was found that the R_2 position on the pyrazole, which is CH_2CF_3 in AA-CS-1-005, can be modified without losing TBK1 cellular engagement. AA-CS-6-006 served as the basis for analogs in a subsequent library. Finally, within the AA-CS-1-017 series, 3-position substitution was the most tolerated, but 4-position substitution also yielded potent compounds in cells. AA-CS-6-005, AA-CS-6-016, and AA-CS-6-022 (boxed in Figure 6) were selected for additional selectivity profiling and served as the basis for additional analogs in a subsequent library.
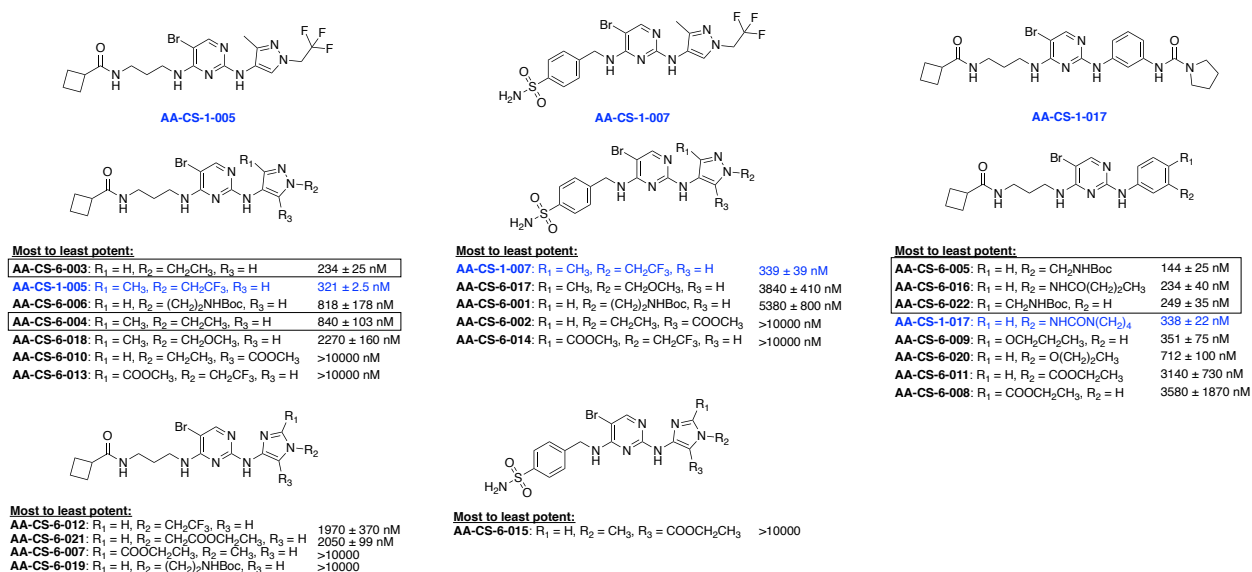
Figure 6. TBK1 cellular target engagement IC_{50} values for TBK1 linker library 1. Blue text corresponds with the parent TBK1 inhibitors, boxed compounds were submitted for kinome-wide profiling.

A second TBK1 linker exploration library was designed and synthesized to further explore modification at the R_2 position of the pyrazole in AA-CS-1-005 and R_1/R_2 of AA-CS-1-017. For this second focused library, 11 compounds were synthesized in total. All compounds were tested using the TBK1 cellular target engagement assay (NanoBRET) in triplicate. For the AA-CS-1-005 series (left in Figure 7), a longer linker at R_2 was tolerated but only when R_1 = H (AA-CS-8-009 versus AA-CS-8-004). Similarly, R_1 = H (AA-CS-6-006) was better tolerated that R_1 = methyl (AA-CS-8-003) for the shorter chain at position R_2. For the series designed around AA-CS-1-017 (right in Figure 7), many potent compounds emerged. The optimal linker length shared by AA-CS-8-008 and AA-CS-8-010 could be attached at either the 3- or 4-position of the aryl ring without changes in potency. A direct alkyl linked chain (AA-CS-8-008 and AA-CS-8-010) was better tolerated than an amide-linked chain (AA-CS-8-001 and AA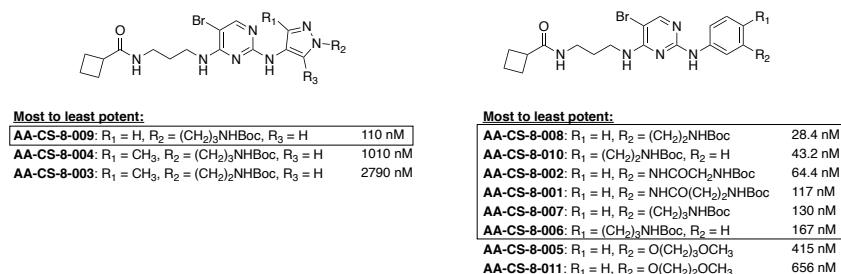-CS-8-002) and longer chains resulted in losses in potency (AA-CS-8-006 and AA-CS-8-007). Given the many potent compounds that were prepared, we opted to profile the kinome-wide selectivity of several (boxed in Figure 7) to ascertain which modifications resulted in promiscuity and which might result in more selective compounds for TBK1.

Figure 7. TBK1 cellular target engagement IC_{50} values for TBK1 linker library 2. Boxed compounds were submitted for kinome-wide profiling.

Table 1. Kinome-wide screening results of TBK1-targeting compounds.

Compound	Parent compound	$S_{10}(1\ \mu M)$	Number of kinases with PoC <10
AA-CS-1-005	N/A	0.154	62
AA-CS-1-007	N/A	0.02	8
AA-CS-1-017	N/A	0.223	90
AA-CS-6-003	AA-CS-1-005	0.333	134
AA-CS-6-004	AA-CS-1-005	0.146	59
AA-CS-6-005	AA-CS-1-017	0.273	110
AA-CS-6-016	AA-CS-1-017	0.218	88
AA-CS-6-022	AA-CS-1-017	0.211	85
AA-CS-8-001	AA-CS-1-017	0.226	91
AA-CS-8-002	AA-CS-1-017	0.303	122
AA-CS-8-006	AA-CS-1-017	0.144	58
AA-CS-8-007	AA-CS-1-017	0.164	66
AA-CS-8-008	AA-CS-1-017	0.134	54
AA-CS-8-009	AA-CS-1-005	0.273	110
AA-CS-8-010	AA-CS-1-017	0.154	62

Since many members of linker libraries 1 and 2 met the potency threshold of <1 µM in the TBK1 NanoBRET assay originally selected as criteria for advancement (Figure 5), we elected to add kinome-wide selectivity screening to help decide on the most suitable warhead to carry forward into ATTAC chemistry. All compounds were screened at a single concentration (1 µM) against 403 human wild-type kinases. Data is included in Table 1 and expressed as a selectivity score ($S_{10}(1\ \mu M)$) and the corresponding number of kinases that demonstrated <10 PoC (percent of control) when screened. Blue highlighting is used to group the analogs designed around AA-1-CS-005, while yellow is used to designate analogs of AA-1-CS-017. While none of the analogs is particularly selective, TBK1 was among the PoC <10 fraction for all compounds screened. For the AA-1-CS-005 series, AA-CS-6-004 showed comparable selectivity to the parent ($R_2 = CH_2CF_3$ versus $R_2 = CH_2CH_3$, respectively) and AA-CS-8-009 was significantly more promiscuous than the parent. Also, incorporation of $R_1 = $ methyl in AA-1-CS-004 versus $R_1 = $ H in AA-1-CS-003 resulted in a substantial increase in kinome-wide selectivity, supporting this position as a way to impart selectivity. For the AA-1-CS-017 series, several analogs with linkers outperformed the parent compound in terms of kinome-wide selectivity, with AA-CS-8-006, AA-CS-8-007, AA-CS-8-008, and AA-CS-8-010 among the best candidates for advancement. These matched pairs of NHBoc-capped analogs with either a 3- or 4-position shorter or longer linker attached will give us options of ATTACs to make.

For the TRAF3-targeting warhead, we began with thermal shift assay (TSA) screening to identify a suitable ligand. We had the RZ3 domain of both TRAF3 and TRAF6 protein synthesized and purified to be able to screen them in parallel, based on the seeming homology between the two proteins, to allow for an initial selectivity analysis. TRAF6 was screened first against two libraries in parallel: the Selleck kinase inhibitor set (856 published kinase inhibitors) and a set of analogs (25 in total) offered by ChemDiv of a putative TRAF6 ligand reported in the literature (C25-140).[18] The Selleck inhibitor set was screened at 12.5 µM using a previously described protocol.[19] Screening the Selleck library yielded 12 hits with shifts >1.6 °C. When repeated twice, only 5 of these hits reproduced in all three runs with average shifts between 1.3–2.5 °C (Table 2).

Table 2. TSA Selleck library results.

Compound	Ave. ΔT_m (°C)
AMG900	2.49
SLx-2119	1.95
BLU9931	1.83
CX6258	1.79
Repotrectinib	1.34

Figure 8. TRAF3 and TRAF6 TSA screening workflow.

Screening the C25-140 ChemDiv library at a higher concentration of 250 µM due to their smaller size yielded many putative hits. Hit follow-up was carried out on any compounds that demonstrated a ΔT_m (change in melting temperature) of 2 or more standard deviations above DMSO. A hit plate was assembled and screened in triplicate to ultimately yield 18 validated hits from the C25-140 ChemDiv library via TSA. Based on the Selleck library results, a fragment set of 422 compounds was selected based on substructure and similarity searching around AMG900 and SLx-2119. This set was screened at 500 µM using the same protocol described for the C25-140 ChemDiv library. 114 hits fit the criteria to be added to the hit plate, which, after screening in triplicate, yielded 47 validated TRAF6 ligands by TSA. This workflow and results are summarized in Figure 8.

Next, the same basic workflow and screening concentrations were used for TRAF3. Both the C25-140 ChemDiv library and fragment library of 422 were profiled via TSA in parallel. Screening of the ChemDiv library was carried out in triplicate, yielding 9 validated hits. Screening the fragment library initially resulted in 96 hits with a ΔT_m of 2 or more standard deviations above DMSO. Assembly and profiling of the hit plate in triplicate resulted in 21 validated fragment hits. Gratifyingly, there was little overlap in the fragment hits identified for TRAF3 and TRAF6, suggesting that ligand selectivity might be feasible.

To next assess whether the binding observed via TSA was recapitulated in an orthogonal assay and to quantify the affinity of ligand binding, surface plasmon resonance (SPR) studies were carried out. TRAF3 was selected for immediate follow-up and the 21 validated fragment hits, two parent compounds (AMG900 and SLx2119) as well as 9 validated ChemDiv hits were provided to the vendor (32 compounds in total). Unfortunately, TRAF3 aggregation, non-specific binding, and low affinity of the parent compounds impeded data collection. Single-concentration screening at 10 µM was successfully accomplished, yielding the graph in Figure 9. It was suggested that lyophilization of the TRAF3 protein upon preparation resulted in difficulties with resuspending it in its biologically relevant form. Thus, the RZ3 TRAF3 protein was remade and provided as a frozen glycerol stock.

Signal at 10 µM, single run

Red bars: start up blanks (1-3); First two green bars: blanks (4-5)
ChemDiv G167: 6, 17, 30, 37
Fragment CSC5515 strong non-specific binding: 22

Figure 9. Single-concentration SPR screening of hits against TRAF3.

A new vendor was contracted for this second round of SPR screening with the newly prepared TRAF3 protein. Using the single-concentration screening (Figure 9) as a guide, the non-specific compound (CSC5515) and an addition 6 compounds that bound non-specifically as well as the parent compounds (AMG900 and SLx2119) were excluded from analysis this round and 23 compounds were provided to the vendor. BRD4, another E3 ligase, was screened in parallel to enable an initial sense of compounds that might bind more promiscuously. Upon thorough screening in dose-response, the compounds were grouped into three categories: compounds that bound only TRAF3, compounds that bind TRAF3 and BRD4, and compounds that do not bind TRAF3. The ChemDiv library yielded only one compound that weakly binds to both TRAF3 and BRD4 (C25-140). For the fragment library, one compound was found to bind non-specifically (**21704**), one compound (**87189**) binds dose-dependently to TRAF3 with an apparent $K_D = 19$ µM and weaker to BRD4 ($K_D \sim 120$ µM), one compound (**92296**) binds weakly to TRAF3 ($K_D > 200$ µM) without apparent binding to BRD4 (NB), and one compound (**54411**) binds weakly to both TRAF3 and BRD4 ($K_D > 200$ µM for both proteins). The remaining compounds did not bind to either protein. It is worth noting that for **87189**, analysis indicates non-specific binding to BRD4 and the K_D fit was forced so it is possibly selective

for TRAF3 over BRD4. Figure 10 shows the structures of the potential lead series (**87189** and **92296**) as well as SLx-2119 and highlights in red that these compounds share structurally similarity. Of note, these were among the compounds that gave the highest signal in the single-concentration SPR screening (Figure 9).

Since TSA and SPR yielded such different results, we are considering a few next steps. For other proteins and projects, we have found that TSA does not yield reproducible results. SPR will be utilized as the primary screening method for TRAF3 moving forward. One certain next step is screening lead compound **87189** via SPR against 1-2 additional proteins from diverse classes to determine whether this compound is binding specifically to TRAF3 or is a promiscuous compound that binds many proteins. In parallel, we have revisited the fragment library and identified 15 close analogs of **87189** that did not emerge as hits via TSA. Rather than investing in additional synthetic efforts, these 15 analogs and 6 additional analogs that bear slight structural modifications will next be screened via SPR to generate structure–activity relationships. Finally, the concentration range for **87189** will be expanded when it is next profiled by SPR to determine if we see the curve shape maintained and can find where the curve plateaus, therein gathering some additional information about whether this compound binds to multiple sites on TRAF3.

Relative to our initial proposed timeline and milestones, the delays posed by COVID-19 have set us back slightly. While we intended to begin ATTAC synthesis before the end of year 1, changes in personnel, including loss of two funded scientists from UNC, have set us back some. TSA assays were delayed and then SPR studies were added to the workflow as a confirmatory step that seems to have been essential. After a few more SPR studies with **87189** and related analogs as well as exploration of where a linker would be tolerated on this scaffold, we should be able to begin ATTAC synthesis.
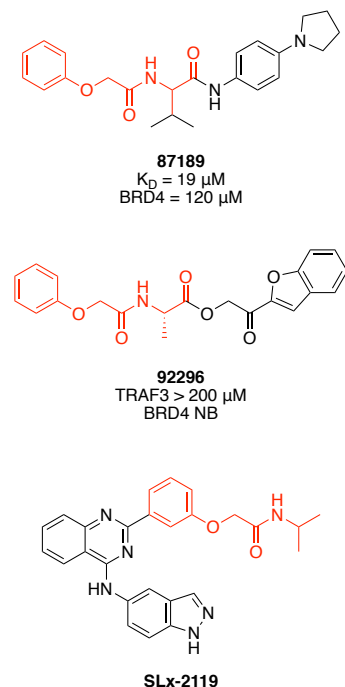

87189
K_D = 19 µM
BRD4 = 120 µM

92296
TRAF3 > 200 µM
BRD4 NB

SLx-2119

Figure 10. Structures of SPR leads and SLx2119.

Aim 3. Develop CK2 inhibitors that inhibit p62 (nucleoporin 62) phosphorylation and indirectly activate TBK1. Autophagy adapter p62 is among the most well-characterized receptors implicated in selective degradation of protein aggregates in mammalian models.[20] Phosphorylation of p62 alters the clearance propensity of p62-associated proteins. CK2, specifically the CK2α catalytic subunit (CSNK2A1), is responsible for phosphorylation of the ubiquitin-binding domain of p62 on S403, increasing its binding affinity for and promoting formation and clearance of p62 inclusions.[21] Moreover, p62 is also phosphorylated by TBK1, amplifying cargo recognition and committing it to degradation.[22] CK2 is unique among protein kinases in that no CK2 mutations have been found to date, yet its elevated expression and activity have been associated with diverse diseases.[23] CK2, which is highly expressed in the mammalian brain and a key regulator of neuronal function, is implicated in the molecular pathology of neurodegenerative disorders, including AD, PD and ALS.[24-27]

CK2 was identified as an essential regulator of TBK1 activation at steady state and under viral infection. Knockdown of CK2 (shCK2α) or genetic ablation of its kinase activity resulted in TBK1 hyperactivation and interferon induction in response to viruses. TBK1 regulation by CK2 was determined to be indirect, mediated by proteins to be defined.[28] As another possible explanation, S403 phosphorylation of p62 is mediated by TBK1, suggesting that TBK1 might be recruited to overcome the shortage of CK2 and execute an essential phosphorylation event to mediate autophagy.[29] Importantly, a SM capable of CK2 inhibition resulted in time- and dose-dependent TBK1 activation and interferon induction in two human cell lines *without* co-stimulation or viral infection.[28] This SM, TBB, does not represent the best choice of inhibitor to study CK2

given its lack of potency (1.6 μM), limited knowledge surrounding its selectivity, and polyhalogenated aromatic nature that may result in undesired toxicity.[30] There is a need for the development of high quality chemical tools to study CK2. We will synthesize the first chemical tools with the goals of studying the mechanism of TBK1 activation via CK2 inhibition, how CK2 inhibition influences TBK1-mediated autophagy, and whether CK2 inhibitors could become ALS therapeutics.
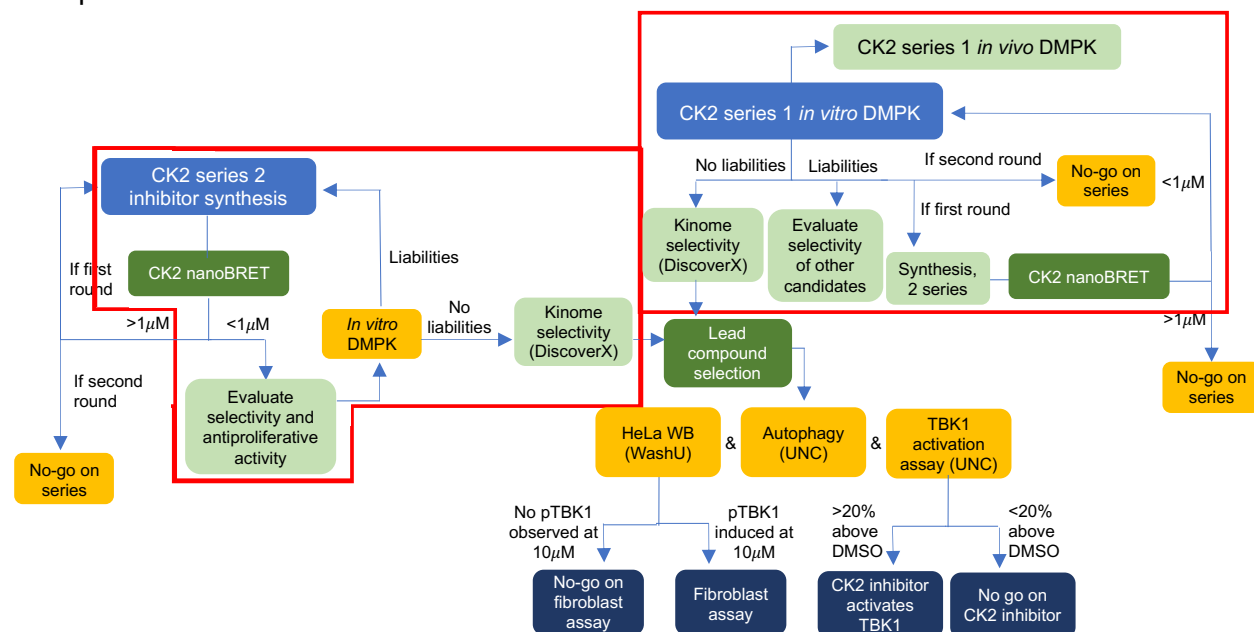

Figure 11. Aim 3 decision tree with current progress boxed in red, edits to the original workflow in light green boxes.

With these goals in mind and in alignment with the workflow in Figure 11, we have synthesized the best available cell-active chemical probe to study the phenotypic changes ascribed to CK2 inhibition. This chemical probe emerged from our "series 1" described in the grant proposal. We published a pre-print in 2020 and peer-reviewed publication in 2021 in *Cell Chemical Biology* on this probe: SGC-CK2-1 (Figure 12).[31, 32] This compound is potent (IC$_{50}$ = 36 nM in the CK2α and IC$_{50}$ = 16 nM in the CK2α' NanoBRET cellular target engagement assays) and selective in cells and, remarkably, demonstrates limited anti-proliferative activity when profiled against nearly 180 distinct cancer cell lines. It greatly outperforms the most commonly used CK2 inhibitor in the literature (CX-4945, the basis for our "series 2"), both in terms of potency and kinome-wide selectivity when profiled at 1 μM against 403 wild-type human kinases (Figure 12). Further, we have examined the sensitivity of human-derived primary cells to SGC-CK2-1. While induced pluripotent stem cells are slightly sensitive to SGC-CK2-1 (IC$_{50}$ = 2 μM), neural progenitor cells were found to be less sensitive and differentiation to motor neurons makes them even less sensitive. A lack of cell sensitivity to our selective CK2

Figure 12. Data for SGC-CK2-1: best available CK2 probe.

probe gives us confidence that targeting CK2 in the brain can be accomplished without collateral toxicity.

We next evaluated the developability of SGC-CK2-1, the entire library from which it was selected, and its negative control compound (SGC-CK2-1N, Figure 12). Table 3 shows the results of these efforts versus literature-reported stability values for other CK2 inhibitors. We analyzed the logD (measure of lipophilicity at pH = 7.4) and kinetic solubility in aqueous buffer for all compounds in our library. Several widely used CK2 inhibitors, including CX-4945, CX-5011 (an analog of CX-4945) and TBB, were sent for kinetic solubility and logD assessment at the same time. Table 3 includes the data, which is colored as a heat map to show the best performers in each respective category in green and the poorest in red. The ideal drug is thought to have a logD between 2–3, giving it passive permeability properties necessary for cell activity, bioavailability, and to avoid efflux by transporters. Many members of our library were found to have sub-optimal kinetic solubility. We consider a kinetic solubility concentration >20 µM as acceptable and >100 µM as desirable. While drugs with low water solubility are predisposed to low and variable oral bioavailability and there are structural modifications known to improve aqueous solubility, ~40% of currently marketed compounds remain poorly water-soluble.[33-35] It has been suggested that kinetic solubility may also play a small role in passive diffusion across the BBB.[36]

Table 3. Developability results for series 1 of CK2 inhibitors.

	logD	Kinetic Solubility (µM)	Microsomal Stability (% remaining, T = 30 min)	Cmax (ng/mL)	T1/2 (h)	Concentration of compound in mouse plasma after 3h (ng/mL)
Aniline I	0.06	104.9	71.3	803.7	1.33	61.8
Aniline J	1.27	89.6	0.0			1.75
Aniline K	1.94	2.4	69.9	5.987	NA	1.71
Aniline L	2.73	0.5	0.0			56.1
SGC-CK2-1	1.95	3.7	40.5	384.7	1.24	43.2
Aniline P	2.03	4.5	54.5			
Aniline Q	2.35	1.8	2.5			<1
Aniline G	0.03	77.5	73.6	1080	1.67	109
Aniline H	1.26	148.7	3.4			4.21
Aniline N	1.89	8.0	48.0			48.9
Indole U	2.15	0.9	20.9			19.0
Indole T	2.13	2.3	59.3	1025	1.46	201
SGC-CK2-1N	2.41	34.7	0.0			
CX-4945	0.83	277.1	83	4740	10.9	
CX-5011	0.14	66.7			6.40	
TBB	1.43	72.8				

We experimentally determined the microsomal stability of our library of pyrazolopyrimidines in mouse liver microsomes. Table 3 shows that <50% of the majority of compounds remained 30 minutes after dosing. For comparison, published data for CX-4945 in rat liver microsomes after 30 minutes is included in Table 3.[37] The four best performers in terms of stability in mouse liver microsomes plus SGC-CK2-1 (compound names highlighted in blue) were then sent for evaluation of *in vivo* PK properties. Groups of three CD-1 mice were dosed at 10 mg/kg IP with each of the compounds and blood plasma samples collected at four time points: 0.5, 1, 3 and 8 hours. Subsequently, another 6 analogs (highlighted in purple) were sent and evaluated in the same manner in terms of number of mice, dose, and route of administration, just with a single timepoint readout of 3 hours. Also included are C_{max} (maximal concentration observed in the blood) and half-life ($T_{1/2}$) as reported in the literature for CX-4945, in male rats when dosed orally at 10 mg/kg, and CX-5011, in rats when dosed orally (no dose provided).[37, 38] The CX compounds outperformed our pyrazolopyrimidines when dosed in vivo. In addition, our chemical probe, SGC-CK2-1, did not demonstrate suitable PK properties for in vivo use since it

is too quickly metabolized. Next, Indole T that bears a slightly different scaffold seems to have slightly better PK properties and this will be taken advantage of in design of next generation analogs. Finally, with a couple of exceptions, trends observed in mouse liver microsomes were found to be generally predictive of *in vivo* results*: higher % remaining after 30 minutes in mouse liver microsomes correlated with longer compound survival *in vivo.*

Finding that series 1 had liabilities motivated a two-prong approach. First, we more thoroughly analyzed the selectivity of another potent compound from the series that had more favorable physiochemical properties than SGC-CK2-1. As shown in Figure 13, Aniline I demonstrated improved aqueous kinetic solubility and microsomal stability versus

SGC-CK2-1
- CK2α1 IC_{50} = 2.8nM
- CK2α2 IC_{50} = 3.1nM
- S_{10} (1μM) = 0.007
- LogD = 1.95
- Solubility = 3.7 μM
- Microsomal Stability T_{30} = 40.5% cmpd remaining

Aniline I
- CK2α1 IC_{50} = 2.4nM
- CK2α2 IC_{50} = 2.9nM
- S_{10} (1μM) = 0.025
- LogD = 0.06
- Solubility = 104.9 μM
- Microsomal Stability T_{30} = 71.3% cmpd remaining

Figure 13. Comparison of properties of SGC-CK2-1 versus Aniline I.

SGC-CK2-1 but suffered from a sub-optimal selectivity score when profiled against 403 wild-type kinases at 1 μM. We determined whether the kinases potently inhibited (PoC <35) in the broad profiling effort (18 in total available at the vendor) were also potently inhibited in corresponding enzymatic assays. Half of the kinases tested, 9 of 18, were inhibited with IC_{50} values <1 μM, confirming the kinome-wide selectivity results and that it demonstrates sub-optimal selectivity for advancement to study CK2 function. As confirmation of this selectivity screening, this compound was also sent to the NCI60 panel and profiled in this same panel as SGC-CK2-1 at the same concentration (10 μM). Aniline I was found to elicit more significant anti-proliferative activity against several cell lines, which supports its inhibition of off-target kinases.
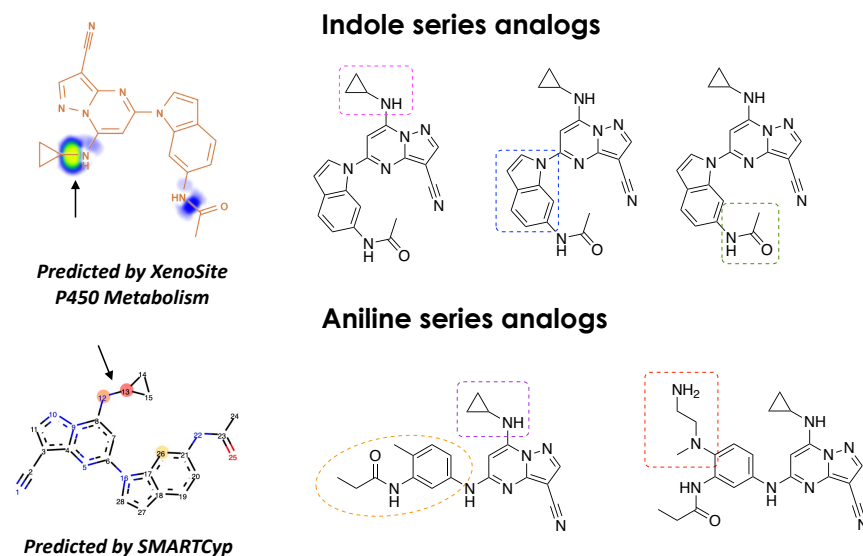

Figure 14. Sites of metabolism and analog design strategy.

In parallel, we have modified both the Aniline (SGC-CK2-1) and Indole (Indole T) scaffolds in parallel to address the metabolic instability of these scaffolds through design. Based on our initial library from which SGC-CK2-1 and Indole T originated as well as several published pyrazolopyrimidines as well as ours and other published corresponding co-crystal structures, we have confidently identified those parts of each scaffold that make essential interactions with CK2. We recently solved the structures of SGC-CK2-1 and Indole T bound to CK2α[31] and plan to continue to work with our collaborators at SGC Frankfurt to solve the co-crystal structures of other lead CK2 pyrazolopyrimidines. We have designed several sub-libraries of analogs that maintain these key interactions to preserve CK2 potency as well as selectivity, and instead target those parts of the molecule that are solvent-exposed and/or

particularly susceptible to metabolism, with BBB penetrance also in mind as part of our design strategy. Using two computati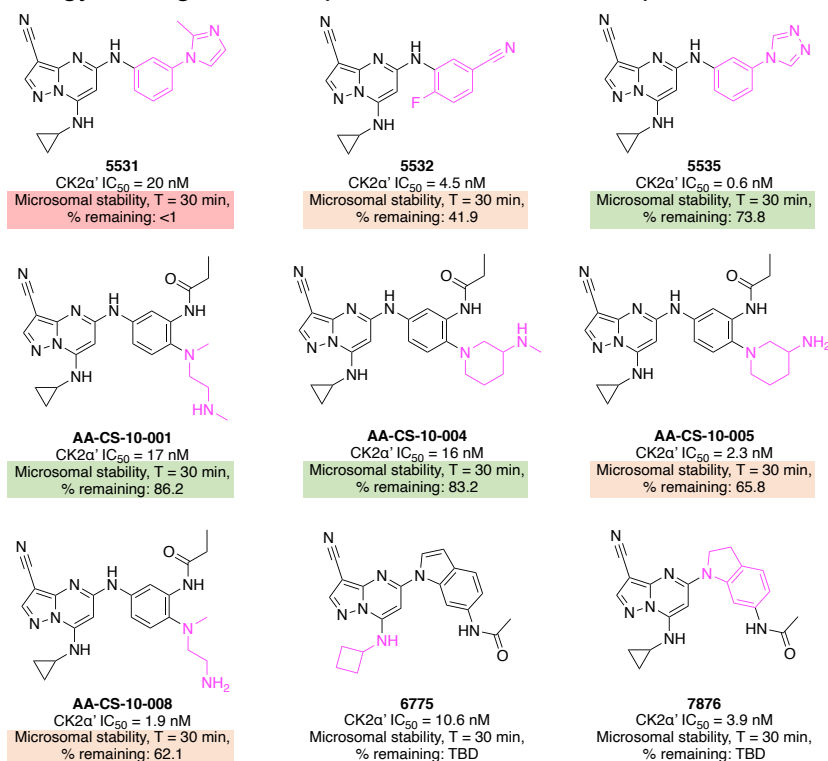onal models that predict sites of P450 metabolism, we have identified a potential metabolic liability at the site of the 7-position cyclopropyl amine (Figure 14).[39, 40]

A library of 30 analogs has been synthesized with different structural modifications to address sites of metabolic liabilities. Upon preparation, this library was analyzed for CK2 cellular target engagement in the CK2α' NanoBRET assay. Figure 15 highlights 9 of the analogs from this library with the structural modifications aimed at addressing liabilities colored pink. These particular analogs demonstrated IC$_{50}$ values ≤20 nM in the CK2α' NanoBRET assay. To build our database and increase understanding of the relationship between structure and microsomal

5531
CK2α' IC$_{50}$ = 20 nM
Microsomal stability, T = 30 min, % remaining: <1

5532
CK2α' IC$_{50}$ = 4.5 nM
Microsomal stability, T = 30 min, % remaining: 41.9

5535
CK2α' IC$_{50}$ = 0.6 nM
Microsomal stability, T = 30 min, % remaining: 73.8

AA-CS-10-001
CK2α' IC$_{50}$ = 17 nM
Microsomal stability, T = 30 min, % remaining: 86.2

AA-CS-10-004
CK2α' IC$_{50}$ = 16 nM
Microsomal stability, T = 30 min, % remaining: 83.2

AA-CS-10-005
CK2α' IC$_{50}$ = 2.3 nM
Microsomal stability, T = 30 min, % remaining: 65.8

AA-CS-10-008
CK2α' IC$_{50}$ = 1.9 nM
Microsomal stability, T = 30 min, % remaining: 62.1

6775
CK2α' IC$_{50}$ = 10.6 nM
Microsomal stability, T = 30 min, % remaining: TBD

7876
CK2α' IC$_{50}$ = 3.9 nM
Microsomal stability, T = 30 min, % remaining: TBD

Figure 15. Newly synthesized potent aniline and indole analogs.

stability, we sent the first 16 prepared for analysis in mouse liver microsomes. Indoles **6775** and **7876**, although promising, were made later and haven't yet been analyzed for their microsomal stability. Of the 16 that were sent for analysis, 12 compounds demonstrated >50% compound remaining after 30 minutes and 5 had ≥80% compound remaining after 30 minutes. As a reminder, SGC-CK2-1 demonstrated 41% compound remaining after 30 minutes and Indole T had 59% compound remaining after 30 minutes (Table 3). The values observed for our new library support that we have improved the *in vitro* microsomal stability of our pyrazolopyrimidines overall and, in some cases, did not see a loss in CK2 potency. Modification of the propionamide in SGC-CK2-1 and/or the pendant amine chain resulted in compounds with variable stability. Those bearing a secondary amine (AA-CS-10-001 and AA-CS-10-004) as well as the triazole-substituted analog (**5535**) were amongst the most stable to liver microsomes.

Next steps for a select set of the compounds in Figure 15 (AA-CS-10-001, AA-CS-10-004, 5535) as well as 4 others that demonstrated ≥74% compound remaining after 30 minutes is analysis of *in vivo* PK in mice. This study will be done collaboratively with Takeda. We will also send the same subset of compounds for analysis of kinome-wide selectivity, as captured in the updated flowchart (Figure 11). Synthetic efforts are ongoing to continue to improve our pyrazolopyrimidine compounds based on the data collected and deliver a suitable compound for use *in vivo*.

CX-4945

CX-5011
Sub-optimal solubility

12 analogs
3 with solubility issues

11 analogs
1 with solubility issues

Figure 16. CK2 series 2 library 1.

With respect to series 1 we are right on track with our proposed milestones and deliverables at the end of year 1. We have added some ad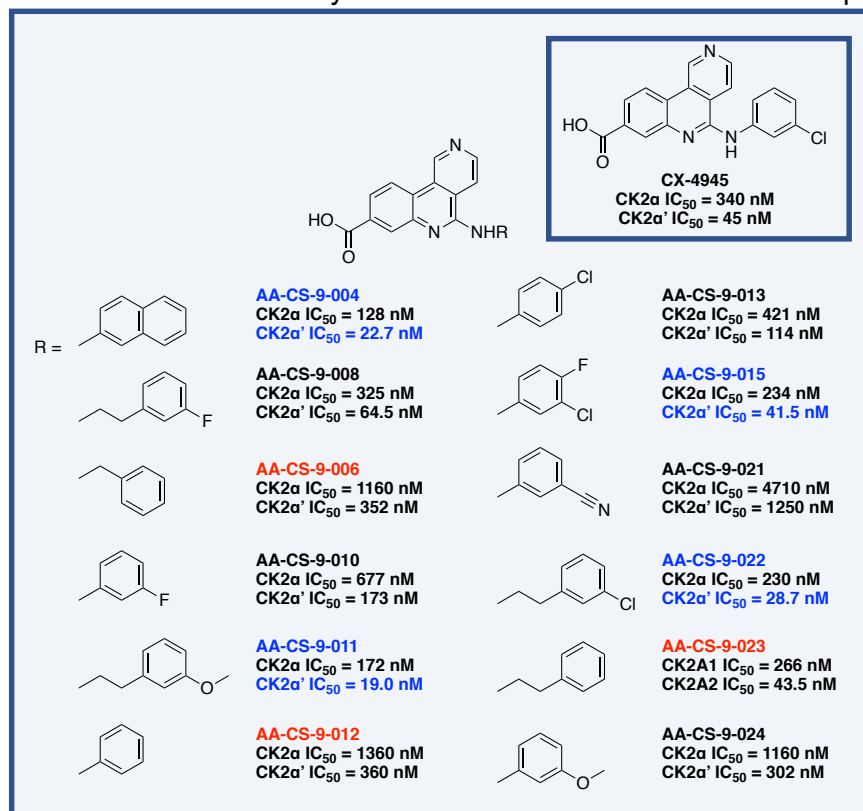ditional profiling around our compounds that has enhanced the compound data we will deliver. Our collaborators at Washington University will be officially added to the workflow in year 2 and we will be selecting our best inhibitors to send to them for profiling.

For series 2, we designed analogs around the CX-4945 and CX-5011 scaffolds. The goal of our first library was to determine whether the biochemical data reported for a large number of CX-4945 analogs translated to cellular activity in our CK2 NanoBRET assays.[23] Through preparation of some exemplified compounds and others that were not reported, we have started to understand the structural elements that contribute to the variable solubility of the naphthyridine scaffold and confirmed that naphthyridines get into cells (at least partially) to potently engage CK2. The two parent compounds and a summary of the 23 analogs prepared are included in Figure 16.

Figure 17 includes all 12 CX-4945 analogs prepared and the corresponding CK2α and CK2α' NanoBRET data. Similarly, Figure 18 includes all 11 CX-5011 analogs prepared with corresponding NanoBRET data. Compounds with IC_{50} values <50 nM in the CK2α' NanoBRET assay without associated

Figure 17. CX-4945 analogs and corresponding CK2 NanoBRET data.
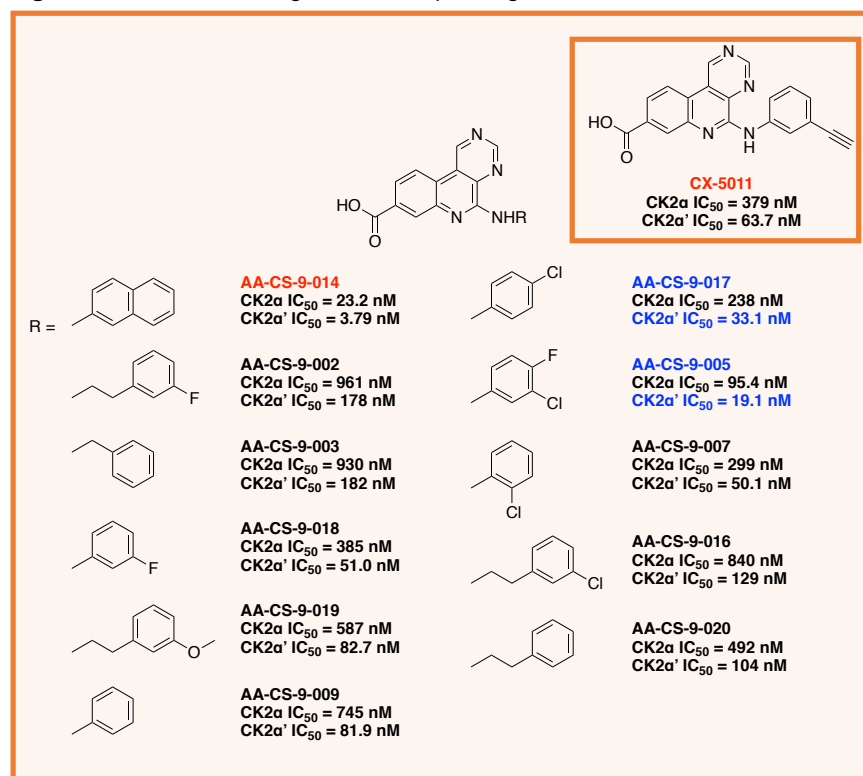
Figure 18. CX-5011 analogs and corresponding CK2 NanoBRET data.

16

solubility problems are highlighted blue. Compounds with solubility problems noted are highlighted in red. While several compounds in each series potently engage CK2 in cells, the promiscuity of CX-4945 (Figure 12) makes us wary of the selectivity of these compounds for CK2 over other kinases. To begin to explore the selectivity of these compounds for CK2, the entire library of 23 compounds was profiled against highly homologous CMGC kinases from the DYRK and HIPK sub-families. All kinases minus DYRK4 were available as enzymatic assays at Eurofins. Profiling results are included in Table 4 versus results for CX-4945 when broadly screened at DiscoverX at 1 μM in their corresponding binding assays. The compounds were profiled at a single concentration (1 μM) in duplicate and % control values reported. The lower % control values (highlighted green) correspond with more potent inhibition of the kinase. We found these compounds to potently inhibit most kinases within the CMGC family. These data indicate that our naphthyridine analogs are less selective than pyrazolopyrimidine leads and likely inhibit many kinases if broadly profiled.

Table 4. Enzymatic profiling data for series 2 against CMGC kinases.

Compound	% Control (1 μM)							
	DYRK1A	DYRK1B	DYRK2	DYRK3	HIPK1	HIPK2	HIPK3	HIPK4
AA-CS-9-002	18	117	52	17	15	6	27	10
AA-CS-9-003	61	124	37	31	70	39	52	63
AA-CS-9-004	2	84	18	4	13	4	7	-10
AA-CS-9-005	1	60	41	8	6	2	12	6
AA-CS-9-006	49	112	27	21	76	51	68	33
AA-CS-9-007	11	122	60	66	13	3	17	-3
AA-CS-9-008	8	106	17	7	13	4	8	-10
AA-CS-9-009	3	62	54	22	11	2	13	103
AA-CS-9-010	0	13	13	0	6	-1	10	1
AA-CS-9-011	12	123	19	11	16	10	21	-8
AA-CS-9-012	6	73	45	7	30	10	20	-2
AA-CS-9-013	2	65	11	2	6	-1	9	116
AA-CS-9-014	-1	41	1	0	1	-3	3	109
AA-CS-9-015	0	22	5	1	8	1	5	75
AA-CS-9-016	44	114	76	37	35	36	38	53
AA-CS-9-017	3	80	33	9	4	-2	7	62
AA-CS-9-018	1	30	33	9	3	-1	5	52
AA-CS-9-019	40	112	59	28	36	22	27	135
AA-CS-9-020	19	123	45	25	18	7	16	29
AA-CS-9-021	-1	10	11	0	5	-1	13	29
AA-CS-9-022	17	112	29	5	20	20	29	47
AA-CS-9-023	10	114	9	3	12	4	8	5
AA-CS-9-024	2	35	14	2	11	2	8	-14
CX-5011	3	87	55	15	17	3	8	35
CX-4945	0.1	0	5.1	NT	0.3	0	1	7.8

As a confirmatory experiment to corroborate the selectivity profiling data, the 23 compounds were evaluated for their antiproliferative activity. The antiproliferative activity of CX-4945 is well documented and has motivated its use in clinical trials for oncology. It has also been hypothesized that it is off-target kinase inhibition rather than CK2 inhibition (or a combination of both) that is responsible for the antiproliferative activity elicited by CX-4945. Collaboratively, we profiled the entire library as well as CX-4945 and CX-5011 (25 compounds in total) against a panel of Ewing's sarcoma and multiple myeloma cell lines. While we did not find the compounds to be broadly antiproliferative, some of the cancer lines were sensitive to treatment. The STA-ET-10 Ewing's sarcoma cell line was the most sensitive of the cell lines tested, with all but 3 of the

compounds tested resulting in at least 40% loss in viability at 1 µM and 20 of the compounds resulting in 50% loss in viability at 1 µM. These 20 compounds had a more significant effect on viability than when SGC-CK2-1 was tested at the same concentration in this cell line. There were, however, examples from the pyrazolopyrimidine series (series 1) that demonstrated more profound impacts on viability than any of the 25 naphthyridines in the STA-ET-10 Ewing's sarcoma cell line as well as against the entire Ewing's sarcoma cell line panel. The remaining 6 The other four Ewing's sarcoma cell lines evaluated showed some response to certain naphthyridines, but with <45% loss in viability at 1 µM. Of the multiple myeloma cell lines tested, only a couple of the 6 cell lines tested were responsive to the 25 naphthyridines in series 2. 3 compounds in the series (AA-9-003, AA-CS-9-013, and AA-CS-9-023) resulted in >50% loss in viability at 1 µM in two cell lines (AMO-1 and L363). The AMO-1 cell line was modestly sensitive to an additional 9 compounds, resulting in >30% loss in viability at 1 µM. The 4 remaining multiple myeloma cell lines tested were not sensitive to this library but demonstrated significant sensitivity to several pyrazolopyrimidine-based CK2 inhibitors from our first series.

XY2-051
CK2α' IC$_{50}$ = 550 nM

XY2-052
CK2α' IC$_{50}$ = 684 nM
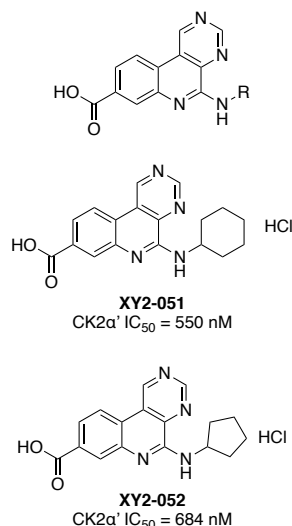
Figure 19. Design strategy for series 2 library 2.

Synthesis of the second library of series 2 compounds has started. Given its standout potency and lack of antiproliferative activity, we have opted to make analogs around AA-CS-9-014 (Figure 18) to try to improve the problematic solubility while maintaining the CK2 potency. Our design hypothesis centers around the theory that the poor solubility is the result of an extremely planar compound and incorporation of groups that break the planarity of the system could improve the solubility of resultant analogs. The design strategy and a couple representative analogs that have been prepared and tested are included in Figure 19. Significant losses in CK2 potency were observed with these first two analogs, but more will need to be made before we can draw conclusions about our strategy.

With respect to series, we have delivered and profiled the first library via NanoBRET assay and have continued to make a few additional analogs. We have opted to not look at the DMPK properties of this series yet because of the liabilities associated with the kinase inhibition profile of these compounds. Additional analogs will be prepared and analyzed for CK2 in-cell target engagement, while compounds from Table 4 are broadly profiled for kinome-wide selectivity to determine whether this series is a viable back-up series to the pyrazolopyrimidines.

Key Research Accomplishments

Aim 1
- Published pre-print about KCGS and submitted same data for publication in *Int J Mol Sci*
- Generated human induced pluripotent stem cells with two ALS-relevant mutant forms of TDP-43 incorporated: G348C and A382T that were successfully used to generate spinal motor neurons
- Characterized transcript and protein levels of mutant versus WT TDP-43 during differentiation, with RNAseq analysis of five replicates across both mutant and control MNs now in progress to identify potential biomarkers for assay screening
- Characterized localization of mutant versus WT TDP-43 in spinal motor neurons without and with treatment with ethacrynic acid
- Confirmed that ethacrynic acid treatment induces translocation of both mutant and WT TDP-43
- Developed methodology to allow quantification of TDP-43 translocation

Aim 2

- Identified several potent TBK1 inhibitors that permeate cells and engage TBK1 in a cellular target engagement assay
- Published pre-print about this series and submitted same data for publication in *J Med Chem*
- Confirmed GSK8612 to be the best available TBK1 inhibitor in terms of cellular potency and kinome-wide selectivity
- Found that GSK8612 was not tolerant of incorporation of a linker without significant losses in TBK1 cellular target engagement potency
- Prioritized several analogs with linkers attached that maintain potent TBK1 cellular target engagement and demonstrated improved kinome-wide selectivity versus the corresponding parent compound
- Selected at least one TBK1-targeting warhead with linker attached for ATTAC chemistry
- Identified several putative TRAF6 ligands via thermal shift assay
- Identified several putative TRAF3 ligands via thermal shift assay
- Confirmed dose-dependent binding of a small molecule ligand to TRAF3 with an apparent K_D = 19 μM and some demonstrated binding selectivity over E3 ligase BRD4
- Selected lead series of TRAF3-targeting compounds for follow-up studies

Aim 3
- Delivered best available chemical probe targeting CK2: SGC-CK2-1
- Published pre-print and publication in *Cell Chem Biol* about SGC-CK2-1
- Validated that selective CK2 inhibition is not toxic to the majority of cancer cell lines or primary cells, especially differentiated motor neurons
- Determined that SGC-CK2-1 has sub-optimal developability properties and requires improvement to be a useful *in vivo* tool compound
- Confirmed that, while it demonstrates improved mouse liver microsomal stability versus SGC-CK2-1, Aniline I suffers from poor kinome-wide selectivity that precludes its use as a high-quality CK2 tool compound
- Delivered several potent CK2 inhibitors that engage CK2 in cells and demonstrate improved mouse liver microsomal stability versus SGC-CK2-1
- Selected a subset of pyrazolopyrimidine-based CK2 inhibitors for evaluation of *in vivo* mouse PK and kinome-wide selectivity
- Determined that naphthyridines based on CX-4945 suffer from poor solubility in DMSO, while those based around CX-5011 demonstrate slightly better solubility
- Confirmed that naphthyridine analogs designed around CX-4945 and CX-5011 demonstrate potent engagement of CK2 in cells, but suffer from sub-optimal selectivity when profiled against highly homologous CMGC kinase families
- Demonstrated that series 2 naphthyridines are not broadly antiproliferative when tested against 12 Ewing's sarcoma and multiple myeloma cell lines
- Selected a lead compound from the naphthyridine series: AA-CS-9-014

Reportable Outcomes

Manuscripts, abstractions, presentations
A. Manuscripts and published abstracts

1. Wells, C.; Drewry, D. H.; Pickett, J. E.; Tjaden, A.; Krämer, A.; Müller, S.; Gyenis, L.; Menyhart, D.; Litchfield, D. W.; Knapp, S.; <u>Axtman, A. D.</u> Development of a potent and selective chemical probe for the pleiotropic kinase CK2. *Cell Chem Biol* **2021**, *28*, 546-558.e10; doi.org/10.1016/j.chembiol.2020.12.013.
2. Wells, C. I.; Al-Ali, H.; Andrews, D. M.; Asquith, C. R. M.; <u>Axtman, A. D.</u>; Dikic, I.; Ebner, D.; Elkins, J.; Ettmayer, P.; Fischer, C.; Frederiksen, M.; Futrell, R. E.; Gray, N. S.; Hatch, S. B.;

Knapp, S.; Lücking, U.; Michaelides, M.; Mills, C. E.; Müller, S.; Owen, D.; Picado, A.; Saikatendu, K. S.; Schröder, M.; Stolz, A.; Tellechea, M.; Turunen, B. J.; Vilar, S.; Wang, J.; Zuercher, W. J.; Willson, T. M.; Drewry, D. H. The Kinase Chemogenomic Set (KCGS): An open science resource for kinase vulnerability identification. *Int J Mol Sci* **2020**, *22*, 566; doi: 10.3390/ijms22020566.

3. Wells, C.; Drewry, D. H.; Pickett, J. E.; Tjaden, A.; Krämer, A.; Knapp, S.; Menyhart, D.; Gyenis, L.; Litchfield, D. W.; <u>Axtman, A. D.</u> Development of the first selective chemical probe for the pleiotropic kinase CK2, an emerging target in neurodegenerative disease. *Alzheimer's Dement* **2020**, 16, e12278; doi: 10.1002/alz.12278.

4. Lindsley, C. W.; <u>Axtman, A. D.</u> NeuroChat with Research Assistant Professor Alison Axtman. *ACS Chem Neurosci* **2020**, *11*, 2783–2785; doi: 10.1021/acschemneuro.0c00548.

5. Krahn, A. I.; Wells, C.; Drewry, D. H.; Beitel, L. K.; Durcan, T. M.; <u>Axtman, A. D.</u> Defining the neural kinome: strategies and opportunities for small molecule drug discovery to target neurodegenerative diseases. *ACS Chem Neurosci* **2020**, *11*, 1871–1886; doi: 10.1021/acschemneuro.0c00176.

B. Preprints

1. Drewry, D.; Annor-Gyamfi, J. K.; Wells, C.; Pickett, J. E.; <u>Axtman, A.</u> Strategy for Lead Identification for Understudied Kinases. *ChemRxiv* **2021**, *14195207*; doi: 10.26434/chemrxiv.14195207.v1.

2. Wells, C.; Drewry, D. H.; Pickett, J. E.; Tjaden, A.; Krämer, A.; Müller, S.; Gyenis, L.; Menyhart, D.; Litchfield, D. W.; Knapp, S.; <u>Axtman, A. D.</u> Development of a potent and selective chemical probe for the pleiotropic kinase CK2. *Cell Press Sneak Peek* **2020**; doi: https://ssrn.com/abstract=3732376.

3. Wells, C.; Drewry, D. H.; Pickett, J. E.; <u>Axtman, A. D.</u> SGC-CK2-1: the first selective chemical probe for the pleiotropic kinase CK2. *ChemRxiv* **2020**, *12296180*; doi: 10.26434/chemrxiv.12296180.

4. Krahn, A. I.; Wells, C.; Drewry, D. H.; Beitel, L. K.; Durcan, T. M.; <u>Axtman, A. D.</u> Defining the neural kinome: strategies and opportunities for small molecule drug discovery to target neurodegenerative diseases. *BioRxiv* **2020**, doi: 10.1101/2020.04.01.020206.

5. Wells, C.; Al-Ali, H.; Andrews, D. M.; Asquith, C. R. M.; <u>Axtman, A. D.</u>; Chung, M.; Dikic, I.; Ebner, D.; Elkins, J.; Ettmayer, P.; Fischer, C.; Frederiksen, M.; Gray, N. S.; Hatch, S.; Knapp, S.; Lee, S.; Lücking, U.; Michaelides, M.; Mills, C. E.; Müller, S.; Owen, D.; Picado, A.; Ramadan, K.; Saikatendu, K. S.; Schröder, M.; Stolz, A.; Tellechea, M.; Treiber, D. K.; Turunen, B. J.; Vilar, S.; Wang, J.; Zuercher, W. J.; Willson, T. M.; Drewry, D. H. The Kinase Chemogenomic Set (KCGS): An open science resource for kinase vulnerability identification. *BioRxiv* **2019**, *886523;* doi: 10.1101/886523.

C. Oral presentations

March 2021: " "Characterizing the Role of the Dark Proteome in Neurodegenerative Disease" SGC Board Meeting, virtual

November 2020: "Design of the first selective chemical probe for the pleiotropic kinase CK2" Target 2035 kick-off webinar, virtual

October 2020: "Progress on Chemical Tools and Role of IDG Dark Kinases in Neurodegeneration" Kinase-DRGC meeting, virtual

October 2020: "Opportunities for Small Molecule Drug Discovery within the Neural Kinome" ATOM-IDG symposium, virtual

April 2020: "CSNK2A1/2 (CK2) probe"
SGC Chemical Probes Joint Management Committee meeting, virtual

D. Poster presentations

February 2021: "Illumination of CK2 uncovers new roles in cell biology"
IDG Face-to-Face Annual Meeting, virtual

December 2020: "Development of the first selective chemical probe for the pleiotropic kinase CK2, an emerging target in neurodegenerative disease"

<table>
<tr><td>*November 2020:*</td><td>CSHL Neurodegenerative Diseases: Biology & Therapeutics, virtual
"Development of the first selective chemical probe for the pleiotropic kinase CK2, an emerging target in neurodegenerative disease"
Alzheimer's Association International Conference Neuroscience Next, virtual</td></tr>
<tr><td>*September 2020:*</td><td>"Identification of novel kinase targets in ALS"
19th Annual NEALS Meeting, virtual</td></tr>
</table>

Funding applied for based on work supported by this training grant

A. Received
1. Clinical NIH Loan Repayment Program award through the National Institute on Aging (Axtman)

B. Applied for
1. "Use of iPSC-based model systems to interrogate novel protein targets that drive neurodegeneration" 2021 NYSCF- Robertson Neuroscience Investigator Award
2. "Optimization of a potent and cell active CK2 chemical probe for use in Alzheimer's disease" NIH PAR-21-029 Discovery of in vivo Chemical Probes for the Nervous System (R01 Clinical Trial Not Allowed)

Employment or research opportunities applied for and/or received based on experience/training supported by this grant

1. Promotion to Research Associate Professor, effective April 1, 2021 (Axtman)
2. Promotion to Associate Professor, effective February 14, 2021 (Durcan)
3. Guest Associate Editors for a co-listed special topic in *Front Cell Neurosci* and *Front Mol Neurosci*: "The Next Generation of Tools and Technologies for Studying Human Neurons in a Dish" (Axtman and Durcan)

Conclusions

Despite setbacks incurred due to COVID-19, we have delivered on many of our milestones and kept to the timelines proposed in the original grant application. We have pivoted in strategy where necessary and are producing a more robust portfolio of deliverables as a result. The many significant research accomplishments as well as several notable reportable outcomes support that we have made measurable and impactful progress toward our aims. We will continue to be productive in year 2 of the award period and provide the research community with useful chemical and biological reagents for use in their own studies.

References

1. Freischmidt, A.; Wieland, T.; Richter, B.; Ruf, W.; Schaeffer, V.; Muller, K.; Marroquin, N.; Nordin, F.; Hubers, A.; Weydt, P.; Pinto, S.; Press, R.; Millecamps, S.; Molko, N.; Bernard, E.; Desnuelle, C.; Soriani, M. H.; Dorst, J.; Graf, E.; Nordstrom, U.; Feiler, M. S.; Putz, S.; Boeckers, T. M.; Meyer, T.; Winkler, A. S.; Winkelman, J.; de Carvalho, M.; Thal, D. R.; Otto, M.; Brannstrom, T.; Volk, A. E.; Kursula, P.; Danzer, K. M.; Lichtner, P.; Dikic, I.; Meitinger, T.; Ludolph, A. C.; Strom, T. M.; Andersen, P. M.; Weishaupt, J. H. Haploinsufficiency of TBK1 causes familial ALS and fronto-temporal dementia. *Nat Neurosci* **2015,** 18, 631-6.
2. Chen-Plotkin, A. S.; Lee, V. M.; Trojanowski, J. Q. TAR DNA-binding protein 43 in neurodegenerative disease. *Nat Rev Neurol* **2010,** 6, 211-20.
3. Oakes, J. A.; Davies, M. C.; Collins, M. O. TBK1: a new player in ALS linking autophagy and neuroinflammation. *Mol Brain* **2017,** 10, 5.
4. Wells, C. I.; Al-Ali, H.; Andrews, D. M.; Asquith, C. R. M.; Axtman, A. D.; Dikic, I.; Ebner, D.; Ettmayer, P.; Fischer, C.; Frederiksen, M.; Futrell, R. E.; Gray, N. S.; Hatch, S. B.; Knapp, S.; Lücking, U.; Michaelides, M.; Mills, C. E.; Müller, S.; Owen, D.; Picado, A.; Saikatendu, K. S.;

Schröder, M.; Stolz, A.; Tellechea, M.; Turunen, B. J.; Vilar, S.; Wang, J.; Zuercher, W. J.; Willson, T. M.; Drewry, D. H. The Kinase Chemogenomic Set (KCGS): An Open Science Resource for Kinase Vulnerability Identification. *Int J Mol Sci* **2021,** 22, 566.

5.   Wells, C. I.; Hassan, A.-A.; Andrews, D. M.; Asquith, C. R. M.; Axtman, A. D.; Chung, M.; Dikic, I.; Ebner, D.; Elkins, J. M.; Ettmayer, P.; Fischer, C.; Frederiksen, M.; Gray, N. S.; Hatch, S.; Knapp, S.; Lee, S.; Lücking, U.; Michaelides, M.; Mills, C. E.; Müller, S.; Owen, D.; Picado, A.; Ramadan, K.; Saikatendu, K. S.; Schröder, M.; Stolz, A.; Tellechea, M.; Treiber, D. K.; Turunen, B.; Vilar, S.; Wang, J.; Zuercher, W. J.; Willson, T. M.; Drewry, D. H. The Kinase Chemogenomic Set (KCGS): An open science resource for kinase vulnerability identification. *BioRxiv* **2019**, 10.1101/2019.12.22.886523.

6.   Buratti, E.; Baralle, F. E. Multiple roles of TDP-43 in gene expression, splicing regulation, and human disease. *Front Biosci* **2008,** 13, 867-78.

7.   Arai, T.; Hasegawa, M.; Akiyama, H.; Ikeda, K.; Nonaka, T.; Mori, H.; Mann, D.; Tsuchiya, K.; Yoshida, M.; Hashizume, Y.; Oda, T. TDP-43 is a component of ubiquitin-positive tau-negative inclusions in frontotemporal lobar degeneration and amyotrophic lateral sclerosis. *Biochem Biophys Res Commun* **2006,** 351, 602-11.

8.   Neumann, M.; Sampathu, D. M.; Kwong, L. K.; Truax, A. C.; Micsenyi, M. C.; Chou, T. T.; Bruce, J.; Schuck, T.; Grossman, M.; Clark, C. M.; McCluskey, L. F.; Miller, B. L.; Masliah, E.; Mackenzie, I. R.; Feldman, H.; Feiden, W.; Kretzschmar, H. A.; Trojanowski, J. Q.; Lee, V. M. Ubiquitinated TDP-43 in frontotemporal lobar degeneration and amyotrophic lateral sclerosis. *Science* **2006,** 314, 130-3.

9.   Iguchi, Y.; Katsuno, M.; Takagi, S.; Ishigaki, S.; Niwa, J.; Hasegawa, M.; Tanaka, F.; Sobue, G. Oxidative stress induced by glutathione depletion reproduces pathological modifications of TDP-43 linked to TDP-43 proteinopathies. *Neurobiol Dis* **2012,** 45, 862-70.

10.   Choksi, D. K.; Roy, B.; Chatterjee, S.; Yusuff, T.; Bakhoum, M. F.; Sengupta, U.; Ambegaokar, S.; Kayed, R.; Jackson, G. R. TDP-43 Phosphorylation by casein kinase Iε promotes oligomerization and enhances toxicity in vivo. *Hum Mol Genet* **2013,** 23, 1025-1035.

11.   Nonaka, T.; Suzuki, G.; Tanaka, Y.; Kametani, F.; Hirai, S.; Okado, H.; Miyashita, T.; Saitoe, M.; Akiyama, H.; Masai, H.; Hasegawa, M. Phosphorylation of TAR DNA-binding Protein of 43 kDa (TDP-43) by Truncated Casein Kinase 1delta Triggers Mislocalization and Accumulation of TDP-43. *J Biol Chem* **2016,** 291, 5473-83.

12.   Hasegawa, M.; Arai, T.; Nonaka, T.; Kametani, F.; Yoshida, M.; Hashizume, Y.; Beach, T. G.; Buratti, E.; Baralle, F.; Morita, M.; Nakano, I.; Oda, T.; Tsuchiya, K.; Akiyama, H. Phosphorylated TDP-43 in frontotemporal lobar degeneration and amyotrophic lateral sclerosis. *Ann Neurol* **2008,** 64, 60-70.

13.   Mohapatra, B.; Ahmad, G.; Nadeau, S.; Zutshi, N.; An, W.; Scheffe, S.; Dong, L.; Feng, D.; Goetz, B.; Arya, P.; Bailey, T. A.; Palermo, N.; Borgstahl, G. E.; Natarajan, A.; Raja, S. M.; Naramura, M.; Band, V.; Band, H. Protein tyrosine kinase regulation by ubiquitination: critical roles of Cbl-family ubiquitin ligases. *Biochim Biophys Acta* **2013,** 1833, 122-39.

14.   Nazio, F.; Carinci, M.; Cecconi, F. ULK1 ubiquitylation is regulated by phosphorylation on its carboxy terminus. *Cell Cycle* **2017,** 16, 1744-1747.

15.   Nguyen, L. K.; Kolch, W.; Kholodenko, B. N. When ubiquitination meets phosphorylation: a systems biology perspective of EGFR/MAPK signalling. *Cell Commun Signal* **2013,** 11, 52.

16.   Drewry, D.; Annor-Gyamfi, J. K.; Wells, C.; Pickett, J. E.; Axtman, A. Strategy for Lead Identification for Understudied Kinases. *ChemRxiv* **2021,** 10.26434/chemrxiv.14195207.v1.

17.   Crew, A. P.; Raina, K.; Dong, H.; Qian, Y.; Wang, J.; Vigil, D.; Serebrenik, Y. V.; Hamman, B. D.; Morgan, A.; Ferraro, C.; Siu, K.; Neklesa, T. K.; Winkler, J. D.; Coleman, K. G.; Crews, C. M. Identification and Characterization of Von Hippel-Lindau-Recruiting Proteolysis Targeting Chimeras (PROTACs) of TANK-Binding Kinase 1. *J Med Chem* **2018,** 61, 583-598.

18.   Brenke, J. K.; Popowicz, G. M.; Schorpp, K.; Rothenaigner, I.; Roesner, M.; Meininger, I.; Kalinski, C.; Ringelstetter, L.; R'kyek, O.; Jürjens, G.; Vincendeau, M.; Plettenburg, O.;

Sattler, M.; Krappmann, D.; Hadian, K. Targeting TRAF6 E3 ligase activity with a small-molecule inhibitor combats autoimmunity. *J Biol Chem* **2018,** 293, 13191-13203.

19.   Fedorov, O.; Niesen, F. H.; Knapp, S. Kinase Inhibitor Selectivity Profiling Using Differential Scanning Fluorimetry. In *Kinase Inhibitors. Methods in Molecular Biology (Methods and Protocols)*, B, K., Ed. Humana Press: 2012; Vol. 795.

20.   Lamark, T.; Kirkin, V.; Dikic, I.; Johansen, T. NBR1 and p62 as cargo receptors for selective autophagy of ubiquitinated targets. *Cell Cycle* **2009,** 8, 1986-90.

21.   Matsumoto, G.; Wada, K.; Okuno, M.; Kurosawa, M.; Nukina, N. Serine 403 phosphorylation of p62/SQSTM1 regulates selective autophagic clearance of ubiquitinated proteins. *Mol Cell* **2011,** 44, 279-89.

22.   Herhaus, L.; Dikic, I. Expanding the ubiquitin code through post-translational modification. *EMBO Rep* **2015,** 16, 1071-83.

23.   Pierre, F.; Chua, P. C.; O'Brien, S. E.; Siddiqui-Jain, A.; Bourbon, P.; Haddach, M.; Michaux, J.; Nagasawa, J.; Schwaebe, M. K.; Stefan, E.; Vialettes, A.; Whitten, J. P.; Chen, T. K.; Darjania, L.; Stansfield, R.; Anderes, K.; Bliesath, J.; Drygin, D.; Ho, C.; Omori, M.; Proffitt, C.; Streiner, N.; Trent, K.; Rice, W. G.; Ryckman, D. M. Discovery and SAR of 5-(3-chlorophenylamino)benzo[c][2,6]naphthyridine-8-carboxylic acid (CX-4945), the first clinical stage inhibitor of protein kinase CK2 for the treatment of cancer. *J Med Chem* **2011,** 54, 635-54.

24.   Perez, D. I.; Gil, C.; Martinez, A. Protein kinases CK1 and CK2 as new targets for neurodegenerative diseases. *Med Res Rev* **2011,** 31, 924-54.

25.   Castello, J.; Ragnauth, A.; Friedman, E.; Rebholz, H. CK2—An Emerging Target for Neurological and Psychiatric Disorders. *Pharmaceuticals* **2017,** 10, 7.

26.   Cozza, G.; Pinna, L. A.; Moro, S. Kinase CK2 inhibition: an update. *Curr Med Chem* **2013,** 20, 671-93.

27.   Guerra, B.; Issinger, O. G. Protein kinase CK2 in human diseases. *Curr Med Chem* **2008,** 15, 1870-86.

28.   Du, M.; Liu, J.; Chen, X.; Xie, Y.; Yuan, C.; Xiang, Y.; Sun, B.; Lan, K.; Chen, M.; James, S. J.; Zhang, Y.; Zhong, J.; Xiao, H. Casein kinase II controls TBK1/IRF3 activation in IFN response against viral infection. *J Immunol* **2015,** 194, 4477-88.

29.   Matsumoto, G.; Shimogori, T.; Hattori, N.; Nukina, N. TBK1 controls autophagosomal engulfment of polyubiquitinated mitochondria through p62/SQSTM1 phosphorylation. *Hum Mol Genet* **2015,** 24, 4429-42.

30.   Sarno, S.; Reddy, H.; Meggio, F.; Ruzzene, M.; Davies, S. P.; Donella-Deana, A.; Shugar, D.; Pinna, L. A. Selectivity of 4,5,6,7-tetrabromobenzotriazole, an ATP site-directed inhibitor of protein kinase CK2 ('casein kinase-2'). *FEBS Lett* **2001,** 496, 44-8.

31.   Wells, C. I.; Drewry, D. H.; Pickett, J. E.; Tjaden, A.; Krämer, A.; Müller, S.; Gyenis, L.; Menyhart, D.; Litchfield, D. W.; Knapp, S.; Axtman, A. D. Development of a Potent and Selective Chemical Probe for the Pleiotropic Kinase CK2. *Cell Chem Biol* **2021,** 28, 546-558.e10.

32.   Wells, C.; Drewry, D. H.; Pickett, J. E.; Axtman, A. D. SGC-CK2-1: the first selective chemical probe for the pleiotropic kinase CK2. *ChemRxiv* **2020**, 10.26434/chemrxiv.12296180.v1.

33.   Williams, H. D.; Trevaskis, N. L.; Charman, S. A.; Shanker, R. M.; Charman, W. N.; Pouton, C. W.; Porter, C. J. Strategies to address low drug solubility in discovery and development. *Pharmacol Rev* **2013,** 65, 315-499.

34.   Walker, M. A. Improvement in aqueous solubility achieved via small molecular changes. *Bioorg Med Chem Lett* **2017,** 27, 5100-5108.

35.   Thomas, V. H.; Bhattachar, S.; Hitchingham, L.; Zocharski, P.; Naath, M.; Surendran, N.; Stoner, C. L.; El-Kattan, A. The road map to oral bioavailability: an industrial perspective. *Expert Opin Drug Metab Toxicol* **2006,** 2, 591-608.

36.   Guha, R.; Dexheimer, T. S.; Kestranek, A. N.; Jadhav, A.; Chervenak, A. M.; Ford, M. G.; Simeonov, A.; Roth, G. P.; Thomas, C. J. Exploratory analysis of kinetic solubility measurements of a small molecule library. *Bioorg Med Chem* **2011,** 19, 4127-4134.

37.   Son, Y. H.; Song, J. S.; Kim, S. H.; Kim, J. Pharmacokinetic characterization of CK2 inhibitor CX-4945. *Arch Pharm Res* **2013,** 36, 840-5.

38.   Siddiqui-Jain, A.; Chua, P.; Darjania, L.; Lim, J.; O'Brien, S.; Pierre, F.; Streiner, N.; Trent, K.; Whitten, J.; Rice, W. The discovery and characterization of CX-5011, a highly selective, potent inhibitor of Protein Kinase CK2. *Cancer Res* **2008,** 68, 4875-4875.

39.   Matlock, M. K.; Hughes, T. B.; Swamidass, S. J. XenoSite server: a web-available site of metabolism prediction tool. *Bioinformatics* **2014,** 31, 1136-1137.

40.   Rydberg, P.; Gloriam, D. E.; Zaretzki, J.; Breneman, C.; Olsen, L. SMARTCyp: A 2D Method for Prediction of Cytochrome P450-Mediated Drug Metabolism. *ACS Med Chem Lett* **2010,** 1, 96-100.

Appendices

Attached are copies of the following:

1. Wells, C.; Drewry, D. H.; Pickett, J. E.; Tjaden, A.; Krämer, A.; Müller, S.; Gyenis, L.; Menyhart, D.; Litchfield, D. W.; Knapp, S.; Axtman, A. D. Development of a potent and selective chemical probe for the pleiotropic kinase CK2. *Cell Chem Biol* **2021**, *28*, 546-558.e10; doi.org/10.1016/j.chembiol.2020.12.013.

2. Wells, C. I.; Al-Ali, H.; Andrews, D. M.; Asquith, C. R. M.; Axtman, A. D.; Dikic, I.; Ebner, D.; Elkins, J.; Ettmayer, P.; Fischer, C.; Frederiksen, M.; Futrell, R. E.; Gray, N. S.; Hatch, S. B.; Knapp, S.; Lücking, U.; Michaelides, M.; Mills, C. E.; Müller, S.; Owen, D.; Picado, A.; Saikatendu, K. S.; Schröder, M.; Stolz, A.; Tellechea, M.; Turunen, B. J.; Vilar, S.; Wang, J.; Zuercher, W. J.; Willson, T. M.; Drewry, D. H. The Kinase Chemogenomic Set (KCGS): An open science resource for kinase vulnerability identification. *Int J Mol Sci* **2020**, *22*, 566; doi: 10.3390/ijms22020566.

3. Drewry, D.; Annor-Gyamfi, J. K.; Wells, C.; Pickett, J. E.; Axtman, A. Strategy for Lead Identification for Understudied Kinases. *ChemRxiv* **2021**, *14195207*; doi: 10.26434/chemrxiv.14195207.v1.

Cell Chemical Biology

Development of a potent and selective chemical probe for the pleiotropic kinase CK2

Graphical Abstract
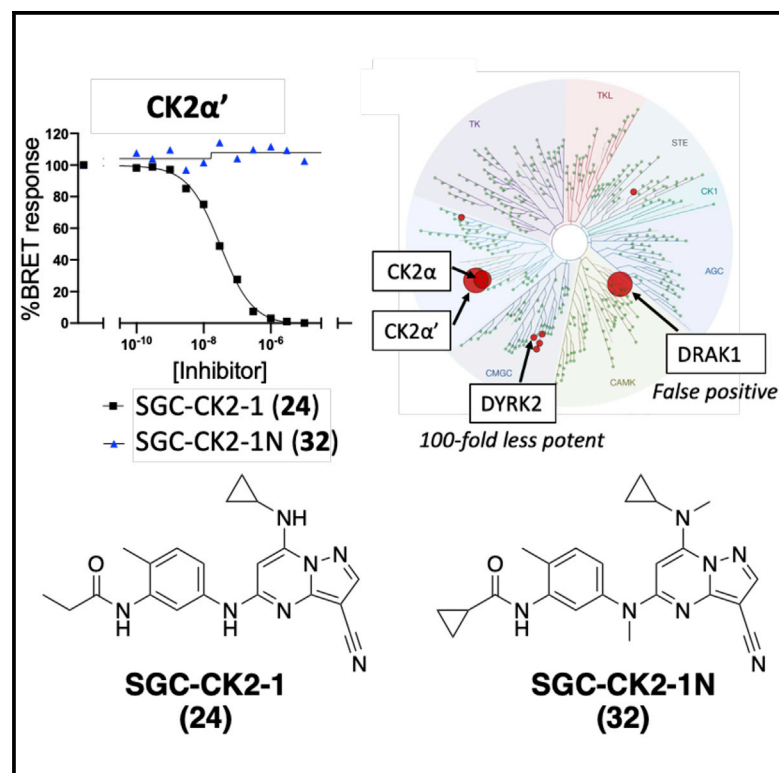
Authors

Carrow I. Wells, David H. Drewry,
Julie E. Pickett, ..., David W. Litchfield,
Stefan Knapp, Alison D. Axtman

Correspondence

alison.axtman@unc.edu

In Brief

Many papers have detailed the function(s) of casein kinase 2 (CK2). Characterization of CK2, however, has been confounded by the use of suboptimal inhibitors. Wells et al. have identified the best available chemical tool to use in illuminating the essential roles of this pleiotropic kinase.

Highlights

- We developed a potent, selective, and cell-active chemical probe for CK2

- We identified a negative control compound to be used with the CK2 probe

- Our selective chemical probe (SGC-CK2-1) is not broadly antiproliferative

- SGC-CK2-1 is the best available chemical tool to define the roles of CK2 in cells

CellPress

Article

Development of a potent and selective chemical probe for the pleiotropic kinase CK2

Carrow I. Wells,[1,2,7] David H. Drewry,[1,2,7] Julie E. Pickett,[1,2] Amelie Tjaden,[3,4] Andreas Krämer,[3,4] Susanne Müller,[3,4] Laszlo Gyenis,[5] Daniel Menyhart,[5] David W. Litchfield,[5,6] Stefan Knapp,[3,4] and Alison D. Axtman[1,2,8,*]

[1]Structural Genomics Consortium (SGC), UNC Eshelman School of Pharmacy, University of North Carolina at Chapel Hill (UNC-CH), Chapel Hill, NC 27599, USA
[2]Division of Chemical Biology and Medicinal Chemistry, UNC Eshelman School of Pharmacy, UNC-CH, Chapel Hill, NC 27599, USA
[3]Institute for Pharmaceutical Chemistry, Johann Wolfgang Goethe-University, Max-von-Laue-Str. 9, 60438 Frankfurt am Main, Germany
[4]Structural Genomics Consortium, Buchman Institute for Life Sciences, Johann Wolfgang Goethe-University, Max-von-Laue-Str. 15, 60438 Frankfurt am Main, Germany
[5]Department of Biochemistry, Schulich School of Medicine & Dentistry, University of Western Ontario, London, Ontario, N6A 5C1, Canada
[6]Department of Oncology, Schulich School of Medicine & Dentistry, University of Western Ontario, London, Ontario, N6A 5C1, Canada
[7]These authors contributed equally
[8]Lead contact
*Correspondence: alison.axtman@unc.edu
https://doi.org/10.1016/j.chembiol.2020.12.013

SUMMARY

Building on the pyrazolopyrimidine CK2 (casein kinase 2) inhibitor scaffold, we designed a small targeted library. Through comprehensive evaluation of inhibitor selectivity, we identified inhibitor 24 (SGC-CK2-1) as a highly potent and cell-active CK2 chemical probe with exclusive selectivity for both human CK2 isoforms. Remarkably, despite years of research pointing to CK2 as a key driver in cancer, our chemical probe did not elicit a broad antiproliferative phenotype in >90% of >140 cell lines when tested in dose-response. While many publications have reported CK2 functions, CK2 biology is complex and an available high-quality chemical tool such as SGC-CK2-1 will be indispensable in deciphering the relationships between CK2 function and phenotypes.

INTRODUCTION

Protein phosphorylation is one of the most common and important post-translational modifications, playing a key role in signal transduction (Ardito et al., 2017). Protein kinases catalyze this reaction, phosphorylating a specific substrate and causing a conformational change that affects protein function (Plattner and Bibb, 2012; Röhm et al., 2020). One protein kinase, CK2 (casein kinase 2 [CSNK2]) has been implicated in the phosphorylation of hundreds of cellular proteins with >10% of the phosphoproteome matching the consensus sequence for CK2 phosphorylation (Meggio and Pinna, 2003; Salvi et al., 2009). Via genetic and biochemical studies in a variety of experimental models, CK2 has been found to be both constitutively active and ubiquitously expressed, making it important in many biological processes (Figure 1 and Table S1) (Ahmed et al., 2002; Meggio and Pinna, 2003; Nuñez de Villavicencio-Diaz et al., 2017; Rabalski et al., 2016). CK2 exists as a tetrameric complex made up of two catalytic subunits, designated CK2α (encoded by the CSNK2A1 gene) and CK2α′ (encoded by the CSNK2A2 gene), and two regulatory subunits, CK2β (Litchfield, 2003). Given the reported involvement of CK2 in a multitude of pathways, selective chemical probes would be indispensable tools for deciphering its complex roles in biological processes (Ahmed et al., 2002).

Although CK2 biology has been well-studied, reflected by >1,000 PubMed references to the human gene, selective and potent inhibitors of CK2 have remained elusive. As shown in Figure 2A, some early reported compounds that bound to CK2 originate from such diverse chemical scaffolds as benzotriazoles (TBB, 4,5,6,7-tetrabromobenzotriazole and TMCB, 4,5,6,7-tetrabromo-2-dimethylamino-1-carboxymethyl-benzimidazole) to thienopyrimidines (TTP 22) to natural product-like flavonoids (fisetin) (Golub et al., 2011; Lolli et al., 2012; Szyszka et al., 1995). TBB was published as a CK2 inhibitor in 1995 and demonstrated modest selectivity for CK2 over CK1 (casein kinase 1) (Szyszka et al., 1995). Evaluation of this compound against a panel of 33 (Sarno et al., 2001) and 70 (Pagano et al., 2008) kinases showed however that, while maintaining reasonable selectivity, it did inhibit several other kinases with >90% inhibition at a screening concentration of 10 μM (DYRK1A, DYRK2, DYRK3, HIPK2, and PIM1–3). In 2010, the compound CX-4945 (silmitasertib) was published, which has since become the most commonly employed CK2 inhibitor. Silmitasertib received orphan drug status in the US for treatment of advanced cholangiocarcinoma and has entered clinical testing in oncology (Gowda et al., 2017; Siddiqui-Jain et al., 2010). Given its antiproliferative activity in several different cancer cell lines, this inhibitor has been advanced and is currently being evaluated in clinical
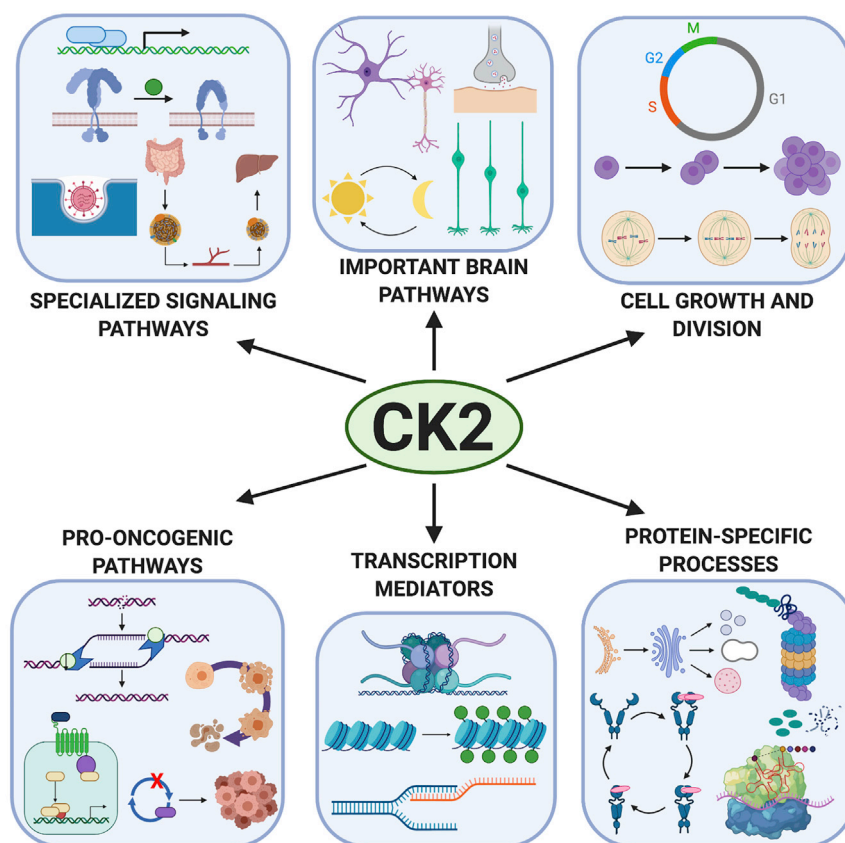
Figure 1. Summary of biological pathways mediated by CK2

tency for CK2 (Figure 2B). They further evaluate this series for both mechanistic and phenotypic endpoints, including pS129-AKT levels and antiproliferative activity (Chuaqui et al., 2013; Dowling et al., 2012, 2013, 2016). While the compounds are potent, the lead structure (**17**) has considerable off-target kinase activity (HIPK1–4, DAPK1–3, DYRK2, and BMPR1B), resulting in the need for further modification of this scaffold for probe development (Dowling et al., 2016). Due to its relatively favorable kinome-wide selectivity profile as well as its good cellular potency, we started our CK2 chemical probe project utilizing this promising starting point (**17**).

RESULTS

Design and synthesis of pyrazolopyrimidine inhibitors of CK2

Based on the published data for pyrazolopyrimidines targeting CK2, we prepared a small library of compounds. We opted to resynthesize a subset of the published molecules so we could further characterize their selectivity and cell activity and also expand into unexplored chemical space by designing and preparing an additional six analogs not described in these papers. Table 1 shows the structures and corresponding CK2 enzymatic activity for the subset of previously exemplified molecules that we resynthesized for further characterization. Three of these compounds (**17**, **22**, **29**) had been previously reported to have narrow selectivity profiles when screened at Ambit/DiscoverX in panels of 324 (**29**) or 402 (**17** and **22**) kinases. The remaining three compounds are close structural analogs with potent enzymatic activity, but for which limited selectivity data had been reported (Chuaqui et al., 2013; Dowling et al., 2012, 2013, 2016). Figure 2B shows the compounds we designed based upon surveying the literature for structures and corresponding data. Structure–activity relationships were developed, and compounds designed that incorporated minor structural changes (**18**, **24**, **26**) and some slightly larger structural perturbations (**19**, **20**, **27**). Analogs **19** and **20** were designed with groups at a position that has proven tolerant to a wide variety of structural modifications from methyl to alkyldiamine chains (Table 1). The morpholine (**19**) and benzylamine (**20**) are bulkier than previously exemplified groups and would explore the spatial tolerance of this portion of the pocket. Analog **27** is devoid of the acetamide that is present in all previously exemplified compounds (Table 1). This modest change is expected to affect binding, as the acetamide has been shown to engage in a network of hydrogen bonds in previously solved and our own solved structures (Dowling et al., 2016). All analogs were prepared

trials for several oncology indications, basal cell carcinoma, multiple myeloma, cholangiocarcinoma, breast cancer, and medulloblastoma, all listed as active or recruiting trials on clinicaltrials.gov (Pierre et al., 2011). Recently, silmitasertib emerged as a candidate for severe acute respiratory syndrome coronavirus 2 (SARS-CoV-2), as pharmacological inhibition of CK2 was found to result in antiviral efficacy (Bouhaddou et al., 2020). Despite being fairly narrow spectrum and displaying modest kinome-wide selectivity, CX-4945 does significantly inhibit other kinases with IC_{50} (half maximal inhibitory concentration) values well below 100 nM, including CDK1, CLK1–CLK3, DAPK3, DYRK1A, DYRK1B, DYRK3, FLT3, HIPK3, PIM1, and TBK1 (Kim et al., 2014, 2016; Pierre et al., 2011). Thus, the off-target activities of this inhibitor confound results when trying to attribute target to function to phenotype. Efforts have aimed at improving the selectivity of CX-4945, producing benzonaphthyridine analogs such as CX-5011, CX-5033, and CX-5279 that display improved selectivity versus CX-4945 (Figure 2A) (Battistutta et al., 2011). Recently, a series of acyclic/macrocyclic pyrazolo[1,5-*a*]pyrimidines (Figure 2A, IC20 and IC19) was published that demonstrates excellent selectivity *in vitro*. However, the required introduction of a carboxylic acid group resulted in modest, low micromolar cellular activity (Krämer et al., 2020).
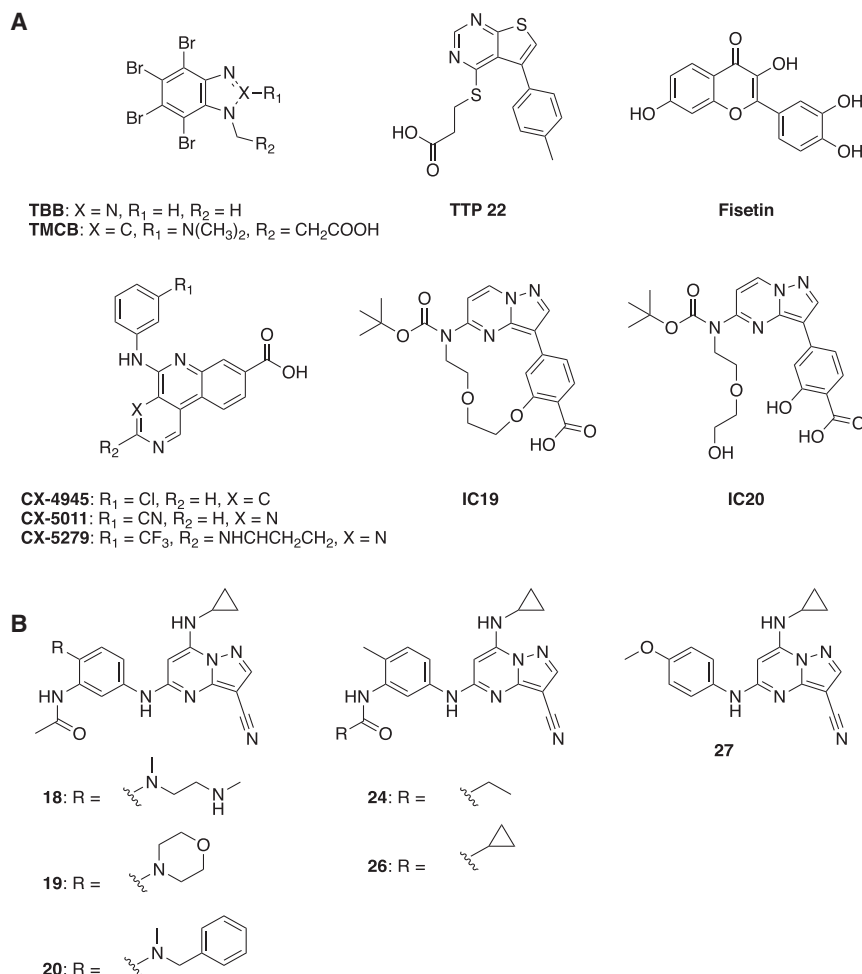
Given both the biological importance of this target and lack of selective inhibitors, we recognized the need for a CK2 chemical probe to enable accurate elucidation of its biological effects. Three recent publications from scientists at AstraZeneca disclose a series of pyrazolopyrimidines with nanomolar (nM) po-

Figure 2. Structures of reported and synthesized pyrazolopyrimidine CK2 inhibitors

(A) Structures of literature-reported CK2 inhibitors used in studies aimed at interrogating CK2 function.

(B) Structures of non-exemplified pyrazolopyrimidines synthesized.

with the other molecules in the set (Table 2 and Figure 3C). Of note, our compounds were significantly more selective than CX-4945, currently the most frequently utilized CK2 inhibitor in the literature (Figure 3C). CX-4945 has an $S_{10}(1\mu M) = 0.069$ with 28 kinases >90%I (%I, percent inhibition) (Figure S1) and compound **24**, for example, has an $S_{10}(1\mu M) = 0.007$ with only three kinases >90%I. By comparison, in smaller assay panels (94 wild-type human kinases) and tested at a lower concentration, CX-4945, CX-5011, CX-5033, and CX-5279 had $S_{10}(0.5\mu M) = 0.064$, 0.032, 0.053, and 0.021, respectively. While it is difficult to compare selectivity scores since the assay panels contain different kinase constructs and were evaluated using different assay platforms and compound concentrations, clearly the more recently generated benzonaphthyridines are more selective than CX-4945 (Battistutta et al., 2011).

In parallel, we assessed the cellular penetrance and target engagement of all compounds using the CK2α and CK2α′ nanoBRET assays in HEK-293 cells. Given the high sequence similarity of the active sites of CK2α and CK2α′, we did not anticipate preferential binding to one versus the other (Lozeman et al., 1990). The nanoBRET assay relies upon bioluminescence resonance energy transfer (BRET) between CK2α–Nluc or CK2α′–Nluc, each tagged with nanoluciferase (Nluc), and a tracer with a red-shifted fluorophore appended. Our analogs, which compete with the tracer for binding to the active site, were introduced in a dose-dependent manner and BRET was plotted versus concentration, allowing us to calculate a target engagement IC_{50} value (Vasta et al., 2017). Our entire series was active in the CK2α and CK2α′ cellular target engagement assays with several inhibitors exhibiting single digit nanomolar potencies (Figure S3). As expected, no significant difference in potency was observed between the two CK2 subunits. Nine of the pyrazolopyrimidines demonstrated CK2α′ nanoBRET in cell target engagement IC_{50} values less than or equal to 20 nM. The remaining three compounds were less potent in the nanoBRET assays, especially compounds **26** and **27**, which demonstrated micromolar IC_{50} values. CX-4945, for comparison, was shown to have a CK2α′ nanoBRET $IC_{50} = 45$ nM.

Off-target kinase inhibition was evaluated for the subset of very selective compounds that inhibited three or fewer kinases. Follow-up was carried out in dose-response using an

using convergent chemistry and, where possible, utilizing previously reported synthetic routes (Dowling et al., 2012, 2013, 2016). Key transformations, including nucleophilic aromatic substitution and Buchwald-Hartwig amination, allowed preparation of all analogs. Detailed routes are included in the Supplemental Information (Scheme S1).
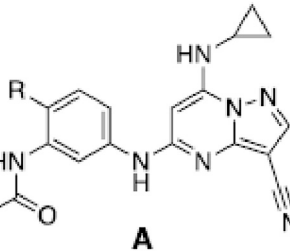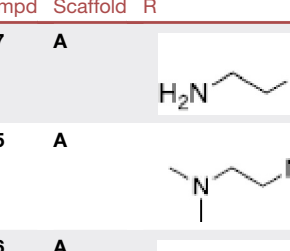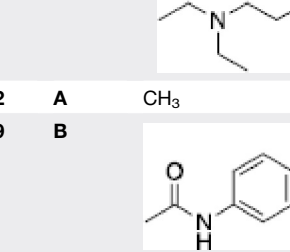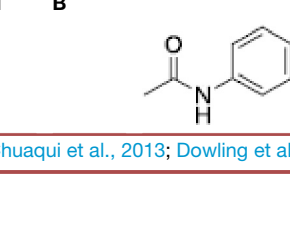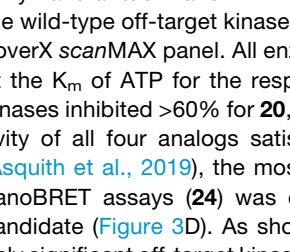
Modulation of pyrazolopyrimidines yields inhibitors with exclusive selectivity for CK2 and potent in cell target engagement

Upon preparation of the analogs shown in Table 1 and Figure 2B, the compound set was sent to Eurofins DiscoverX to be profiled against 403 wild-type human kinases using their *scan*MAX platform to characterize kinome-wide selectivity. Table 2 summarizes our findings related to the cellular potency and kinome-wide selectivity of the compounds we prepared. The selectivity score ($S_{10}(1\mu M)$) is calculated by dividing the number of inhibited kinases having an experimental value greater than 90% inhibition (I) by the total number of tested kinases. A low $S_{10}(1\mu M)$ value reflects high compound selectivity whereas a high $S_{10}(1\mu M)$ value represents poor selectivity (Bosc et al., 2017). From the entire set of compounds, four of our six non-exemplified pyrazolopyrimidines from Figure 2B (**20**, **24**, **26**, and **27**) exhibited higher kinome-wide selectivity compared

Table 1. Reported CK2 inhibitors and biochemical activity

Cmpd	Scaffold	R	Reported CK2 IC$_{50}$ (nM)
17	A		<3
15	A		<3
16	A		9
22	A	CH$_3$	<3
29	B		10
31	B		26

(Chuaqui et al., 2013; Dowling et al., 2012, 2013, 2016).

enzymatic and/or nanoBRET assay corresponding to each of the wild-type off-target kinases that inhibited >60% in the DiscoverX *scan*MAX panel. All enzymatic assays were carried out at the K$_m$ of ATP for the respective kinase. Table 2 lists the kinases inhibited >60% for **20**, **24**, **26**, and **27**. While the selectivity of all four analogs satisfy our chemical probe criteria (Asquith et al., 2019), the most potent compound in the CK2 nanoBRET assays (**24**) was chosen as the chemical probe candidate (Figure 3D). As shown in Table 2, DYRK2 was the only significant off-target kinase to demonstrate an IC$_{50}$ value < 1 μM. Of note, the potency of **24** in the CK2α and CK2α′ enzymatic assays was such that 100-fold selectivity for CK2 over DYRK2, its most potently inhibited off-target kinase, was observed. Since it seemed to be a common off target of compounds in our library, all analogs in Table 2 were tested in the DYRK2 nanoBRET assay. Only **17** was found to be active at <1 μM against DYRK2 in cells (Figure S4, IC$_{50}$ = 160 nM). An IC$_{50}$ value of 3.7 μM was determined for **24** in the DYRK2 nanoBRET assay (Figure S4). Impressively, the 100-fold selectivity for CK2 over DYRK2 in the respective enzymatic assays was maintained in the cell-based system.

Global methylation of nitrogens results in the identification of a negative control

With our chemical probe identified, we shifted our attention to furnishing a negative control compound that could be used in tandem in biological experiments. A negative control compound is structurally similar to the probe yet devoid of activity at the primary target and is useful to add rigor to the conclusion that a phenotypic response is due to the target in question. If the negative control is active in the phenotypic assay, the response is likely due to an off target. Given its modest CK2 activity in the nanoBRET assay, narrow selectivity profile, and structural similarity to **24**, **26** was chosen as a chemical starting point from which to synthesize a negative control. To convert **26** to a structurally similar negative control, we methylated the aniline that connects the 5-position of the pyrazolopyrimidine core to the aryl side chain as well as the 7-position pyrazolopyrimidine aniline bearing a cyclopropyl ring. These methylations were designed to interrupt key interactions between the pyrazolopyrimidine scaffold and the CK2 ATP binding site, thus abolishing binding affinity. As shown in Scheme S1, **26** was globally methylated using methyl iodide, the various products were separated, and structural assignments made via spectroscopy. Compound **32** was profiled to determine both its kinome-wide selectivity and cellular target engagement of CK2α′. Based on no inhibition of any kinases >80% at 1 μM and no cellular activity in the CK2α′ nanoBRET assay up to 10 μM, **32** (SGC-CK2-1N) was chosen as the negative control: a structurally related compound that lacks CK2 affinity. In addition to a lack of cellular activity, **32** was also found to be devoid of CK2α and CK2α′ potency in the corresponding enzymatic assays (Table 2).

SGC-CK2-1 assumes a canonical ATP-competitive binding mode

The CK2-targeting pyrazolopyrimidines from which our non-exemplified compounds were designed bind in the ATP site of CK2. X-ray crystallographic structures have been reported for **15**, **17**, and **22** (Dowling et al., 2016). To determine how our compounds bind relative to these, we solved structures corresponding to compounds **24** and **29**. Compound **24** (SGC-CK2-1) was chosen since it was the nominated chemical probe, while compound **29** represents a structurally different inhibitor with good kinome-wide selectivity and potency in the CK2α and CK2α′ nanoBRET assays. Through solving the structures of diverse compounds, we hoped to maximize our information learned about the plasticity of the CK2 ATP binding pocket. As shown in Figures 3A and 3B, compounds **24** and **29**, similar to **15**, **17**, and **22**, act as type I kinase inhibitors and occupy the ATP pocket exclusively. All compounds adopt nearly identical orientations and make similar interactions. In agreement with previously solved structures, the backbone of H115 and V116 in the hinge makes key hydrogen bonds with the pyrazolopyrimidine core and 7-cyclopropylamine. The 3-carbonitrile interacts via a water molecule with a network of hydrogen bonds that includes the oxygen and nitrogen of the propionamide in **24** and the acetamide in **15**, **17**, **22**, and **29**. Our structures show that key interactions are made with the DWG (D, aspartic acid, W, tryptophan, and G, glycine)-motif (D175), αC helix (E81), and K68 as part of this hydrogen bond network. These structures also support that the methyl groups on negative control **32** likely disrupt a hydrogen bond with V116 in the hinge

Table 2. Potency and selectivity of CK2-targeting pyrazolopyrimidines

Cmpd	S_{10}(1 μM)	# kinases >90%I at 1 μM	CK2α NB IC_{50} (nM)	CK2α' NB IC_{50} (nM)	Wild-type kinases >90%I at 1 μM (%I)	Enzymatic IC_{50} values (nM)	Wild-type kinases >35%I at 1 μM (%I)	Off-target IC_{50} or enzymatic assay values (nM)
17	0.042	17	5.3	4.4	Figure S2	NT[a]		
15	0.02	8	2.7	1.3	Figure S2	NT[a]		
16	0.012	5	15	7.6	Figure S2	NT[a]		
22	0.032	13	3.2	1.8	Figure S2	NT[a]		
29	0.015	6	11	3.9	Figure S2	NT[a]		
31	0.027	11	94	20	Figure S2	NT[a]		
18	0.025	10	3.3	2.6	Figure S2	NT[a]		
19	0.025	10	67	15	Figure S2	NT[a]		
20	0.005	2	280	130	CSNK2A2 (100) CSNK2A1 (96.7)	CSNK2A2: 94 CSNK2A1: 91		
24	0.007	3	36	16	CSNK2A2 (100) DRAK1 (100) CSNK2A1 (99.5)	CSNK2A2: 2.3 DRAK1: >10,000 CSNK2A1: 4.2	DYRK2 (86) PLK4 (77) HIPK2 (74) MEK5 (72) HIPK1 (68) HIPK3 (66)	DYRK2: 440 PLK4: >10,000 HIPK2: 3400 MEK5: 0%I at 1μM HIPK1: 3,700 HIPK3: 8,100
26	0.002	1	7,700	2,700	CSNK2A2 (100)	CSNK2A2: 120	CSNK2A1 (80) SGK1 (68) SGK3 (67)	CSNK2A1: 150 SGK1: >10,000 SGK3: >10,000
27	0.007	3	2,200	1,000	CSNK2A2 (99.3) CLK2 (97.6) PHKG2 (95.6)	CSNK2A2: 240 CLK2: 2995 PHKG2: >10,000	CAMK2A (84) SGK1 (73) CHEK2 (72) BLK (67) DAPK3 (66) SGK3 (65) DYRK2 (63)	CAMK2A: >10,000 SGK1: 3,600 CHEK2: >10,000 BLK: >10,000 DAPK3: >10,000 SGK3: >10,000 DYRK2: 720
32	0.00	0	NT	>10,000	None >90% CSNK2A2 (35) CSNK2A1 (0)	CSNK2A1: >10,000 CSNK2A2: >10,000		
CX-4945	0.069	28	340	45	Figure S1	NT[a]		

[a]NT: compound not tested.

region of the ATP binding pocket as well as change the binding orientation due to steric clash with the ATP site in the region of M168 such that other key interactions cannot be maintained. In Figure 3A, the pyrazolopyrimidine core and pendant aryl ring are co-planar. The addition of a methyl group is proposed to rotate the aryl ring such that the two rings will not maintain co-planarity, thus preventing many key hydrogen interactions from being made with aryl ring substituents.

Selective CK2 inhibition results in narrow antiproliferative activity in cancer cell lines

Multiple studies link CK2 inhibition to a reduction of proliferation for a range of cancer cells. We wanted to see if the antiproliferative activity held for our non-exemplified compounds, especially SGC-CK2-1, which has enhanced selectivity. Our working hypothesis was that a narrower set of cell lines would be responsive to a more selective compound and highlight true dependencies on CK2. Based upon reports that the previously exemplified pyrazolopyrimidines in our library inhibited the growth of HCT-116 colorectal carcinoma cells and that **17** exhibited a high level of activity as a monotherapy in HCT-116 xenografts (Dowling et al., 2016),

we evaluated the antiproliferative activity of our entire library in this colon cancer cell line. Table S2 shows the previously reported cytotoxicity data in HCT-116 cells alongside the data we collected following 72 h of continuous treatment. Compounds that had previously been reported as cell growth inhibitors demonstrated antiproliferative activity in our hands as well. This was also true of the non-selective CK2 inhibitor CX-4945 (Pierre et al., 2011). Our non-exemplified analogs (**18**, **19**, **20**, **24**, **26**, and **27**) showed variable growth inhibition. Our negative control (**32**) did not demonstrate antiproliferative activity. Remarkably, the most selective compounds, **20**, **24**, **26**, and **27**, demonstrated no antiproliferative activity in this assay.

Driven by our findings with respect to HCT-116 proliferation, we expanded our exploration of the antiproliferative activity of the chemical probe **24**. CK2 inhibition has been linked with suppressing glioblastoma invasiveness as well as pro-survival signaling pathways and growth (Pencheva et al., 2017; Zheng et al., 2013). As these published studies employed U-87 MG cells, we tested the antiproliferative activity of **24** in this glioblastoma cell line after 72 h of continuous compound treatment. As was observed in HCT-116 cells, **24** demonstrated no antiproliferative
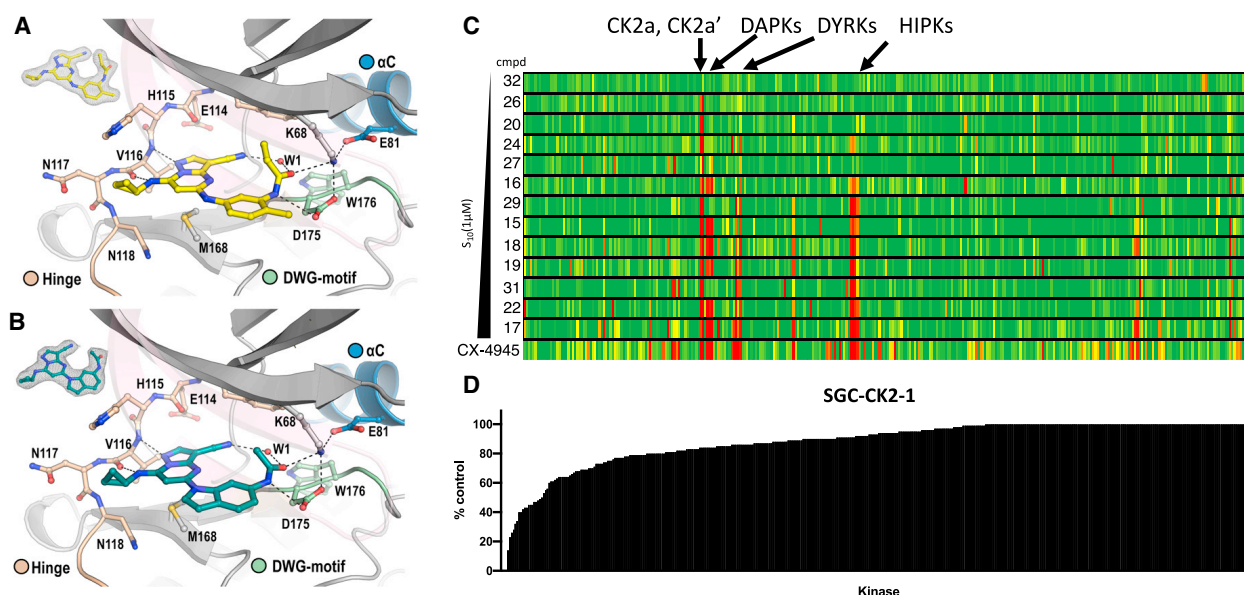
Figure 3. X-ray crystallographic structure of human CK2α in complex with pyrazolopyrimidines and kinome-wide selectivity of the library
(A) and (B) **24** (A, PDB: 6Z83) is shown in yellow and **29** (B, PDB: 6Z84) in teal stick representation, respectively. The hinge region is colored brown, the αC helix blue, the DWG motif green, and water molecules are shown as red spheres. The pink P loop was made transparent for better view of the interaction. Hydrogen bonds are indicated as black dashed lines. The insert on the upper left corner of each panel shows the electron density map ($2F_o{-}F_c$) of the bound ligand contoured at 1σ.
(C) Heatmap of kinome-wide selectivity of all analogs and CX-4945, ranked from most (top) to least (bottom) selective, when profiled against 403 wild-type kinases at 1 μM in the DiscoverX scanMAX platform.
(D) Kinome-wide selectivity of SGC-CK2-1 (**24**) displayed as % control and ranked from most (left) to least (right) inhibited when profiled against 403 wild-type kinases at 1 μM in the DiscoverX scanMAX platform.

activity when tested up to a concentration of 10 μM. We also investigated whether **24** could activate caspase 3/7 in U-87 MG cells (Rahnel et al., 2017). At multiple time points, no caspase 3/7 activation was observed when tested up to a concentration of 10 μM.

Motivated by the lack of antiproliferative activity of SGC-CK2-1 (**24**) in HCT-116 and U-87 MG cells, we opted to further profile this compound in multiple large panels of cancer cell lines (Figure 4). We profiled **24** against 140 cancer cell lines in eight-point dose-response. Remarkably, we found that **24** only inhibited cell proliferation below 500 nM in one cell line, a pro-monocytic, human histiocytic lymphoma line U-937 (Figures 4A and 4B). Figure 4C and Table S3 contain antiproliferative results for all 140 cell lines tested. In parallel, we profiled SGC-CK2-1 (**24**) and SGC-CK2-1N (**32**) using the NCI60 panel at 10 μM (Figures 4E–4H) (Shoemaker, 2006). As shown in Figure 4D and Table S3, 23 cell lines are shared in common between the 140 and NCI60 panels. We profiled SGC-CK2-1 in 176 distinct cancer cell lines in total. SGC-CK2-1 elicited minor lethality (8%–22%) in A498, HS 578T, RXF 393, and SNB-75 cells and inhibited growth >90% in an additional six cell lines at the single 10 μM dose (Figures 4E and 4F). SGC-CK2-1N was devoid of significant antiproliferative activity (Figures 4G and 4H).

SGC-CK2-1 potently modulates downstream cellular activity

With a chemical probe in hand that possesses exquisite kinase selectivity, binds to CK2 in cells, and does not elicit widespread

antiproliferative activity, we sought to verify that this target engagement with CK2 leads to the expected inhibition of downstream phosphorylation events mediated by CK2. To explore the impact of SGC-CK2-1 (**24**) on known downstream CK2 targets we treated HCT-116 cells in dose-response for either 3 h or 24 h. We opted to use HCT-116 cells since they had been used previously in exploring downstream phosphorylation in response to pyrazolopyrimidine-based CK2 inhibitors and to probe whether CK2 is inhibited in these cells despite the lack of evidence of any antiproliferative activity when treated with of SGC-CK2-1 (**24**) (Dowling et al., 2016). CK2 has been shown to phosphorylate AKT at serine 129 (S129), leading to multiple direct and indirect consequences, and phosphorylation at this site has been used to confirm CK2 is active (Di Maira et al., 2005; Girardi and Ruzzene, 2015; Zanin et al., 2012). As shown in Figures 5A and 5B, we observed a dose-dependent decrease in AKT S129 phosphorylation due to treatment of HCT-116 cells at both time points, confirming that CK2 inhibition by **24** results in disruption of its downstream signaling inside the cell. This finding is in alignment with previously reported CK2 inhibitors.

Additional studies targeted at studying CK2 downstream signaling were performed using EIF2S2, a known substrate and interacting partner for CK2, as a biomarker for CK2 inhibition (Llorens et al., 2003). These analyses were performed using human osteosarcoma (U2OS) cells engineered to express wild-type CK2α or a double mutant of CK2α (designated DM, harboring V66A/I174A substitutions) under the control of tetracycline. Both wild-type and DM CK2α incorporate HA epitope tags
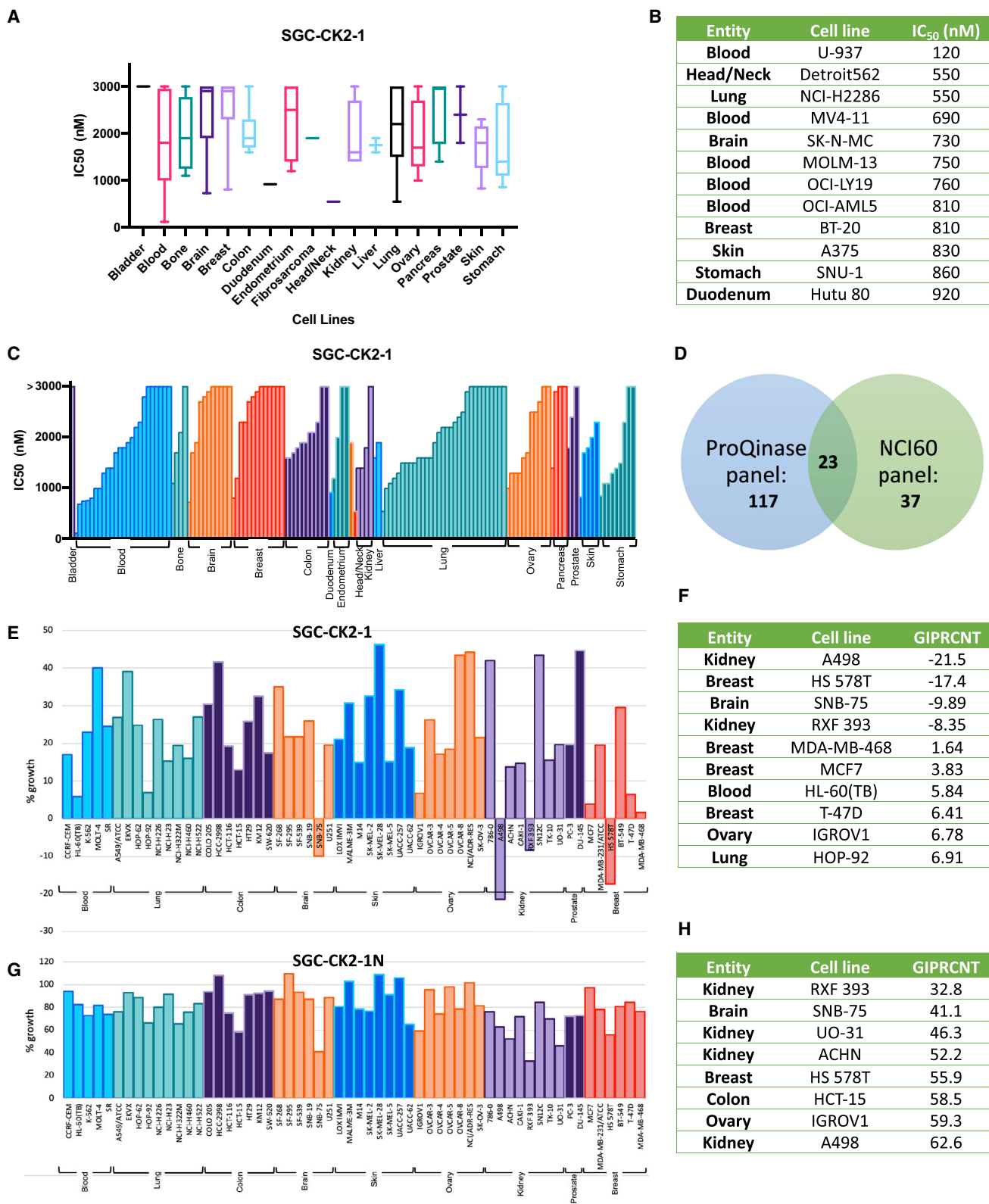
Figure 4. SGC-CK2-1 (24) evaluated for antiproliferative activity

(A) Potency data for 140 cell lines grouped by origin.

(B) Growth inhibited cell lines within 140 panel with an IC$_{50}$ value < 1 μM.
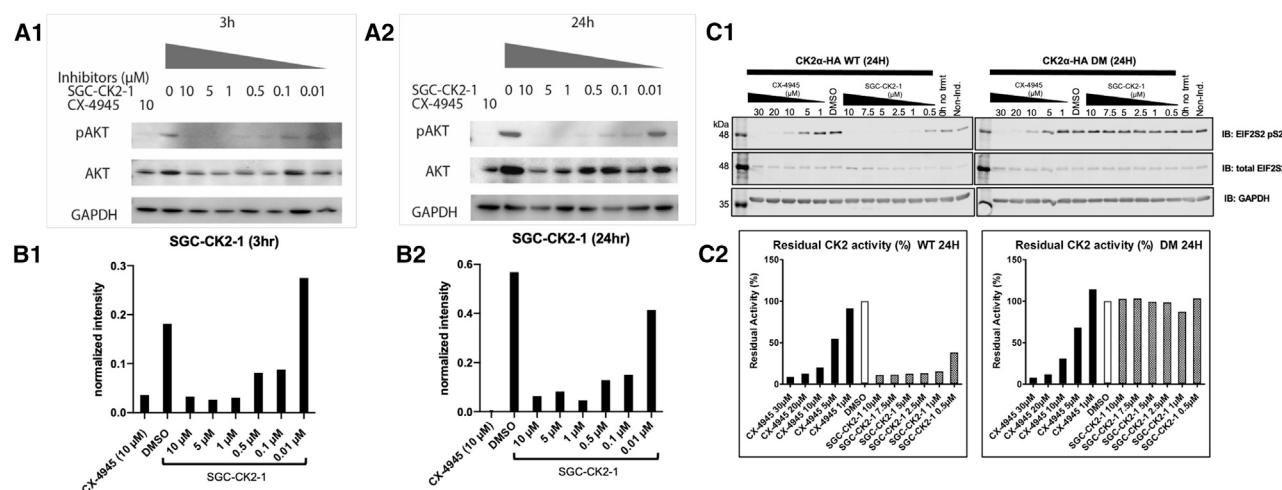
Figure 5. Western blot analysis and quantification in response to SGC-CK2-1 (24)

(A) Western blot for HCT-116 cell protein extracts (20 μg) treated with decreasing doses of SGC-CK2-1 and CX-4945 as positive control (from left to right: CX-4945 10 μM, DMSO 0.1%, SGC-CK2-1 10 μM, 5 μM, 1 μM, 0.5 μM, 0.1 μM, and 0.01 μM). The inhibition of phosphorylated AKT (S129) and AKT1 was analyzed after 3 h (A1) and 24 h (A2) of inhibitor treatment. Glyceraldehyde-3-phosphate dehydrogenase (GAPDH) was used as a loading control.

(B) Intensity levels of phosphorylated AKT (S129) normalized against GAPDH loading control of western blot analysis after 3 h (B1) and 24 h (B2) of compound treatment.

(C) Phosphorylation of EIF2S2 in FT-U2OS cells expressing wild-type (WT) or DM, V66A/I174A CK2α. Expression of exogenous CK2α was induced with tetracycline for 48 h and cells were then treated for 24 h with decreasing doses of CX-4945 or SGC-CK2-1: CX-4945 (30, 20, 10, 5, 1 μM), SGC-CK2-1 (10, 7.5, 5, 2.5, 1, 0.5 μM). As controls, cells were also subjected to treatment with DMSO (vehicle control) or were analyzed either without induction of exogenous CK2α or without any treatment as indicated. (C1) Phosphorylation of EIF2S2 was assessed by immunoblot analysis (top panels) together with analysis of total levels of EIF2S2 (middle panels) and GAPDH (bottom panels) as loading controls. (C2) Residual CK2 activity reflects phosphorylation of EIF2S2 expressed as the percentage of the level of phosphorylation detected in the absence of the inhibitor.

to enable detection. Mutations in the DM (V66A/I174A) are within the ATP binding site and abolish binding of high-affinity type I inhibitors. While dose-dependent inhibition of EIF2S2 pS2 was observed in the case of wild-type CK2α-HA, SGC-CK2-1 did not affect phosphorylation of EIF2S2 in the cells harboring the DM CK2α-HA (Figure 5C). This is in contrast to CX-4945, which exhibited dose-dependent inhibition of EIF2S2 pS2 in cells with wild-type and DM CK2α-HA. Of note, SGC-CK2-1 demonstrated robust inhibition of CK2 and its downstream signaling at a concentration at least 10× less than CX-4945.

DISCUSSION

While it was anticipated that the minor structural changes to the pyrazolopyrimidine lead structure would result in compounds of similar potency and selectivity to their progenitors, analogs with more significant structural changes were designed to probe the pocket and determine which interactions were favorable and what changes might lead to enhanced selectivity. Comparison of the CK2 nanoBRET data corresponding with analogs **19** and **20** with that generated for analogs **15–18**, **22**, and **24** confirm that the portion of the binding pocket that accommodates the

morpholine (**19**) or benzylamine (**20**) is also sensitive to changes in steric bulk. While the other analogs bear a methyl or alkyldiamine group, incorporation of the bulkier morpholine and especially the benzylamine results in significant loss in CK2 cellular target engagement. These data support that cyclic side chains at this position do not increase affinity for CK2.

An interesting observation was made in examining the structures of **22**, **24**, and **26** and their corresponding biological data. While the difference in structures is only a methyl group (acetamide in **22** and propionamide in **24**), **24** inhibits considerably fewer off-target kinases than **22**. This finding is supported by our follow-up data in Table 2 for **24**, and the data provided in the original publication for **22**. CK2, DYRK1–3, HIPK1–3, and DAPK1–3 were all inhibited with residual activity <45% at 0.1 μM, supporting our finding that **22** is less selective than **24** (Dowling et al., 2013). While our X-ray crystallography structures of **24** and **29**, like those solved for other pyrazolopyrimidines, support that the CK2α ATP pocket has space to accommodate the homologated amide, it appears that other kinases may not be as tolerant. This part of the CK2α pocket is only moderately tolerant, as there is a 10-fold loss in CKα cellular target engagement in moving from **22** to **24** and a significant 200-fold loss in

(C) Proliferation data as IC$_{50}$ values for all 140 cancer cell lines profiled.

(D) Overlapping cell lines in antiproliferative panels.

(E) NCI60 results for SCG-CK2-1 when tested at 10 μM. Bars above zero indicate growth inhibition, while bars below zero indicate lethality.

(F) Cell lines with growth inhibited percentage (GIPRCNT) < 10 when treated with 10 μM SGC-CK2-1.

(G) NCI60 results for SCG-CK2-1N when tested at 10 μM. All bars reflect growth inhibition.

(H) Cell lines with GIPRCNT < 65 when treated with 10 μM SGC-CK2-1N.

moving from **24** to **26**. So changing from acetamide to propiona-mide to cyclopropanecarboxamide, while subtly different in structure, results in significantly reduced CK2 cellular target engagement as well as number of kinases inhibited in broad profiling (S_{10} score, Table 2). We propose that modifying this part of the pyrazolopyrimidine scaffold and/or accessing this part of the ATP binding site may be key to building in selectivity for CK2 versus other kinases.

The exquisite selectivity of **24** for CK2 was explored from a structural perspective. CK2 shares closest structural homology with the DYRKs, HIPKs, CLKs, and SPRKs within the CMGC subfamily. The main differences between CK2 and DYRK family members are in the hinge (H115 in CK2α or Y116 in CK2α′ versus M/L in DYRKs) and key hydrophobic contact in β-sheet 7 (M163 in CK2α or M164 in CK2α′ versus L/V in DYRKs). We hypothesize that the larger xDFG/pre-DFG residue (I174 for CK2α or I175 for CK2α′ versus V for DYRK1A/B) also contributes to better binding to CK2, a strategy that has been used by others in the field to impart selectivity (Martin et al., 2012; Rudolph et al., 2015; Schröder et al., 2020; Tong et al., 2013). This hypothesis is further supported by our studies with DM CK2α (Figure 5C), in which I174 is mutated to A174. Since critical interactions with V66 are not observed (Figures 3 and S6), the I174A mutation seems responsible for obliteration of SGC-CK2-1 binding to CK2α, demonstrating the sensitivity of SGC-CK2-1 to subtle changes in the CK2α ATP binding site. The overlay of **24** bound to CK2 versus DYRK2 and DYRK1A (Figure S6) shows improved hydrophobic contacts in the case of CK2. It is also interesting to note that we do not observe any CLK family inhibition despite their high structural homology. CLK family kinases are often an off target of CK2 inhibitors, including CX-4945.

We found that the most selective compounds, **20**, **24**, **26**, and **27**, demonstrated no antiproliferative activity in our HCT-116 antiproliferation assay. Since these compounds were found to only inhibit CK2α and CK2α′, a working hypothesis is that the antiproliferative activity exhibited by less selective compounds was likely due to inhibition of an off-target kinase or combination of kinases and not due solely to inhibition of CK2. From examina-tion of the inhibition profiles of the most potent inhibitors of pro-liferation in HCT-116 cells, **15**, **17**, **18**, and **22**, potent inhibition (>80%I) of DAPK1–3, DYRK2, HIPK1–3, and RPS6KA4 at 1 μM in the DiscoverX binding assay emerged (Figure S5). Our follow-up K_d determinations at DiscoverX for **17** confirmed that it potently inhibits all of these kinases with values <8 nM. Com-pounds **20**, **24**, **26**, **27**, and **32** were devoid of activity for these same kinases (<50%I for most) at 1 μM in the DiscoverX binding assay, while the remainder of compounds tested showed less consistent potent inhibition of these same kinases. We followed up on off-target kinases potently inhibited in the DiscoverX panel using the corresponding enzymatic assays run at the K_m of ATP for the compounds that inhibit proliferation of HCT-116 cells (**15**, **17**, **18**, and **22**). Although the binding data implicate several ki-nases, published and collected enzymatic data point to inhibition of DAPKs as driving the antiproliferative activity (Figure S5) (Dowling et al., 2016). The most potent antiproliferative agents in the series (**17** and **18**) demonstrate significant inhibition of both DAPK2 and DAPK3 in addition to CK2 (IC$_{50}$ values <130 nM). Antiproliferative activity is reduced with less potent in-hibition of DAPK2 and/or DAPK3 by **15** and especially **22**. The

DAPK family has been reported to have effects on cell proliferation (Elbadawy et al., 2018). Furthermore, dual DAPK1 and DAPK3 inhibition has been shown to result in HCT-116 apoptosis (Elbadawy et al., 2018; Farag and Roh, 2019). We hypothesize that inhibiting a combination of DAPK1–3 and CK2 may be causing the antiproliferative effects that we are observing with our most potent growth inhibitors (**15**, **17**, **18**, and **22**).

Anti-tumor drugs are known to display different anti-prolifera-tive efficacy depending on the cell lines used in the assay. We have shown that SGC-CK2-1 (**24**) does not demonstrate signifi-cant antiproliferative activity against a panel of 140 different cancer cell lines originating from 18 different locations within the body. The most sensitive cell line, U937, is a human myeloid leukemia cell line. An association between CK2 inhibition and leukemia has been previously reported, with higher expression levels of CK2 being associated with a poorer prognosis (Kim et al., 2007). It was gratifying to see no significant antiproliferative activity elicited by SGC-CK2-1N in the NCI60 panel. Cell lines that demonstrated some lethality in response to SGC-CK2-1 in the NCI60 panel include one brain cancer cell line (SNB-75), two kidney cell lines (A498 and RXF 393), and one breast cancer cell line (HS 578T). Of note, two of these four were the most in-hibited (>58%I, Figure 4H) cell lines by SGC-CK2-1N (SNB-75 and RXF 393), so there is clearly some sensitivity to the scaffold that is not related to CK2 inhibition. A498 cells were also included in the 140-cell line panel. While an IC$_{50}$ = 1.8 μM was determined for growth inhibition in these cells in the larger panel study, 10 μM SGC-CK2-1 induced some cell death. The last cell line that demonstrated lethality in response to SGC-CK2-1 (HS 578T) is a breast cancer cell line that has been shown to overexpress CK2 and depend on CK2 for its survival (Romieu-Mourez et al., 2001, 2002). Other cancer cell lines in common between the two panels that demonstrated >93% growth inhibition in response to 10 μM SGC-CK2-1 include HL-60, MCF7, MDA-MB-468, and T-47D (IC$_{50}$ values 1.2–2.8 μM). Generally, we found leukemia (HL-60 and U937) and breast (MCF7, MDA-MB-468, T-47D, and HS 578T) cancer cells to be most respon-sive to our chemical probe in terms of proliferation.

In general, we found no correlation between CK2 expression and sensitivity of a particular cell line to our chemical probe. One hypothesis that could explain why our compound does not affect proliferation in nearly all of these diverse hyperprolifer-ating cell lines is that they have evolved to shunt around CK2 control of processes such as DNA damage repair and p53 acti-vation (Rabalski et al., 2016). One reported role of CK2 is DNA damage cell cycle checkpoint control, while another related role is regulation of p53 function (McKendrick et al., 1999; Mon-tenarh, 2016). If cancer cells are able to circumvent these regu-latory pathways to promote their survival and growth, they become less sensitive to CK2 inhibition. Subcellular localization of CK2 has also been described as key to its function and certain sub-populations may be more critical for survival/viability, add-ing another layer of complexity to CK2 biology (Faust and Mon-tenarh, 2000).

Using the same experimental context (same cell line and same dose range), we confirmed the inability of SGC-CK2-1 (**24**) to counteract proliferation of HCT-116 cells despite suppression of endogenous CK2 activity. While the literature strongly supports that CK2 drives proliferation and oncogenesis as a

pro-survival protein kinase overexpressed in cancer (Chua et al., 2017; Di Maira et al., 2019; Trembley et al., 2009), our results challenge this paradigm. The use of CK2 inhibitors with suboptimal kinome-wide selectivity has added to this notion, through ascribing results to CK2 that are likely due to off-target kinase inhibition. Our studies have demonstrated that SGC-CK2-1 is more selective and potent in cellular target engagement as well as inhibition of downstream signaling elicited by CK2α (generally the predominant catalytic subunit of CK2) than CX-4945 and that it lacks the antiproliferative effects that have been reported for CX-4945 and have motivated its use in clinical trials for multiple oncological indications (Chon et al., 2015; Eroglu et al., 2020; Siddiqui-Jain et al., 2010; Zakharia et al., 2019). While inhibition of CK2α by either SGC-CK2-1 or CX-4945 can be prevented by expression of a V66A/I174A DM of CK2α, phosphorylation is recovered (or inhibition is prevented) nearly completely by SGC-CK2-1. These experiments demonstrate that SGC-CK2-1 more efficiently inhibits CK2 than CX-4945, as a 10 times lower concentration is required to elicit the same response. That inhibition by SGC-CK2-1 is more effectively prevented with the CK2 mutant supports that SGC-CK2-1 yields a much "cleaner" analysis of CK2-dependent effects within cells. Reduction of CK2 activity via knockout of CK2α has been found to significantly enhance the cytotoxicity of approved chemotherapeutics so a combination strategy may prove fruitful when using SGC-CK2-1 in a cancer context (Di Maira et al., 2019).

In addition to its potential applications in deciphering the biological roles of CK2 at the cellular level, a highly selective probe for CK2 may also have important implications related to CK2 as a potential therapeutic target. For example, CK2 is highly expressed in the brain and has been implicated in the molecular pathology of neurodegenerative diseases (Castello et al., 2017). The non-toxic nature our selective CK2 probe suggests that CK2 inhibition could be a viable approach for treating disorders of the brain. Roles for CK1 and CK2 have recently been discovered in the molecular pathology of different neurodegenerative disorders, such as Alzheimer disease (AD), Parkinson disease (PD), amyotrophic lateral sclerosis (ALS), and frontotemporal dementia (FTD) (Perez et al., 2011). CK2 has been shown to be involved in the neuroinflammatory response in AD mediated by astrocytes, to co-localize with α-synuclein in Lewy bodies in PD patient brains, and to contribute to the formation of TDP-43 aggregates in ALS and FTD (Hasegawa et al., 2008; Rosenberger et al., 2016; Ryu et al., 2008). In addition, the recent finding that host cell CK2 activity is hijacked by SARS-CoV-2 indicates that a non-toxic inhibitor of CK2 could be a valuable antiviral agent (Bouhaddou et al., 2020). Overall, the identification of specific, non-toxic inhibitors of CK2, like SGC-CK2-1, could represent a therapeutic option to treat neurodegenerative diseases and viral infections.

SIGNIFICANCE

We have described the design, synthesis, and biological evaluation of a series of pyrazolopyrimidines as selective inhibitors of CK2α and CK2α′. We have demonstrated that our probe is CK2 active using three orthogonal assay formats: binding assay at DiscoverX, radiometric enzyme assay at Eurofins, and nanoBRET cellular target engagement assays.

Compound 24 (SGC-CK2-1) emerged as our chemical probe candidate. This compound outperforms all published inhibitors in terms of kinome-wide selectivity. When combined with its potent cellular activity and confirmed inhibition of downstream CK2 signaling, our chemical probe represents a high-quality tool to interrogate CK2 biology. Importantly, this confirmed inhibitor of CK2 does not elicit significant antiproliferative activity when broadly profiled. This is in stark contrast to widely studied and less selective inhibitors of CK2 and opens the door to exploring the roles of CK2 beyond oncology, such as in the areas of neuroscience and virology. With so many putative substrates, CK2 is clearly a pleiotropic kinase. Additional studies aided by this chemical probe and the negative control are underway that aim to deconvolute CK2 biology and refine its roles in key disease-propagating pathways.

STAR★METHODS

Detailed methods are provided in the online version of this paper and include the following:

- KEY RESOURCES TABLE
- RESOURCE AVAILABILITY
  - Lead Contact
  - Materials Availability
  - Data and Code Availability
- EXPERIMENTAL MODEL AND SUBJECT DETAILS
  - Cell lines
- METHOD DETAILS
  - General information for chemical synthesis
  - Kinome screening
  - *In vitro* kinase radiometric kinaseprofiler and LANCE assays
  - NanoBRET measurements
  - HCT-116 and U-87 MG 72hr AlamarBlue cell proliferation assay
  - Caspase-Glo 3/7 assay
  - ProQinase broad tumor cell line profiling
  - NCI60 profiling
  - HCT-116 western blot analyses
  - U2OS western blot analyses
  - Crystallography Methods
- QUANTIFICATION AND STATISTICAL ANALYSIS
  - Statistical analysis
- ADDITIONAL RESOURCES

SUPPLEMENTAL INFORMATION

Supplemental information can be found online at https://doi.org/10.1016/j.chembiol.2020.12.013.

AUTHOR CONTRIBUTIONS

Conceptualization, C.I.W., D.H.D., and A.D.A.; Validation, C.I.W., S.K., L.G., D.W.L., and A.D.A.; Formal Analysis, C.I.W., A.K., and L.G.; Investigation, C.I.W., J.E.P., A.T., A.K., D.M., L.G., and A.D.A.; Resources C.I.W., S.K., D.W.L., and A.D.A.; Writing – Original Draft, C.I.W. and A.D.A.; Writing – Review & Editing, all authors; Visualization, C.I.W., A.T., A.K., L.G., and A.D.A.; Supervision, C.I.W., S.M., S.K., L.G., D.W.L., and A.D.A.; Project Administration, A.D.A.; Funding Acquisition, A.D.A.

DECLARATION OF INTERESTS

The authors declare no competing interests.

REFERENCES

Ahmed, K., Gerber, D.A., and Cochet, C. (2002). Joining the cell survival squad: an emerging role for protein kinase CK2. Trends Cell Biol. 12, 226–230.

Ardito, F., Giuliani, M., Perrone, D., Troiano, G., and Lo Muzio, L. (2017). The crucial role of protein phosphorylation in cell signaling and its use as targeted therapy. Int J. Mol. Med. 40, 271–280.

Asquith, C.R.M., Berger, B.-T., Wan, J., Bennett, J.M., Capuzzi, S.J., Crona, D.J., Drewry, D.H., East, M.P., Elkins, J.M., Fedorov, O., et al. (2019). SGC-GAK-1: a chemical probe for cyclin G associated kinase (GAK). J. Med. Chem. 62, 2830–2836.

Banerjee, S., Wei, T., Wang, J., Lee, J.J., Gutierrez, H.L., Chapman, O., Wiley, S.E., Mayfield, J.E., Tandon, V., Juarez, E.F., et al. (2019). Inhibition of dual-specificity tyrosine phosphorylation-regulated kinase 2 perturbs 26S proteasome-addicted neoplastic progression. Proc. Natl. Acad. Sci. U S A 116, 24881–24891.

Battistutta, R., Cozza, G., Pierre, F., Papinutto, E., Lolli, G., Sarno, S., O'Brien, S.E., Siddiqui-Jain, A., Haddach, M., Anderes, K., et al. (2011). Unprecedented selectivity and structural determinants of a new class of protein kinase CK2 inhibitors in clinical trials for the treatment of cancer. Biochemistry 50, 8478–8488.

Bosc, N., Meyer, C., and Bonnet, P. (2017). The use of novel selectivity metrics in kinase research. BMC Bioinformatics 18, 17.

Bouhaddou, M., Memon, D., Meyer, B., White, K.M., Rezelj, V.V., Correa Marrero, M., Polacco, B.J., Melnyk, J.E., Ulferts, S., Kaake, R.M., et al. (2020). The global phosphorylation landscape of SARS-CoV-2 infection. Cell 182, 685–712.

Castello, J., Ragnauth, A., Friedman, E., and Rebholz, H. (2017). CK2—an emerging target for neurological and psychiatric disorders. Pharmaceuticals 10, 7.

Chon, H.J., Bae, K.J., Lee, Y., and Kim, J. (2015). The casein kinase 2 inhibitor, CX-4945, as an anti-cancer drug in treatment of human hematological malignancies. Front. Pharmacol. 6, 70.

Chua, M.M.J., Ortega, C.E., Sheikh, A., Lee, M., Abdul-Rassoul, H., Hartshorn, K.L., and Dominguez, I. (2017). CK2 in cancer: cellular and biochemical mechanisms and potential therapeutic target. Pharmaceuticals 10, 18.

Chuaqui, C.E., Dowling, J.E., Lyne, P., Pontz, T., and Ye, Q. (2013). 3-cyano-5-arylamino-7-cycloalkylaminopyrrolo[1, 5 -a]pyrimidine derivatives and their use as antitumor agents, WO2013144532A1 (AstraZeneca UK Limited).

Davis, M.I., Hunt, J.P., Herrgard, S., Ciceri, P., Wodicka, L.M., Pallares, G., Hocker, M., Treiber, D.K., and Zarrinkar, P.P. (2011). Comprehensive analysis of kinase inhibitor selectivity. Nat. Biotechnol. 29, 1046–1051.

Di Maira, G., Gentilini, A., Pastore, M., Caligiuri, A., Piombanti, B., Raggi, C., Rovida, E., Lewinska, M., Andersen, J.B., Borgo, C., et al. (2019). The protein kinase CK2 contributes to the malignant phenotype of cholangiocarcinoma cells. Oncogenesis 8, 61.

Di Maira, G., Salvi, M., Arrigoni, G., Marin, O., Sarno, S., Brustolon, F., Pinna, L.A., and Ruzzene, M. (2005). Protein kinase CK2 phosphorylates and upregulates Akt/PKB. Cell Death Differ. 12, 668–677.

Dowling, J.E., Alimzhanov, M., Bao, L., Block, M.H., Chuaqui, C., Cooke, E.L., Denz, C.R., Hird, A., Huang, S., Larsen, N.A., et al. (2013). Structure and property based design of pyrazolo[1,5-a]pyrimidine inhibitors of CK2 kinase with activity in vivo. ACS Med. Chem. Lett. 4, 800–805.

Dowling, J.E., Alimzhanov, M., Bao, L., Chuaqui, C., Denz, C.R., Jenkins, E., Larsen, N.A., Lyne, P.D., Pontz, T., Ye, Q., et al. (2016). Potent and selective CK2 kinase inhibitors with effects on wnt pathway signaling in Vivo. ACS Med. Chem. Lett. 7, 300–305.

Dowling, J.E., Chuaqui, C., Pontz, T.W., Lyne, P.D., Larsen, N.A., Block, M.H., Chen, H., Su, N., Wu, A., Russell, D., et al. (2012). Potent and selective inhibitors of CK2 kinase identified through structure-guided hybridization. ACS Med. Chem. Lett. 3, 278–283.

Elbadawy, M., Usui, T., Yamawaki, H., and Sasaki, K. (2018). Novel functions of death-associated protein kinases through mitogen-activated protein kinase-related signals. Int. J. Mol. Sci. 19, 3031.

Emsley, P., and Cowtan, K. (2004). Coot: model-building tools for molecular graphics. Acta Crystallogr. D Biol. Crystallogr. 60, 2126–2132.

Eroglu, Z., Cowey, C.L., Soong, J., McCormick, D., Fan, P., Chen, J., Elgendy, M., Jang, S., and Chang, A.L.S. (2020). A phase I study of CX-4945 administered orally twice daily to patients with advanced basal cell carcinoma. J. Clin. Oncol. 38, TPS10080.

Farag, A.K., and Roh, E.J. (2019). Death-associated protein kinase (DAPK) family modulators: current and future therapeutic outcomes. Med. Res. Rev. 39, 349–385.

Faust, M., and Montenarh, M. (2000). Subcellular localization of protein kinase CK2. A key to its function? Cell Tissue Res. 301, 329–340.

Gandin, V., Masvidal, L., Cargnello, M., Gyenis, L., McLaughlan, S., Cai, Y., Tenkerian, C., Morita, M., Balanathan, P., Jean-Jean, O., et al. (2016). mTORC1 and CK2 coordinate ternary and eIF4F complex assembly. Nat. Commun. 7, 11127.

Girardi, C., and Ruzzene, M. (2015). CK2 function in the regulation of akt pathway. In Protein Kinase CK2 Cellular Function in Normal and Disease States, vol 12, K. Ahmed, O.G. Issinger, and R. Szyszka, eds. (Springer), pp. 125–140.

Golub, A.G., Bdzhola, V.G., Briukhovetska, N.V., Balanda, A.O., Kukharenko, O.P., Kotey, I.M., Ostrynska, O.V., and Yarmoluk, S.M. (2011). Synthesis and biological evaluation of substituted (thieno[2,3-d]pyrimidin-4-ylthio)carboxylic acids as inhibitors of human protein kinase CK2. Eur. J. Med. Chem. 46, 870–876.

Gowda, C., Sachdev, M., Muthusami, S., Kapadia, M., Petrovic-Dovat, L., Hartman, M., Ding, Y., Song, C., Payne, J.L., Tan, B.H., et al. (2017). Casein

kinase II (CK2) as a therapeutic target for hematological malignancies. Curr. Pharm. Des. 23, 95–107.

Gyenis, L., Duncan, J.S., Turowec, J.P., Bretner, M., and Litchfield, D.W. (2011). Unbiased functional proteomics strategy for protein kinase inhibitor validation and identification of bona fide protein kinase substrates: application to identification of EEF1D as a substrate for CK2. J. Proteome Res. 10, 4887–4901.

Hasegawa, M., Arai, T., Nonaka, T., Kametani, F., Yoshida, M., Hashizume, Y., Beach, T.G., Buratti, E., Baralle, F., Morita, M., et al. (2008). Phosphorylated TDP-43 in frontotemporal lobar degeneration and amyotrophic lateral sclerosis. Ann. Neurol. 64, 60–70.

Haynes, K.A., and Silver, P.A. (2011). Synthetic reversal of epigenetic silencing. J. Biol. Chem. 286, 27176–27182.

Kabsch, W. (2010). Xds. Acta Crystallogr. D Biol. Crystallogr. 66, 125–132.

Kim, H., Choi, K., Kang, H., Lee, S.-Y., Chi, S.-W., Lee, M.-S., Song, J., Im, D., Choi, Y., and Cho, S. (2014). Identification of a novel function of CX-4945 as a splicing regulator. PLoS One 9, e94978.

Kim, H., Lee, K.-S., Kim, A.-K., Choi, M., Choi, K., Kang, M., Chi, S.-W., Lee, M.-S., Lee, J.-S., Lee, S.-Y., et al. (2016). A chemical with proven clinical safety rescues Down-syndrome-related phenotypes in through DYRK1A inhibition. Dis. Model. Mech. 9, 839–848.

Kim, J.S., Eom, J.I., Cheong, J.W., Choi, A.J., Lee, J.K., Yang, W.I., and Min, Y.H. (2007). Protein kinase CK2alpha as an unfavorable prognostic marker and novel therapeutic target in acute myeloid leukemia. Clin. Cancer Res. 13, 1019–1028.

Krämer, A., Kurz, C.G., Berger, B.-T., Celik, I.E., Tjaden, A., Greco, F.A., Knapp, S., and Hanke, T. (2020). Optimization of pyrazolo[1,5-a]pyrimidines lead to the identification of a highly selective casein kinase 2 inhibitor. Eur. J. Med. Chem. 208, 112770.

Lebedev, A.A., Vagin, A.A., and Murshudov, G.N. (2008). Model preparation in MOLREP and examples of model improvement using X-ray data. Acta Crystallogr. D Biol. Crystallogr. 64, 33–39.

Lechner, C., Flasshoff, M., Falke, H., Preu, L., Loaec, N., Meijer, L., Knapp, S., Chaikuad, A., and Kunick, C. (2019). [b]-Annulated halogen-substituted indoles as potential DYRK1A inhibitors. Molecules 24, 4090.

Litchfield, D.W. (2003). Protein kinase CK2: structure, regulation and role in cellular decisions of life and death. Biochem. J. 369, 1–15.

Llorens, F., Roher, N., Miró, F.A., Sarno, S., Ruiz, F.X., Meggio, F., Plana, M., Pinna, L.A., and Itarte, E. (2003). Eukaryotic translation-initiation factor eIF2beta binds to protein kinase CK2: effects on CK2alpha activity. Biochem. J. 375, 623–631.

Lolli, G., Cozza, G., Mazzorana, M., Tibaldi, E., Cesaro, L., Donella-Deana, A., Meggio, F., Venerando, A., Franchin, C., Sarno, S., et al. (2012). Inhibition of protein kinase CK2 by flavonoids and tyrphostins. A structural insight. Biochemistry 51, 6097–6107.

Lozeman, F.J., Litchfield, D.W., Piening, C., Takio, K., Walsh, K.A., and Krebs, E.G. (1990). Isolation and characterization of human cDNA clones encoding the alpha and the alpha' subunits of casein kinase II. Biochemistry 29, 8436–8447.

Martin, M.P., Zhu, J.-Y., Lawrence, H.R., Pireddu, R., Luo, Y., Alam, R., Ozcan, S., Sebti, S.M., Lawrence, N.J., and Schönbrunn, E. (2012). A novel mechanism by which small molecule inhibitors induce the DFG flip in aurora A. ACS Chem. Biol. 7, 698–706.

McKendrick, L., Milne, D., and Meek, D. (1999). Protein kinase CK2-dependent regulation of p53 function: evidence that the phosphorylation status of the serine 386 (CK2) site of p53 is constitutive and stable. Mol. Cell Biochem 191, 187–199.

Meggio, F., and Pinna, L.A. (2003). One-thousand-and-one substrates of protein kinase CK2? FASEB J. 17, 349–368.

Montenarh, M. (2016). Protein kinase CK2 in DNA damage and repair. Transl Cancer Res. 5, 49–63.

Nuñez de Villavicencio-Diaz, T., Rabalski, A.J., and Litchfield, D.W. (2017). Protein kinase CK2: intricate relationships within regulatory cellular networks. Pharmaceuticals 10, 27.

Pagano, M.A., Bain, J., Kazimierczuk, Z., Sarno, S., Ruzzene, M., Di Maira, G., Elliott, M., Orzeszko, A., Cozza, G., Meggio, F., et al. (2008). The selectivity of inhibitors of protein kinase CK2: an update. Biochem. J. 415, 353–365.

Pencheva, N., de Gooijer, M.C., Vis, D.J., Wessels, L.F.A., Wurdinger, T., van Tellingen, O., and Bernards, R. (2017). Identification of a druggable pathway controlling glioblastoma invasiveness. Cell Rep. 20, 48–60.

Perez, D.I., Gil, C., and Martinez, A. (2011). Protein kinases CK1 and CK2 as new targets for neurodegenerative diseases. Med. Res. Rev. 31, 924–954.

Pierre, F., Chua, P.C., O'Brien, S.E., Siddiqui-Jain, A., Bourbon, P., Haddach, M., Michaux, J., Nagasawa, J., Schwaebe, M.K., Stefan, E., et al. (2011). Discovery and SAR of 5-(3-chlorophenylamino)benzo[c][2,6]naphthyridine-8-carboxylic acid (CX-4945), the first clinical stage inhibitor of protein kinase CK2 for the treatment of cancer. J. Med. Chem. 54, 635–654.

Plattner, F., and Bibb, J.A. (2012). Chapter 25 - serine and threonine phosphorylation. In Basic Neurochemistry, Eighth Edition, S.T. Brady, G.J. Siegel, R.W. Albers, and D.L. Price, eds. (Academic Press), pp. 467–492.

Rabalski, A.J., Gyenis, L., and Litchfield, D.W. (2016). Molecular pathways: emergence of protein kinase CK2 (CSNK2) as a potential target to inhibit survival and DNA damage response and repair pathways in cancer cells. Clin. Cancer Res. 22, 2840–2847.

Rahnel, H., Viht, K., Lavogina, D., Mazina, O., Haljasorg, T., Enkvist, E., and Uri, A. (2017). A selective biligand inhibitor of CK2 increases caspase-3 activity in cancer cells and inhibits platelet aggregation. ChemMedChem 12, 1723–1736.

Röhm, S., Krämer, A., and Knapp, S. (2020). Function, structure and topology of protein kinases. In Topics in Medicinal Chemistry (Springer), pp. 1–24.

Romieu-Mourez, R., Landesman-Bollag, E., Seldin, D.C., and Sonenshein, G.E. (2002). Protein kinase CK2 promotes aberrant activation of nuclear factor-κB, transformed phenotype, and survival of breast cancer cells. Cancer Res. 62, 6770–6778.

Romieu-Mourez, R., Landesman-Bollag, E., Seldin, D.C., Traish, A.M., Mercurio, F., and Sonenshein, G.E. (2001). Roles of IKK kinases and protein kinase CK2 in activation of nuclear factor-κb in breast cancer. Cancer Res. 61, 3810–3818.

Rosenberger, A.F.N., Morrema, T.H.J., Gerritsen, W.H., van Haastert, E.S., Snkhchyan, H., Hilhorst, R., Rozemuller, A.J.M., Scheltens, P., van der Vies, S.M., and Hoozemans, J.J.M. (2016). Increased occurrence of protein kinase CK2 in astrocytes in Alzheimer's disease pathology. J. Neuroinflam 13, 4.

Rudolph, J., Aliagas, I., Crawford, J.J., Mathieu, S., Lee, W., Chao, Q., Dong, P., Rouge, L., Wang, W., Heise, C., et al. (2015). Leveraging the pre-DFG residue thr-406 to obtain high kinase selectivity in an aminopyrazole-type PAK1 inhibitor series. ACS Med. Chem. Lett. 6, 711–715.

Ryu, M.Y., Kim, D.W., Arima, K., Mouradian, M.M., Kim, S.U., and Lee, G. (2008). Localization of CKII beta subunits in Lewy bodies of Parkinson's disease. J. Neurol. Sci. 266, 9–12.

Salvi, M., Sarno, S., Cesaro, L., Nakamura, H., and Pinna, L.A. (2009). Extraordinary pleiotropy of protein kinase CK2 revealed by weblogo phosphoproteome analysis. Biochim. Biophys. Acta 1793, 847–859.

Sarno, S., Reddy, H., Meggio, F., Ruzzene, M., Davies, S.P., Donella-Deana, A., Shugar, D., and Pinna, L.A. (2001). Selectivity of 4,5,6,7-tetrabromobenzotriazole, an ATP site-directed inhibitor of protein kinase CK2 ('casein kinase-2'). FEBS Lett. 496, 44–48.

Schröder, M., Bullock, A.N., Fedorov, O., Bracher, F., Chaikuad, A., and Knapp, S. (2020). DFG-1 residue controls inhibitor binding mode and affinity, providing a basis for rational design of kinase inhibitor selectivity. J. Med. Chem. 63, 10224–10234.

Shoemaker, R.H. (2006). The NCI60 human tumour cell line anticancer drug screen. Nat. Rev. Cancer 6, 813–823.

Siddiqui-Jain, A., Drygin, D., Streiner, N., Chua, P., Pierre, F., O'Brien, S.E., Bliesath, J., Omori, M., Huser, N., Ho, C., et al. (2010). CX-4945, an orally bioavailable selective inhibitor of protein kinase CK2, inhibits prosurvival and angiogenic signaling and exhibits antitumor efficacy. Cancer Res. 70, 10288–10298.

Szyszka, R., Grankowski, N., Felczak, K., and Shugar, D. (1995). Halogenated benzimidazoles and benzotriazoles as selective inhibitors of protein-kinases

CK I and CK II from *Saccharomyces cerevisiae* and other sources. Biochem. Biophys. Res. Commun. *208*, 418–424.

Tong, Y., Stewart, K.D., Florjancic, A.S., Harlan, J.E., Merta, P.J., Przytulinska, M., Soni, N., Swinger, K.K., Zhu, H., Johnson, E.F., et al. (2013). Azaindole-based inhibitors of Cdc7 kinase: impact of the pre-DFG residue, val 195. ACS Med. Chem. Lett. *4*, 211–215.

Trembley, J.H., Wang, G., Unger, G., Slaton, J., and Ahmed, K. (2009). Protein kinase CK2 in health and disease: CK2: a key player in cancer biology. Cell Mol. Life Sci. *66*, 1858–1867.

Vagin, A.A., Steiner, R.A., Lebedev, A.A., Potterton, L., McNicholas, S., Long, F., and Murshudov, G.N. (2004). REFMAC5 dictionary: organization of prior chemical knowledge and guidelines for its use. Acta Crystallogr. D Biol. Crystallogr. *60*, 2184–2195.

Vasta, J.D., Corona, C.R., Wilkinson, J., Zimprich, C.A., Hartnett, J.R., Ingold, M.R., Zimmerman, K., Machleidt, T., Kirkland, T.A., Huwiler, K.G., et al. (2017). Quantitative, wide-spectrum kinase profiling in live cells for assessing the effect of cellular ATP on target engagement. Cell Chem. Biol. *25*, 206–214.

Wells, C., Couñago, R.M., Limas, J.C., Almeida, T.L., Cook, J.G., Drewry, D.H., Elkins, J.M., Gileadi, O., Kapadia, N.R., Lorente-Macias, A., et al. (2019). SGC-AAK1-1: a chemical probe targeting AAK1 and BMP2K. ACS Med. Chem. Lett. *11*, 340–345.

Zakharia, K., Miyabe, K., Wang, Y., Wu, D., Moser, C.D., Borad, M.J., and Roberts, L.R. (2019). Preclinical in vitro and in vivo evidence of an antitumor effect of CX-4945, a casein kinase II inhibitor, in cholangiocarcinoma. Transl Oncol. *12*, 143–153.

Zanin, S., Borgo, C., Girardi, C., O'Brien, S.E., Miyata, Y., Pinna, L.A., Donella-Deana, A., and Ruzzene, M. (2012). Effects of the CK2 inhibitors CX-4945 and CX-5011 on drug-resistant cells. PLoS One *7*, e49193.

Zheng, Y., McFarland, B.C., Drygin, D., Yu, H., Bellis, S.L., Kim, H., Bredel, M., and Benveniste, E.N. (2013). Targeting protein kinase CK2 suppresses prosurvival signaling pathways and growth of glioblastoma. Clin. Cancer Res. *19*, 6484–6494.

STAR★METHODS

KEY RESOURCES TABLE

Reagent or Resource	Source	Identifier
Antibodies		
pS129 AKT1	Abcam	Cat# ab133458; RRID: AB_10895993
AKT1	Cell Signaling Technology	Cat 2920; RRID: AB_1147620
GAPDH	Invitrogen	Cat# MA5-15738; RRID: AB_10977387
GAPDH	Millipore	Cat# MAB374; RRID: AB_2107445
EIF2S2 pS2	YenZym	N/A
Total-EIF2S2	Novus	Cat# H00008894-M09; RRID: AB_1236902
IRDye® 800CW Goat anti-Rabbit IgG Secondary Antibody	LICOR	Cat# 926-32211; RRID: AB_621843
IRDye® 680RD Goat anti-Mouse IgG Secondary Antibody	LICOR	Cat# 926-68070; RRID: AB_10956588
Anti-mouse HRP-linked	Cell Signaling Technology	Cat 7076; RRID: AB_330924
Anti-rabbit HRP-linked	Cell Signaling Technology	Cat# 7074; RRID: AB_2099233
Bacterial and Virus Strains		
E. Coli BL21 Rosetta DE3	Novagen	Cat# 70954
Chemicals, Peptides, and Recombinant Proteins		
FuGENE HD	Promega	Cat# E2311
Opti-MEM reduced serum medium, no phenol red	Gibco	Cat# 11058021
Dulbecco's Modified Eagle Medium (DMEM)	Gibco	Cat# 11965
Fetal bovine serum (FBS)	Corning	Cat #35-010-CV
AlamarBlue	Invitrogen	Cat# DAL1100
McCoy's 5A media	Corning	Cat# 10-050-CV
Minimal essential medium (MEM)	Gibco	Cat# 11090-081
DMEM w/ High Glucose and L-Glutamine; w/o Sodium Pyruvate, L-Arg, and L-Lys	Wisent	Cat# 319-119-CL
Premium Dialyzed FBS, US Origin	Wisent	Cat# 080-950
Blasticidin S HCl	Wisent	Cat# 400-190-EM
Hygromycin B	Wisent	Cat# 450-141-IG
Penicillin-Streptomycin	Thermo (Gibco)	Cat# 15140-122
Arginin L-Arginine-HCl (non-labeled)	Sigma-Aldrich	Cat# A4599-100G
L-Lysin-HCl (non-labeled)	Sigma-Aldrich	Cat# L7039-100G
L-Proline	Sigma-Aldrich	Cat# P8865-100G
CX-4945 (Silmitasertib)	MedKoo	Cat# 200843
Dimethyl Sulfoxide	Fisher	Cat# BP231-1
Critical Commercial Assays		
CK2a1 NanoBRET	Promega	Cat# NV2981
CK2a2 NanoBRET	Promega	Cat# NV1191
Caspase-Glo 3/7 Assay System	Promega	Cat# G8090
Deposited Data		
CK2 alpha bound to chemical probe SGC-CK2-1 generated	This paper	6Z83
CK2 alpha bound to chemical probe SGC-CK2-1 derivative generated	This paper	6Z84
DYRK2 crystal structure used in analysis	Banerjee et al., 2019	6K0J

(Continued on next page)

Continued

Reagent or Resource	Source	Identifier
DYRK1A crystal structure used in analysis	Lechner et al., 2019	6T6A
All associated data for SGC-CK2-1 and SGC-CK2-1N	This paper	https://www.thesgc.org/chemical-probes/SGC-CK2-1
Experimental Models: Cell Lines		
HEK-293	ATCC	Cat# CRL-1573
HCT-116	ATCC	Cat# CCL-247
U-87 MG	ATCC	Cat# HTB-14
Flp-In™ T-REx U2OS	(Haynes and Silver, 2011)	N/A
Software and Algorithms		
GraphPad Prism 8.2.0	GraphPad Software, Inc.	http://www.graphpad.com
CCP4 suite (includes used Programs: AIMLESS, REFMAC5, MOLREP and Coot)	Collaborative Computational Project No. 4	https://www.ccp4.ac.uk/
XDS	MPI Heidelberg	http://xds.mpimf-heidelberg.mpg.de/
PYMOL	Schrödinger Inc	https://pymol.org/2/
Image Lab Software 6.1	Bio-Rad	https://www.bio-rad.com/de-de/product/image-lab-software?ID=KRE6P5E8Z

RESOURCE AVAILABILITY

Lead Contact
Further information and requests for resources and reagents should be directed to and will be fulfilled by the Lead Contact, Alison Axtman (alison.axtman@unc.edu).

Materials Availability
SGC-CK2-1 and SGC-CK2-1N can be requested at https://www.thesgc.org/chemical-probes/SGC-CK2-1. All other compounds can be requested through contacting the Lead Contact.

Data and Code Availability
The accession numbers for the crystal structures reported in this paper are PDB: 6Z83 and PDB: 6Z84. Original data have been deposited for SGC-CK2-1 and SGC-CK2-1N to https://www.thesgc.org/chemical-probes/SGC-CK2-1.

EXPERIMENTAL MODEL AND SUBJECT DETAILS

Cell lines
HCT-116
Human colorectal carcinoma cells; diploid; male (adult). Cells were purchased from ATCC and were cultured in McCoy's 5a Medium (Corning) supplemented with 10% fetal bovine serum (FBS, Corning). Cells were incubated in 5% CO_2 at 37C. Cell lines were passaged every 72 hours with trypsin and not allowed to reach confluency.
HEK293
Human embryonic kidney cells; hypotriploid; female (fetal). Cells were purchased from ATCC and grown in Dulbecco's Modified Eagle's medium (DMEM, Gibco) supplemented with 10% (v/v) fetal bovine serum (FBS, Corning). Cells were incubated in 5% CO_2 at 37C. Cell lines were passaged every 72 hours with trypsin and not allowed to reach confluency.
U-87 MG
Human glioblastoma astrocytoma cells; hypodiploid; female. Cells were purchased from ATCC and were cultured in MEM (Gibco) supplemented with 10% FBS (Corning). Cells were incubated in 5% CO_2 at 37C. Cell lines were passaged every 72 hours with trypsin and not allowed to reach confluency.
U2OS
Human osteosarcoma U2OS cells expressing the tetracycline responsible element of Flp-In™ T-REx system (FT-U2OS, gift from Karmella Haynes, Arizona State University, (Haynes and Silver, 2011)) were cultured in Dulbecco's Modified Eagle's medium without sodium pyruvate, L-Arg, and L-Lys (DMEM, Wisent) supplemented with 10% of 10 kDa cut-off fetal bovine serum (Wisent), 100 μg/mL streptomycin, 100 units/mL penicillin (Thermo), 15 μg/mL blasticidin (Wisent), and 150 μg/mL hygromycin

B (Wisent). The cell media was also supplemented with 0.398 mM L-Arg, 0.274 mM L-Lys, and 3.47 mM L-Pro. The cells were grown at 37°C with 5% CO_2 in 10 cm dishes (TPP, FroggaBio) or in 6-well plates (Greiner Bio-One). Following the recommendations of Flp-In™ T-REx cell line development of ThermoFisher Scientific (http://www.thermofisher.com/), we developed cell lines stably expressing the wild-type CSNK2A1-HA (WT) or the inhibitor resistant forms of double mutant (DM, V66A/I174A) of the kinase with tight tetracycline regulation. The exogenous CSNK2A1 has a C-terminal HA tag to be able to distinguish from the endogenous kinase. The cell lines were induced 48h prior to inhibitor treatment with 1 μg/mL tetracycline and were kept induced during the inhibitor treatment. Cells were challenged in two independent experiment with a range of inhibitor concentrations as indicated in the figures.

METHOD DETAILS

General information for chemical synthesis

Reagents were purchased from commercial suppliers and used without further purification. Unless otherwise stated, temperatures are given in degrees Celsius (°C); operations were carried out at room or ambient temperature ("rt" or "RT"), typically a range of from about 18–25°C; evaporation of solvent was carried out using a rotary evaporator under reduced pressure (typically 4.5–30 mm Hg) with a bath temperature of up to 60°C; the course of reactions was typically followed by thin layer chromatography (TLC); products exhibited satisfactory 1H-NMR and/or microanalytical data; and the following conventional abbreviations are also used: L (liters), mL (milliliters), mmol (millimoles), g (grams), mg (milligrams), min (minutes), and h (hours). Reactions were conducted under a blanket of nitrogen unless otherwise stated. Compounds were visualized under UV lamp (254 nM). ^{1}H and ^{13}C NMR spectra were collected in DMSO-d_6, acetonitrile-d_4, chloroform-d, or methanol-d_4 and recorded on Varian Inova 400 or Bruker Avance 300 or 700 MHz spectrometers. Peak positions are given in parts per million (ppm) downfield from tetramethylsilane as the internal standard, in some cases; J values are expressed in hertz. Purity was assessed via analytical HPLC using an Agilent SB- C18 3.5 μm column (150 x 4.6 mm) with a 90%/10% gradient of water (0.02% TFA)/methanol as the mobile phase (flow rate = 0.8 mL/min) monitored at a wavelength of 254 nm at 30°C. Reaction schemes and procedures can be found in Supplemental Information Scheme S1.

15
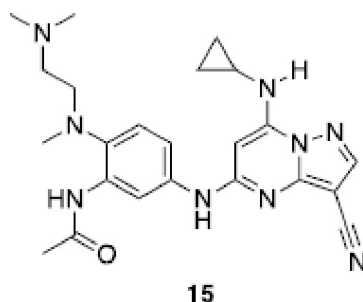
The analytical data for **15** matches that previously reported (Dowling et al., 2016); ^{1}H NMR (300 MHz, methanol-d_4) δ 8.19 (d, J = 2.4 Hz, 1H), 8.08 (s, 1H), 7.77 (m, 1H), 7.25 (d, J = 8.7 Hz, 1H), 6.03 (s, 1H), 3.03 (m, 2H), 2.63 (m, 4H), 2.45 (m, 2H), 2.30 (s, 6H), 2.20 (s, 3H), 0.89 (m, 2H), 0.74 (d, J = 3.9 Hz, 2H); HRMS-ESI (m/z): [M + H]$^+$ calcd for $C_{23}H_{30}N_9O$, 448.26; found 448.35; Purity (HPLC): 95.4%. Appearance: yellow solid.


16
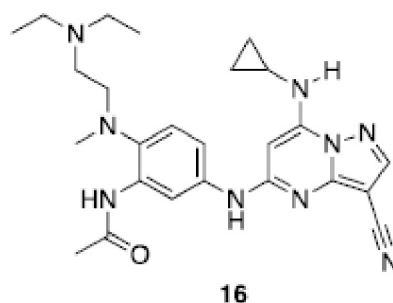
The analytical data for **16** matches that previously reported (Dowling et al., 2016); ^{1}H NMR (300 MHz, chloroform-d) δ 9.78 (s, 1H), 8.37 d, J = 2.1 Hz, 1H), 7.99 (s, 1H), 7.46 (d, J = 7.8 Hz, 1H), 7.24 (m, 1H), 7.05 (s, 1H), 6.33 (s, 1H), 6.02 (s, 1H),

2.87 (t, J = 5.1 Hz, 2H), 2.69 (s, 3H), 2.62 (m, 5H), 2.49 (t, J = 5.1 Hz, 2H), 2.20 (s, 3H), 1.04 (t, J = 7.2 Hz, 6H), 0.94 (d, J = 7.8 Hz, 2H), 0.74 (m, 2H); HRMS-ESI (m/z): [M + H]$^+$ calcd for $C_{25}H_{34}N_9O$, 476.29; found 476.35; Purity (HPLC): 99.1%. Appearance: yellow solid.

17
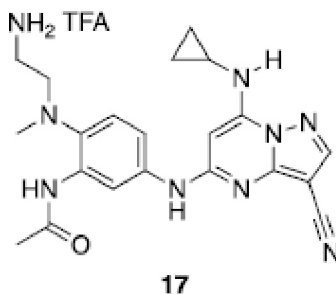
The analytical data for **17** matches that previously reported (Dowling et al., 2016); ^{1}H NMR (300 MHz, methanol-d_4) δ 8.09 (s, 1H), 8.01 (d, J = 2.1 Hz, 1H), 7.82 (d, J = 8.7 Hz, 1H), 7.22 (d, J = 8.7 Hz, 1H), 5.99 (s, 1H), 3.30 (m, 2H), 3.08 (m, 2H), 2.63 (t, J = 3.6 Hz, 4H), 2.23 (s, 3H), 0.90 (m, 2H), 0.74 (m, 2H); HRMS-ESI (m/z): [M + H]$^+$ calcd for $C_{21}H_{26}N_9O$, 420.23; found 420.26; HRMS-ESI (m/z): [M + Na]$^+$ calcd for $C_{21}H_{25}N_9NaO$, 442.21; found 442.21; Purity (HPLC): 95.5%. Appearance: yellow solid.

18
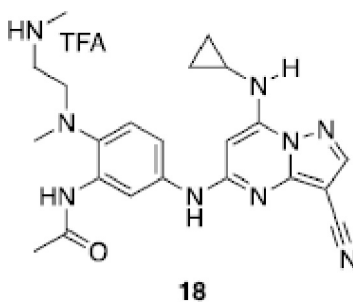
^{1}H NMR (300 MHz, methanol-d_4) δ 8.09 (s, 1H), 7.92 (d, J = 2.4 Hz, 1H), 7.80 (dd, J = 2.4, 6.3 Hz, 1H), 7.23 (d, J = 8.7 Hz, 1H), 5.98 (s, 1H), 3.31 (m, 2H), 3.12 (m, 2H), 2.68 (s, 6H), 2.64 (m, 1H), 2.21 (s, 3H), 0.90 (m, 2H), 0.74 (m, 2H); ^{13}C NMR (176 MHz, DMSO-d_6) δ 168.8, 157.8, 156.9, 150.9, 148.2, 145.0, 137.0, 133.7, 121.8, 115.3, 114.9, 112.6, 76.4, 51.3, 45.6, 42.7, 32.5 (2C), 24.4, 23.3, 6.5 (2C); HRMS-ESI (m/z): [M + H]$^+$ calcd for $C_{22}H_{28}N_9O$, 434.24; found 434.26; Purity (HPLC): 96.3%. Appearance: yellow solid.


19
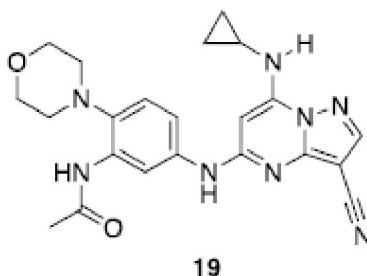
^{1}H NMR (300 MHz, chloroform-d) δ 8.58 (s, 1H), 8.34 (d, J = 2.1 Hz, 1H), 8.00 (s, 1H), 7.54 (d, J = 6.9 Hz, 1H), 7.22 (d, J = 8.7 Hz, 1H), 6.94 (s, 1H), 6.35 (s, 1H), 5.99 (s, 1H), 3.89 (t, J = 4.5 Hz, 4H), 2.89 (t, J = 4.5 Hz, 4H), 2.67 (m, 1H), 2.23 (s, 3H), 0.91 (m, 2H), 0.77 (m, 2H); ^{13}C NMR (176 MHz, DMSO-d_6) δ 168.4, 157.0, 151.0, 148.3, 145.2, 137.4, 136.6, 133.1, 120.5, 115.4, 115.0, 112.9, 76.4,

66.6 (4C), 52.2, 24.3, 23.4, 6.7 (2C); HRMS-ESI (*m/z*): [M + H]$^+$ calcd for C$_{22}$H$_{25}$N$_8$O$_2$, 433.21; found 433.24; Purity (HPLC): 99.2%. Appearance: yellow solid.

20
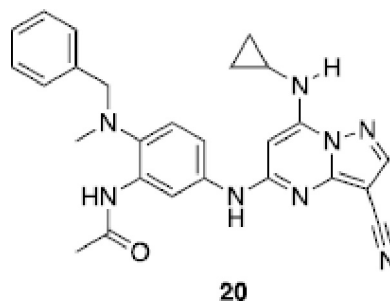
^{1}H NMR (300 MHz, chloroform-*d*) δ 8.60 (s, 1H), 8.30 (d, *J* = 2.4 Hz, 1H), 8.00 (s, 1H), 7.50 (d, *J* = 8.4 Hz, 1H), 7.33 (m, 6H), 6.89 (s, 1H), 6.33 (s, 1H), 5.99 (s, 1H), 3.95 (s, 2H), 2.66 (s, 4H), 2.12 (s, 3H), 0.89 (m, 2H), 0.76 (m, 2H); ^{13}C NMR (176 MHz, DMSO-*d$_6$*) δ 168.3, 157.0, 151.0, 148.3, 145.1, 138.3, 137.6, 136.4, 133.5, 128.8 (2C), 128.3 (2C), 127.2, 121.6, 115.0 (2C), 113.0, 76.4, 60.3 (2C), 42.1, 24.3, 23.4, 6.7 (2C); HRMS-ESI (*m/z*): [M + H]$^+$ calcd for C$_{26}$H$_{27}$N$_8$O, 467.23; found 467.34; Purity (HPLC): 96.6%. Appearance: yellow solid.

22
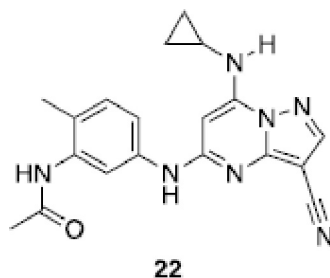
The analytical data for **22** matches that previously reported (Dowling et al., 2013); ^{1}H NMR (300 MHz, DMSO-*d$_6$*) δ 9.61 (s, 1H), 9.26 (s, 1H), 8.34 (s, 1H), 8.21 (s, 1H), 7.64 (m, 2H), 7.15 (d, *J* = 8.4 Hz, 1H), 6.01 (s, 1H), 2.59 (m, 1H), 2.16 (s, 3H), 2.07 (s, 3H), 0.79 (m, 2H), 0.70 (m, 2H); HRMS-ESI (*m/z*): [M + H]$^+$ calcd for C$_{19}$H$_{20}$N$_7$O, 362.17; found 361.95; HRMS-ESI (*m/z*): [M + Na]$^+$ calcd for C$_{19}$H$_{19}$N$_7$NaO, 384.15; found 384.22; Purity (HPLC): 99.4%. Appearance: yellow solid.

24
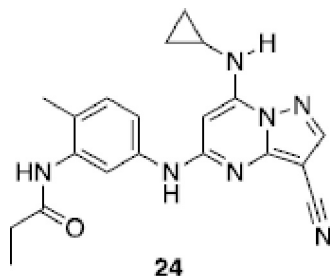
^{1}H NMR (300 MHz, DMSO-*d$_6$*) δ 9.61 (s, 1H), 9.21 (s, 1H), 8.34 (s, 1H), 8.22 (s, 1H), 7.68 (s, 1H), 7.62 (d, *J* = 7.5 Hz, 1H), 7.15 (d, *J* = 8.4 Hz, 1H), 6.01 (s, 1H), 2.59 (m, 1H), 2.34 (q, *J* = 7.5 Hz, 2H), 2.16 (s, 3H), 1.11 (t, *J* = 7.5 Hz, 3H), 0.80 (m, 2H), 0.72 (m, 2H); ^{13}C NMR (176 MHz, DMSO-*d$_6$*) δ 172.1, 157.1, 151.0, 148.4, 145.2, 138.2, 136.7, 130.4, 125.5, 116.6 (2C), 115.0, 76.4, 76.2, 29.2, 23.4, 17.3, 10.2, 6.6 (2C); HRMS-ESI (*m/z*): [M + H]$^+$ calcd for C$_{20}$H$_{22}$N$_7$O, 376.19;

found 376.24; HRMS-ESI (*m/z*): [M + Na]⁺ calcd for $C_{20}H_{21}N_7NaO$, 398.17; found 398.24; Purity (HPLC): 98.5%. Appearance: yellow solid.


26
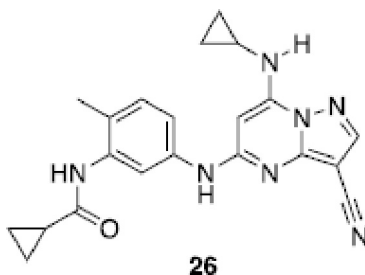
¹H NMR (300 MHz, DMSO-*d₆*) δ 9.60 (s, 1H), 9.49 (s, 1H), 8.34 (s, 1H), 8.22 (s, 1H), 7.70 (s, 1H), 7.62 (d, J = 7.5 Hz, 1H), 7.15 (d, J = 8.4 Hz, 1H), 6.00 (s, 1H), 2.58 (m, 1H), 2.19 (s, 3H), 1.91 (m, 1H), 0.78 (m, 6H), 0.71 (m, 2H); ¹³C NMR (176 MHz, DMSO-*d₆*) δ 171.7, 157.0, 151.0, 148.4, 145.2, 138.2, 136.7, 130.4, 125.0, 116.4, 116.3, 115.0, 76.4, 76.3, 23.4, 17.4, 14.1, 7.1 (2C), 6.6 (2C); HRMS-ESI (*m/z*): [M + H]⁺ calcd for $C_{21}H_{22}N_7O$, found 388.19; found 388.27; Purity (HPLC): 97.1%. Appearance: yellow solid.

27
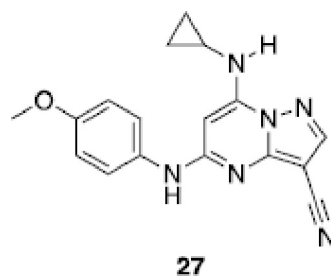
¹H NMR (300 MHz, chloroform-*d*) δ 7.98 (s, 1H), 7.32 (d, J = 8.7 Hz, 2H), 6.95 (d, J = 8.7 Hz, 2H), 6.79 (s, 1H), 6.31 (s, 1H), 5.73 (s, 1H), 3.84 (s, 3H), 2.56 (m, 1H), 0.84 (m, 2H), 0.71 (m, 2H); ¹³C NMR (176 MHz, DMSO-*d₆*) δ 157.0, 154.9, 151.1, 148.2, 145.0, 133.3, 121.5, 115.0, 114.0 (3C), 76.1, 75.8, 55.2, 23.3, 6.5 (2C); HRMS-ESI (*m/z*): [M + H]⁺ calcd for $C_{17}H_{17}N_6O$, 321.15; found 321.22; Purity (HPLC): 99.5%. Appearance: yellow solid.

29
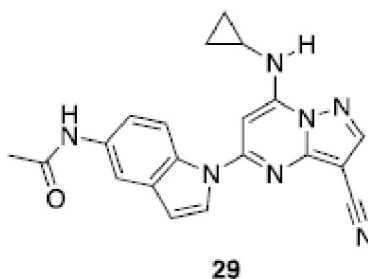
The analytical data for **29** matches that previously reported (Dowling et al., 2012); ¹H NMR (300 MHz, DMSO-*d₆*) δ 10.03 (s, 1H), 9.06 (s, 1H), 8.87 (s, 1H), 8.65 (s, 1H), 8.05 (d, J = 3.6 Hz, 1H), 7.58 (d, J = 8.4 Hz, 1H) 7.24 (dd, J = 1.2, 8.4 Hz, 1H), 6.80 (s, 1H), 6.77 (m, 1H), 2.85 (m, 1H), 2.07 (s, 3H), 0.98 (m, 2H), 0.82 (m, 2H); HRMS-ESI (*m/z*): [M + Na]⁺ calcd for $C_{20}H_{17}N_7NaO$, 394.14; found 393.98; Purity (HPLC): 97.2%. Appearance: yellow solid.

31
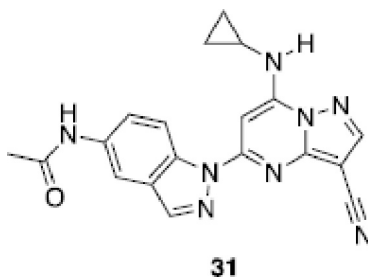
The analytical data for **31** matches that previously reported (Dowling et al., 2012); ^{1}H NMR (300 MHz, DMSO-d_6) δ 10.28 (s, 1H), 9.19 (s, 1H), 8.99 (s, 1H), 8.65 (s, 1H), 8.46 (s, 1H), 7.82 (d, J = 8.7 Hz, 1H), 7.47 (dd, J = 1.2, 8.7 Hz, 1H), 7.16 (s, 1H), 2.50 (m, 1H), 2.12 (s, 3H), 0.91 (m, 2H), 0.81 (m, 2H); HRMS-ESI (m/z): [M + H]+ calcd for $C_{19}H_{17}N_8O$, 373.15; found 373.15; HRMS-ESI (m/z): [M + Na]+ calcd for $C_{19}H_{16}N_8NaO$, 395.13; found 395.15; Purity (HPLC): 97.2%. Appearance: yellow solid.

32
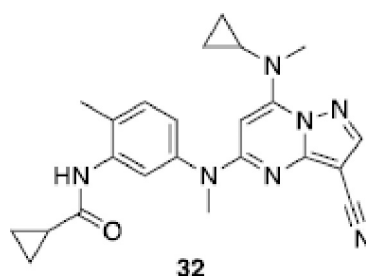
32: ^{1}H NMR (400 MHz, acetonitrile-d_4) δ 8.08 (s, 1H), 8.03 (s, 1H), 7.75 (s, 1H), 7.31 (d, J = 8.1 Hz, 1H), 7.07 (dd, J = 2.3, 5.7 Hz, 1H), 5.81 (s, 1H), 3.48 (s, 3H), 3.32 (s, 3H), 2.39 (m, 1H), 2.30 (s, 3H), 1.78 (m, 1H), 0.87 (m, 2H), 0.81 (m, 2H), 0.65 (m, 2H), 0.51 (m, 2H); ^{13}C NMR (176 MHz, acetonitrile-d_4) δ 173.2, 159.9 (2C), 154.2, 152.7, 145.4, 143.9, 138.7, 132.4, 123.7, 122.7, 115.8, 84.5, 77.4, 40.5, 38.8, 34.7, 17.9, 15.4, 9.1 (2C), 7.9 (2C); HRMS-ESI (m/z): [M + H]+ calcd for $C_{23}H_{26}N_7O$, 416.22; found 416.22; Purity (LCMS): >95%.

33
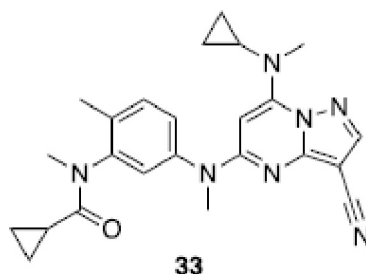
^{1}H NMR (400 MHz, acetonitrile-d_4) δ 8.05 (s, 1H), 7.46 (d, J = 8.0 Hz, 1H), 7.32 (m, 2H), 5.78 (s, 1H), 3.51 (s, 3H), 3.34 (s, 3H), 3,16 (s, 3H), 2.41 (m, 1H), 2.29 (s, 3H), 1.27 (m, 3H), 0.82 (m, 2H), 0.64 (m, 2H), 0.53 (m, 2H); ^{13}C NMR (176 MHz, acetonitrile-d_4) 173.6, 159.8, 154.1, 152.9, 145.5, 145.0, 144.9, 136.2, 133.3, 127.8, 127.5, 115.7, 84.2, 77.4, 40.6, 38.9, 36.4, 34.7, 17.3, 12.5, 9.2, 9.1, 8.5, 8.0; HRMS-ESI (m/z): [M + H]+ calcd for $C_{24}H_{28}N_7O$, 430.24; found 430.23; Purity (LCMS): >95%.

Kinome screening

The *scan*MAX assay was used to assess the selectivity of each compound at 1 μM at Eurofins DiscoverX Corporation as a commercial assay service. This assay platform screens against 403 wild-type human kinases providing percent inhibition values. This method has been previously described (Davis et al., 2011).

In vitro kinase radiometric kinaseprofiler and LANCE assays

Eurofins kinase enzymatic radiometric assays were carried out at the K_m of ATP in dose-response (9-pt curve in duplicate) for each kinase for which it was offered. The CSNK2A1/CK2α (14-445KP) and CSNK2A2/CK2α' (14-689KP) assays were both carried out at 10 μM. The peptide substrate used for CSNK2A1/CK2α and CSNK2A2/CK2α' was RRRDDDSDDD. Eurofins kinase enzymatic LANCE assay was carried out at the K_m of ATP for MEK5 at a single concentration (10 μM) in duplicate. Details about the substrate used, protein constructs, controls, and assay protocol for each kinase assay can be found at https://www.eurofinsdiscoveryservices.com.

NanoBRET measurements

Constructs for NanoBRET measurements of CK2α, CK2α', and DYRK2 were kindly provided by Promega. NanoBRET assays were executed as described previously (Wells et al., 2019).

Example protocol for CK2α': The *C*-terminal Nanoluciferase (NL)/ CK2α' fusion (CK2α'-NL) was encoded in pFN32K expression vector, including flexible Gly-Ser-Ser-Gly linkers between NL and CK2α' (Promega). For cellular NanoBRET target engagement experiments, a 10 μg/mL solution of DNA in Opti-MEM without serum was made containing 9 μg/mL of Carrier DNA (Promega) and 1 μg/mL of CK2α'-NL for a total volume of 1.05 mL. To this solution was then added 31.5 μL of FuGENE HD (Promega) to form a lipid:DNA complex. The solution was then mixed by inversion 8 times and incubated at room temperature for 20 min. The resulting transfection complex (1.082 mL) was then gently mixed with 21 mL of HEK-293 cells (ATCC) suspended at a density of 2 x 105 cells/mL in DMEM (Gibco) + 10% FBS (Corning). This solution was then dispensed (100 μL) into 96-well tissue culture treated plates (Corning #3917) followed by incubation (37°C / 5 % CO2) for 24 hours.

After 24 hours the media was removed and replaced with 85 μL of room temperature Opti-MEM without phenol red. NanoBRET Tracer K5 (Promega) was used at a final concentration of 1.0 μM as previously determined to be the optimal concentration in a titration experiment. A total of 5 μL per well (20x working stock of NanoBRET Tracer K5 [20 μM] in Tracer Dilution Buffer (Promega N291B)) was added to all wells, except the "no tracer" control wells. All test compounds were prepared initially as concentrated (10 mM) stock solutions in 100% DMSO (Sigma), and then diluted in Opti-MEM media (99%) to prepare 1% DMSO working stock solutions. A total of 10 μL per well of the 10-fold test compound stock solutions (final assay concentration of 0.1% DMSO) were added. For "no compound" and "no tracer" control wells, a total of 10 μL per well of Opti-MEM plus DMSO (9 μL Opti-MEM with 1 μL DMSO) was added for a final concentration of 1% DMSO. 96-well plates containing cells with NanoBRET Tracer K5 and test compounds (100 μL total volume per well) were equilibrated (37°C / 5 % CO2) for 2 hours.

After 2 hours the plates were cooled to room temperature for 15 min. To measure NanoBRET signal, NanoBRET NanoGlo substrate (Promega) at a ratio of 1:166 to Opti-MEM media in combination with extracellular NanoLuc Inhibitor (Promega) diluted 1:500 (10 μL [30 mM stock] per 5 mL Opti-MEM plus substrate) were combined to create a 3X stock solution. A total of 50 μL of the 3X substrate/extracellular NL inhibitor were added to each well. The plates were read within 10 min on a GloMax Discover luminometer (Promega) equipped with 450 nm BP filter (donor) and 600 nm LP filter (acceptor), using 0.3 s integration time according to the "NanoBRET 618" protocol.

Test compounds were evaluated at eleven concentrations in competition with NanoBRET Tracer K5 in HEK-293 cells transiently expressing the NL-CK2α or CK2α' fusion protein. Raw milliBRET (mBRET) values were obtained by dividing the acceptor emission values (600 nm) by the donor emission values (450 nm), and then multiplying by 1000. Averaged control values were used to represent complete inhibition (no tracer control: Opti-MEM + DMSO only) and no inhibition (tracer only control: no compound, Opti-MEM + DMSO + Tracer K5 only) and were plotted alongside the raw mBRET values. The data with n=3 biological replicates was first normalized and then fit using Sigmoidal, 4PL binding curve in Prism Software (version 8, GraphPad, La Jolla, CA, USA). All error bars are based on n=3 and are +/- standard error (SE).

HCT-116 and U-87 MG 72hr AlamarBlue cell proliferation assay

This assay was performed as previously described (Dowling et al., 2016). Briefly, this is a fluorometric assay to determine cell viability upon dosing with CK2 inhibitors as compared to vehicle control (DMSO) and staurosporine (control). Specifically, the system incorporates a resazurin-based reagent that upon entering living cells is reduced causing both a change in color and an increase in fluorescence. The CK2 inhibitors were evaluated in both HCT-116 and U-87 MG cells. For each compound a GI_{50} (Growth Inhibition Concentration 50%) was calculated, using the fluorescence corresponding with cells treated for 72hrs with 10 μM staurosporine as the assay minimum (positive control) and DMSO vehicle as the maximum (negative control). HCT-116 and U-87 MG cells were seeded at 2500 cells/well in Costar Flat bottomed 96 well plates (Black wall/clear bottom) in 90 μL of phenol-red free McCoy's 5a (HCT-116) or MEM (U-87 MG) with 10% FBS and incubated overnight in 37°C, 5% CO2. Compound plates were then treated with 1 μL of 100X compound (10 pt dose response) and incubated for 72hrs at 37°C, 5% CO2. The AlamarBlue reagent (Thermo) was then added to each well (10 μL) incubated for 4hrs at 37°C, 5% CO2. Fluorescence was measured at 535 nm (excitation) and 590 nm (emission) using a GloMax plate reader.

Caspase-Glo 3/7 assay

This assay was performed according to manufacturer instructions (Promega G8090). Briefly U-87 MG cells were plated in a Corning white walled flat bottom plate (cat # 3917) at a density of 20,000 cells/well. Cells were plated in all wells except for the no cell control wells. After the cells adhered to the plate, they were treated with compound for 16 hours. After 16 hours to each well was added 100uL of Caspase 3/7 glo reagent. The plate was mixed at 300rpm for 30sec. The plate was allowed to incubate at room temperature for 30 min, and then the plate was read. Compound **24** did not demonstrate significant Caspase 3/7 activation.

ProQinase broad tumor cell line profiling

Analysis of the impact of SGC-CK2-1 on the proliferation of 140 tumor cell lines was carried out at ProQinase. The IC_{50} values were determined for SGC-CK2-1 and reference compound bortezomib in parallel. Compound treatment of cells started one day after seeding with a final DMSO concentration of 0.1% and was performed by nanodrop-dispensing using a Tecan Dispenser. 0.1% DMSO (solvent) and staurosporine (10 μM) served as high control (100% viability) and low control (0% viability), respectively. SGC-CK2-1 was dosed with effective concentrations between 3 μM and 0.9 nM, with 3-fold dilutions in between. Bortezomib was dosed with effective concentrations between 1 μM and 0.3 nM, with 3-fold dilutions in between.

Cells were cultured in different recommended media, which varied by cell line. For the assays, cells were seeded in white cell culture-treated flat and clear bottom multi-well plates and incubated at 37°C overnight before compounds were added. After incubation for 72h at 37°C at 5% or 10% CO_2 dependent on the medium, cell plates were equilibrated to room temperature for one hour, CellTiterGlo reagent (Promega) was added and luminescence was measured approximately an hour later using a luminometer.

Raw data were converted into percent cell viability relative to the high and low control, which were set to 100% and 0%, respectively. IC_{50} calculation was performed using GraphPad Prism software with a variable slope sigmoidal response fitting model using 0% viability as bottom constraint and 100% viability as top constraint.

NCI60 profiling

SGC-CK2-1 and SGC-CK2-1N were profiled against 59 cancer cells lines at a single dose of 10 μM as has been described previously (Shoemaker, 2006). The one-dose data was reported as a mean graph of the percent growth of treated cells. A value was also reported, corresponding to the growth relative to the no-drug control and relative to the time zero number of cells. This allowed for detection of both growth inhibition (values between 0 and 100) and lethality (values less than 0).

HCT-116 western blot analyses

HCT-116 cells (ATCC® CCL-247™) were cultured in McCoy's 5A plus L-Glutamine medium (Gibco) supplemented by 10 % FBS (Gibco) and Penicillin/Streptomycin (Gibco). 200,000 cells per well (6-well tissue culture plate) were incubated at 37°C and 5% CO_2 for 24h prior to inhibitor treatment. The inhibitors were diluted to a 1000x fold assay concentration in DMSO and further diluted in culture medium. Successively, the medium of the cells was aspirated and replaced with the medium containing the inhibitor dilutions. Cells were treated for 3h or 24h, washed with PBS and lysed (50 mM Tris pH 8, 150 mM NaCl, 1% NP40, 20 mM NaF, 2 mM Na_3VO_4, 2 mM beta-phosphoglycerol, 1x protease inhibitor (Merck)) on ice. The total amount of protein was determined by BCA assay (Pierce, Thermo Fisher Scientific).

Samples were analyzed on a precast 4-12% Bis-Tris gradient gel (Criterion XT, Bio-Rad). Proteins were blotted by a Trans-Blot Turbo Semi-dry blotter (Bio-Rad) on a PVDF membrane (Bio-Rad). The membranes were blocked with 5% bovine serum albumin (Roth) and subsequently incubated with either anti-AKT1 antibody (Akt (pan) 40D4 mouse mAB, SignalingTechnology), anti-phosphoAKT1 antibody (Rb mAB to AKT1 (phospho S129) EPR6150, ab133458, Abcam) and anti-GAPDH (Invitrogen, GA1R, MA5-15738) as a loading control followed by an HRP-conjugated anti-mouse (anti-AKT1 antibody, GAPDH antibody) or anti-rabbit (anti-phosphoAKT1 antibody) antibody and ClarityTM Western ECL substrate (Bio-Rad) on a ChemiDoc XRS+ system (Bio-Rad). Intensity levels of the different bands were determined using the Image Lab Software 6.1 (Bio-Rad). In total, two independent biological repeats of the experiment were performed.

U2OS western blot analyses

Immunoblotting was done as described previously (Gyenis et al., 2011). Briefly, antibody incubations with primary antibodies were performed with the indicated dilutions in 3% BSA in TBST (contains 0.05% Tween 20) for rabbit antibodies or PBST (contains 0.1% Tween 20) for mouse antibodies. Incubations with secondary antibodies were performed with 1% BSA in TBST or PBST for secondary antibodies. Phosphospecific antibodies detecting pS2 of EIF2S2 (used at 1:10,000) are rabbit polyclonal antibodies (Gandin et al., 2016). For EIF2S2 pS2 signal normalization we immunoblotted with total EIF2S2 (1:500, Novus). The anti-Glyceraldehyde-3-Phosphate Dehydrogenase (GAPDH), clone 6C5 (1:1,000, Millipore) antibody was used as a loading control to ensure equal loading. The EIF2S2 pS2/total EIF2S2 normalized signal was used to calculate residual CSNK2 activity with the signal for DMSO treatment considered to be 100% kinase activity. Infrared IRDye-labeled antibodies (1:10,000, LiCor) were used for immunoblot visualization and quantification was performed on the LiCor Odyssey Infrared Imaging System with the Odyssey V3.0 and Image Studio Lite Ver 5.2 software.

Crystallography Methods

Expression and purification

Expression and purification were performed as described previously (Krämer et al., 2020). Briefly, transformed BL21(DE3) cells were grown in Terrific Broth medium containing 50 mg/mL kanamycin. Protein expression was induced at an OD_{600} of 2 by using 0.5 mM isopropyl-thio-galactopyranoside (IPTG) at 18°C for 12 hours. Cells expressing His_6-tagged CK2α were lysed in lysis buffer containing 50 mM HEPES pH 7.5, 500 mM NaCl, 25 mM imidazole, 5% glycerol, and 0.5 mM Tris(2-carboxyethyl)phosphine (TCEP) by sonication. After centrifugation, the supernatant was loaded onto a Nickel-Sepharose column equilibrated with 30 mL lysis buffer. The column was washed with 60 mL lysis buffer. Proteins were eluted by an imidazole step gradient (50, 100, 200, 300 mM). Fractions containing protein were pooled together and dialyzed overnight using 1L of final buffer (25 mM HEPES pH 7.5, 500 mM NaCl, 0.5 mM TCEP) at 4°C. Additionally, TEV protease was added (protein:TEV 1:20 molar ratio) to remove the tag. The next day the protein solution was loaded onto Nickel-Sepharose column beads again to remove the TEV protease and cleaved Tag. The combined flow through fraction and the wash fraction (25 mM imidazole) containing the protein was concentrated to approximately 4-5 mL and loaded onto Superdex 75 16/60 Hi-Load gel filtration column equilibrated with final buffer. The protein was concentrated to approximately 9 mg/mL.

Crystallization

CK2α was crystallized using the sitting-drop vapor diffusion method by mixing protein (9 mg/mL) and well solutions in 2:1, 1:1, and 1:2 ratios. The reservoir solution contained 0.2 M ammonia sulfate, 0.1 M bis-tris pH 5.5 and 23-26% (v/v) PEG 3350. Complex structures were achieved by soaking the apo crystals for at least 24h with the desired inhibitor dissolved in reservoir solution. Final concentration of the inhibitor was 0.5 mM.

Data collection, structure solution and refinement

Diffraction data were collected at beamline X06DA (Villigen, CH) at a wavelength of 1.0 Å at 100 K. The reservoir solution supplemented with 20% ethylene glycol was used as cryoprotectant. Data were processed using XDS (Kabsch, 2010) and scaled with aimless. The PDB structure with the accession code 3PE2 (Battistutta et al., 2011) was used as an initial search MR model using the program MOLREP (Lebedev et al., 2008). The final model was built manually using Coot (Emsley and Cowtan, 2004) and refined with REFMAC5 (Vagin et al., 2004).

QUANTIFICATION AND STATISTICAL ANALYSIS

Statistical analysis

Statistical tests and the associated error bars are identified in the corresponding figure legends. Typical replicate numbers describe the number of technical replicates analyzed in a single experiment. GraphPad Prism 8.2.0 software was used for analyses.

ADDITIONAL RESOURCES

All associated data for SGC-CK2-1 and SGC-CK2-1N has been deposited at https://www.thesgc.org/chemical-probes/SGC-CK2-1.

Article

The Kinase Chemogenomic Set (KCGS): An Open Science Resource for Kinase Vulnerability Identification

Carrow I. Wells [1], Hassan Al-Ali [2,3], David M. Andrews [4], Christopher R. M. Asquith [1], Alison D. Axtman [1], Ivan Dikic [5,6,7], Daniel Ebner [8], Peter Ettmayer [9], Christian Fischer [10], Mathias Frederiksen [11], Robert E. Futrell [1], Nathanael S. Gray [12,13], Stephanie B. Hatch [14], Stefan Knapp [6,15,16], Ulrich Lücking [17], Michael Michaelides [18], Caitlin E. Mills [19], Susanne Müller [6,15,16], Dafydd Owen [20], Alfredo Picado [1], Kumar S. Saikatendu [21], Martin Schröder [6,15,16], Alexandra Stolz [5,6,15], Mariana Tellechea [5,6,15], Brandon J. Turunen [22], Santiago Vilar [3], Jinhua Wang [12,13], William J. Zuercher [1], Timothy M. Willson [1] and David H. Drewry [1,*]

1 Structural Genomics Consortium, UNC Eshelman School of Pharmacy, University of North Carolina at Chapel Hill, Chapel Hill, NC 27599, USA
2 The Miami Project to Cure Paralysis, Peggy and Harold Katz Family Drug Discovery Center, Sylvester Comprehensive Cancer Center, Departments of Neurological Surgery and Medicine, University of Miami Miller School of Medicine, Miami, FL 33136, USA
3 Truvitech LLC, Miami, FL 33136, USA
4 AstraZeneca, Darwin Building, Cambridge Science Park, Cambridge CB4 0WG, UK
5 Institute of Biochemistry 2, Faculty of Medicine, Goethe University Frankfurt, Theodor-Stern-Kai 7, 60438 Frankfurt am Main, Germany
6 Buchmann Institute for Molecular Life Sciences, Goethe University Frankfurt, Max-von-Laue-Str. 15, 60438 Frankfurt am Main, Germany
7 Max Planck Institute of Biophysics, Max-von-Laue-Str. 3, 60438 Frankfurt am Main, Germany
8 Nuffield Department of Medicine, Target Discovery Institute, University of Oxford, Oxford OX3 7FZ, UK
9 Boehringer Ingelheim RCV GmbH & Co KG, 1121 Vienna, Austria
10 MSD, 33 Avenue Louis Pasteur, Boston, MA 02115, USA
11 Novartis Institutes for BioMedical Research, Novartis Campus, 4056 Basel, Switzerland
12 Department of Biological Chemistry and Molecular Pharmacology, Harvard Medical School, Boston, MA 02115, USA
13 Department of Cancer Biology, Dana-Farber Cancer Institute, Boston, MA 02215, USA
14 MRC Oxford Institute for Radiation Oncology, Department of Oncology, University of Oxford, Roosevelt Drive, Oxford OX3 7XB, UK
15 Structural Genomics Consortium, Buchmann Institute for Molecular Life Sciences, Goethe University Frankfurt, Max-von-Laue-Straße 15, 60438 Frankfurt am Main, Germany
16 Institute for Pharmaceutical Chemistry, Johann Wolfgang Goethe-University, Max-von-Laue-Str. 9, 60438 Frankfurt am Main, Germany
17 Bayer Pharma AG, Drug Discovery, Müllerstrasse 178, 13353 Berlin, Germany
18 Oncology Discovery, AbbVie, 1 North Waukegan Road, North Chicago, IL 60064, USA
19 Laboratory of Systems Pharmacology, Department of Systems Biology, Harvard Medical School, Boston, MA 02115, USA
20 Discovery Network Group, Pfizer Medicine Design, Cambridge, MA 02139, USA
21 Global Research Externalization, Takeda California, Inc., 9625 Towne Center Drive, San Diego, CA 92121, USA
22 GlaxoSmithKline, Chemical Biology, 1250 S Collegeville Rd, Collegeville, PA 19426, USA
* Correspondence: David.Drewry@unc.edu

check for updates

Abstract: We describe the assembly and annotation of a chemogenomic set of protein kinase inhibitors as an open science resource for studying kinase biology. The set only includes inhibitors that show potent kinase inhibition and a narrow spectrum of activity when screened across a large panel of kinase biochemical assays. Currently, the set contains 187 inhibitors that cover 215 human kinases. The kinase chemogenomic set (KCGS), current Version 1.0, is the most highly annotated set of selective kinase inhibitors available to researchers for use in cell-based screens.

Keywords: protein kinase; kinase inhibitor; chemogenomic set; phenotypic screening; small molecules; KCGS; drug discovery; druggable genome; understudied kinase

1. Introduction

The protein kinases have emerged as one of the most productive families of drug targets in the 21st century. Over 60 small molecule kinase inhibitors have been approved by the FDA since 2001 for the treatment of cancer, inflammation, and fibrosis [1]. Many of these drugs, specifically those that are used in oncology, owe their efficacy to inhibition of multiple kinases [2]. For some targets second- and third-generation inhibitors have been designed to block the activity of mutant kinases that cause drug resistance after first line therapy. Collectively these drugs target only a small fraction of the 500+ human kinases. We and others have proposed that the remaining kinases represent an untapped trove of new drug targets [3–5].

Despite the concerted efforts of academic and industrial scientists over the past 25 years, the vast majority of the human kinases remain understudied. Various bibliographic analyses show that, similar to many other protein families, 90% of the research effort has been expended on <20% of the kinases [6]. Initiatives such as the NIH-sponsored Illuminating the Druggable Genome (IDG) program have sought to change this dynamic by making available high-quality data sets and research tools for the "dark" kinases [7]. The availability of a set of potent and selective inhibitors of the understudied kinases could greatly aid the study of their biology and uncover new targets for drug development.

An ever-growing number of kinase inhibitors are commercially available. Many of these compounds have advanced to clinical studies and may be useful for investigators seeking to repurpose kinase drugs for a secondary indication but they do little to expand the number of new kinase targets [8]. Notably, the commercially available kinase inhibitors vary widely in the amount and depth of annotation provided. Their vendors typically list the primary target of each inhibitor and perhaps a handful of off-targets but only rarely provide kinase selectivity profiles. Although the amount of kinase profiling data that can be found in public databases is growing [9], for many compounds broad profiling is either unavailable or described in a multitude of assay formats in the supporting information that accompanies a primary publication. While commercially available kinase sets contain valuable inhibitors of the well-studied kinases, they do little to provide tools to expand research across the breadth of the kinome.

The public availability of a high-quality chemical probe for every understudied kinase would be an ideal way to embolden researchers to explore the therapeutic potential of each kinase target [10]. However, the development of potent and selective chemical probes for over 500 kinases would be an insurmountable task using current resources and technologies. A chemogenomic set [11] of kinase inhibitors provides a practical solution to the problem [12]. The majority of kinase inhibitors, by virtue of competing with the common cofactor adenosine triphosphate (ATP) in a highly conserved binding site, invariably show some cross-activity on multiple kinases. Landmark studies by Bristol-Myers Squibb and GlaxoSmithKline scientists showed that kinome-wide profiling could identify inhibitors with collateral activity on the understudied kinases [13,14]. Building on these observations, the kinase inhibitor sets PKIS [15] and PKIS2 [16] were assembled as collections of published kinase inhibitors using the principles that chemical diversity and the inclusion of multiple exemplars of each chemotype would increase the breadth of kinase coverage and aid analysis of phenotypic screening data [17]. Both sets have found widespread use in the research community and demonstrated that repurposed inhibitors from past projects could be used to probe the biology of the kinase they were made to target and their off-targets as well. However, the full kinase profile of each inhibitor in PKIS and PKIS2 was not known in advance of their selection, and as a result both sets contained many inhibitors that were either too promiscuous (inhibition of too many kinases) or lacked sufficient target potency to be useful contributors to a chemogenomic set [18]. In spite of this limitation, PKIS and PKIS2 contained many valuable inhibitors for a broad set of understudied kinases. Encouraged by these results, we proposed a community experiment to build an optimized kinase chemogenomic set (KCGS) to cover every human kinase [16].

Each inhibitor would have its full kinome profile determined in advance and only those compounds that met a prespecified potency and selectivity would be added to KCGS.

From the start, we chose to make KCGS an open science experiment. All of the compound structures and associated kinase inhibition and selectivity data would be made publicly available. KCGS would be distributed under a Material Trust Agreement (Supplementary File S1) that supported its use as a public resource and prevented the recipients from blocking other researchers from using the set [19]. Eight pharmaceutical companies answered the call to donate kinase inhibitors from their internal compound collections to the effort. Many but not all of these companies were current partners in the Structural Genomics Consortium (SGC) [20]. In addition, several leading academic groups contributed compounds to the initiative. To date, over 1200 kinase inhibitors have been profiled as candidates for inclusion into KCGS. Here, we present the first version of KCGS as well as its initial characterization and examples of its use in cell-based assays. The set will be broadly useful to the scientific community for phenotypic screening to identify the roles of various kinases in biology and disease.

2. Results

2.1. Compound Selection

Candidate kinase inhibitors were received from GlaxoSmithKline, Pfizer, Takeda, Abbvie, MSD, Bayer, Boehringer Ingelheim, and AstraZeneca. In addition, Vertex gave permission to include their commercially available inhibitors. Academic laboratories that donated inhibitors were Cancer Research UK, Nathanael Gray, and multiple SGC sites. In total, 250 new inhibitors were donated to the initiative as candidates to complement the 950 inhibitors of PKIS and PKIS2.

At the outset, we selected the DiscoverX scanMAX assay to profile all kinase inhibitors donated to the initiative [21]. The scanMAX assay provided kinase binding data on 401 wild type human kinases (Table 1), which was at the time the broadest coverage by any single assay panel [22]. All kinase inhibitors were profiled at a concentration of 1 μM. Using a cut-off of 10% activity remaining (PoC, equivalent to 90% inhibition), an activity profile was determined for each inhibitor and a selectivity index (S_{10}) was calculated as the fraction of kinases meeting the cut-off. Compounds with an S_{10} (1 μM) < 0.04 were initially selected for consideration for inclusion in KCGS. For these compounds, we performed full-dose response experiments in order to determine K_D values for all kinases with PoC < 10% in the scanMAX experiment.

Table 1. Kinase coverage by kinase chemogenomic set (KCGS) version 1. The human kinases are divided into 10 subfamilies [23]. Kinases: the number of human kinases in each subfamily. Assays: the number of kinases in the DiscoverX scanMAX panel. KCGS: The number of kinases covered by an inhibitor. %: The percentage of kinases screened that are covered by an inhibitor.

	Kinases	Assays	KCGS	%
AGC	63	46	20	43
Atypical	34	7	5	71
CAMK	74	58	28	48
CK1	12	8	3	38
CMGC	64	60	37	62
Lipid	20	13	10	77
Other	81	51	26	51
STE	47	42	13	31
TK	90	81	54	67
TKL	43	35	19	54
Total	215	401	528	54

For inclusion in KCGS, an inhibitor was selected if the DiscoverX assay panel showed K_D < 100 nM on its target kinase and S_{10} (1 μM) < 0.025 in a full panel kinase screen [16].

For inhibitors from PKIS, the assay data from the Nanosyn screening panel of 230 kinases was used to calculate the selectivity index in lieu of submitting the compounds to scanMAX. For inhibitors from PKIS2 and the newly donated compounds, the data from the DiscoverX scanMAX panel of 401 kinases was used to calculate the selectivity index. Compounds that met the inclusion criteria were manually triaged to maximize the coverage of the human kinome. Our aspirational goal was to include two unique chemotypes for each kinase and care was taken not to over-represent kinases that had been more heavily studied (such as EGFR, MAPK14, and GSK3B). For the poorly studied dark kinases, there was often only one or two compounds to select that met the inclusion criteria. Finally, in those cases where two compounds had equivalent kinase profiles, preference was given to inclusion of the chemotype with fewer exemplars in the set. Using these guidelines, version 1.0 of KCGS was assembled with a total of 187 kinase inhibitors. Summary information for each inhibitor is contained in Table S1 and the full kinase profiles can be accessed at www.randomactsofkinase.org.

2.2. Kinase Coverage

The set covered a total of 215 human kinases, which was more than 50% of the full scanMAX assay panel (Tables 1 and S2). Across the branches of the kinome, broad coverage was found in the TK family (67%) and CMGC family (62%). While KCGS appears to cover 71% of the atypical kinases, only a small fraction of these kinases have assays in the scanMAX panel. Lower coverage was obtained for the CK1 (38%) and STE (31%) families. In total, 114 kinases were covered by two or more inhibitors, while the remaining 98 kinases have only one useful inhibitor in the current set (Table S1). Ideally, every kinase would be covered by inhibitors from multiple chemotypes to aid analysis of phenotypic screening data. This remains a goal for future expansion of the set.

Despite the tractability of kinases as drug targets, the majority of the kinome is poorly annotated and remains dark with respect to its role in human biology, in part due to a paucity of reagents. The NIH IDG initiative has nominated 162 dark kinases (Figure 1 and Table S2) for development of chemical and biological tools in an effort to seed research on these understudied proteins [7]. KCGS contains inhibitors of 37 of the IDG dark kinases (Table S2), which may be useful as initial chemical tools to study these kinases. These KCGS compounds can also be used as starting points for development of high-quality chemical probes as the biological function of their kinase targets becomes better understood and the investment in additional optimization is warranted. We utilized a recent data set [24,25] annotated to human protein-coding genes and their genetic relevance to look at the frequency of PubMed publications on individual kinases. Figure 1 depicts the publication counts for kinases covered by KCGS. The set contains inhibitors of most of the more highly studied (top 25%) kinases, but importantly it also contains inhibitors that cover some of the darkest kinases. Future expansion of KCGS will focus on filling the gaps in coverage of the dark kinases.
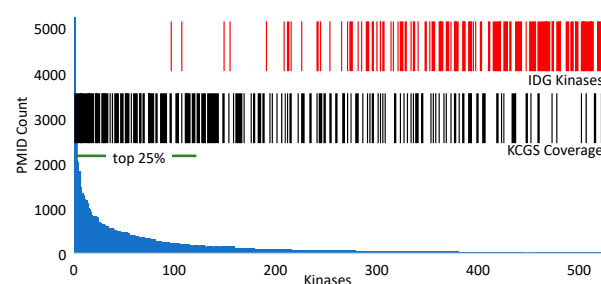

Figure 1. Analysis of kinase coverage in KCGS by publication frequency. The blue histogram indicates the number of publications for each kinase in PubMed (Table S2) [24,25] ordered by frequency with the top 25% noted by the horizontal bar. The red vertical bars indicate the 162 poorly studied dark kinases nominated by the NIH Illuminating the Druggable Genome (IDG) initiative [7]. The black vertical bars indicate the 215 kinases covered by an inhibitor in KCGS version 1.

2.3. Chemotype Analysis

To aid analysis of screening data and to support future expansion of KCGS, a method was developed to assign each inhibitor to a specific chemotype based on the chemical structure of its hinge-binding moiety. To accomplish this, 119 known kinase hinge-binder substructures were defined manually and codified using SMILES (Simplified Molecular Input Line Entry System) arbitrary target specification (SMARTS) [26]. To resolve issues where an inhibitor could be assigned to multiple bins, SMARTS were given a priority order. Kinase inhibitors that lacked an obvious hinge-binding group were grouped separately into an additional SMARTS bin. Applying this analysis to the 187 KCGS inhibitors, the compounds were found to occupy 67 of the 120 SMARTS bins (Figure 2A and Table S3). Nine of the bins contained six or more inhibitors, 27 bins had two to five members, and 31 bins contained only one exemplar. The nine most highly populated SMARTS bins contain well-known kinase inhibitor scaffolds, such as indazoles, oxindoles, quinazolines, quinolines, and pyrimidines. Six KCGS compounds that lack an obvious hinge-binder group were placed in the "other" bin. They include an allosteric PAK inhibitor and two allosteric MEK inhibitors. For bins containing multiple exemplars, the individual inhibitors often showed activity on kinases located in several different branches of the kinome. For example, the 13 oxindoles in KCGS showed a cluster of activity on CMGC kinases, but they also inhibited TK, TKL, and STE kinases (Figure 2B). While the oxindole chemotype has been found in many highly promiscuous kinase inhibitors, the inclusion of several oxindoles in KCGS demonstrated that this chemotype can also produce highly selective kinase inhibitors by judicious optimization of the molecules. KCGS contained nine exemplars in the 4-anilino-quinazolines bin (Figure 2C). Six FDA-approved kinase inhibitors that target EGFR and ERBB2 also fall into this bin. However, the SMARTS analysis highlights that modification of the 4-anilino-quinazoline chemotype can also generate inhibitors with activity on several adjacent kinase subfamilies.
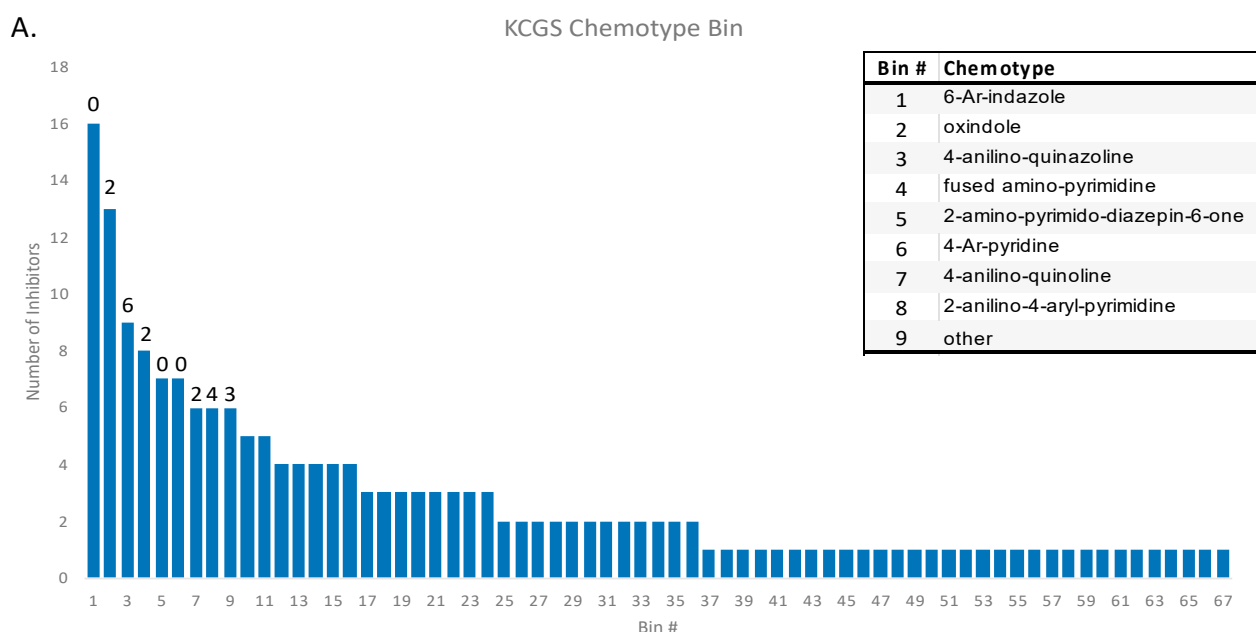
A.

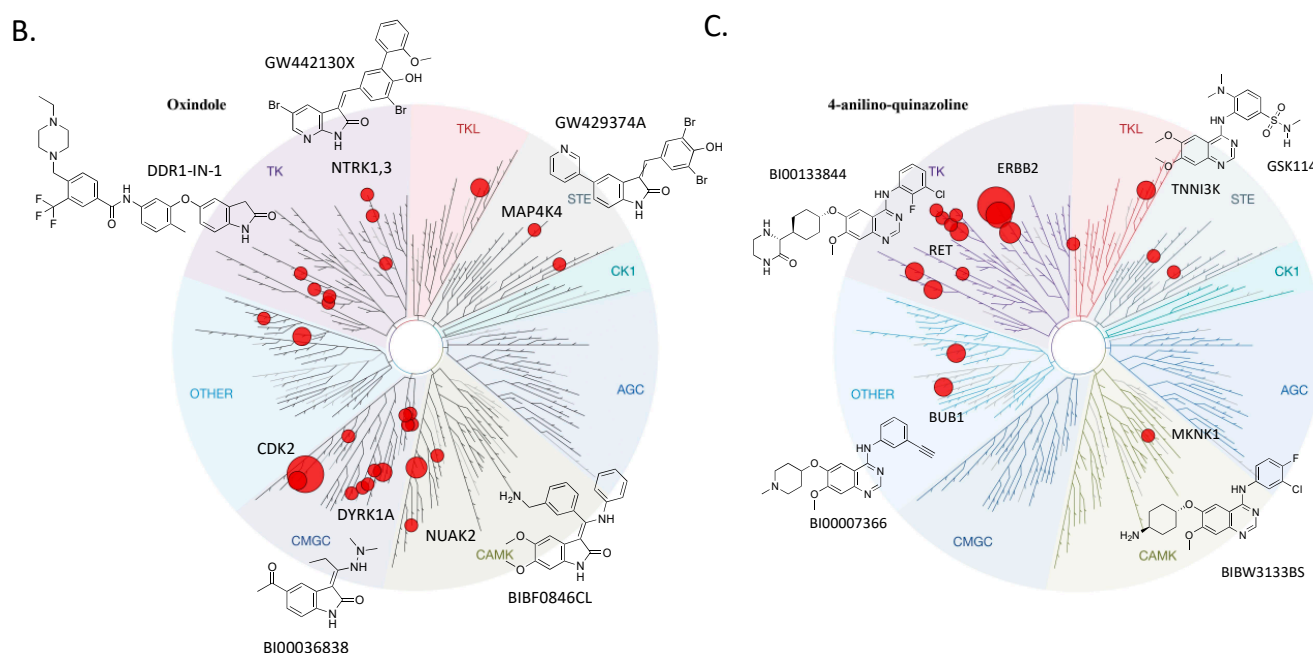| Bin #	Chemotype
1	6-Ar-indazole
2	oxindole
3	4-anilino-quinazoline
4	fused amino-pyrimidine
5	2-amino-pyrimido-diazepin-6-one
6	4-Ar-pyridine
7	4-anilino-quinoline
8	2-anilino-4-aryl-pyrimidine
9	other

Figure 2. *Cont.*

Figure 2. KCGS contains inhibitors from 67 distinct chemotypes. (**A**) This graph displays the number of inhibitors in each SMILES arbitrary target specification (SMARTS) bin. The numbers above the left-most 9 bars represent the number of FDA approved kinase inhibitors in these chemotype bins at the time the manuscript was written. The inset provides names of the 9 most highly populated bins. (**B**) Tree plot of the human kinases with each subfamily uniquely shaded. Kinases covered by a member of the oxindole SMARTS bin are displayed as red dots, scaled by the number of compounds inhibiting a specific kinase. Representative chemical structures form the oxindole SMARTS bin are shown. (**C**) Kinases covered by the 4-anilino-quinazoline SMARTS bin with representative chemical structures. (# = number).

2.4. Calculated Properties

All of the inhibitors in KCGS were originally the product of medicinal chemistry projects to target specific kinases. As such, many of them had been optimized with an eye on physicochemical properties and cellular activity. To evaluate the overall quality of the set, the calculated properties of each inhibitor from KCGS were determined in SwissADME [27] and compared to a set of 52 FDA-approved kinase inhibitors [28]. SMILES strings representing each inhibitor were input into SwissADME to generate the predicted solubility and calculated lipophilicity (Table S1). For predicted solubility, the inhibitors were binned into four categories ranging from poorly to very soluble. The solubility profile of both inhibitor sets was similar (Figure 3A). The majority of compounds were predicted to be moderately soluble or better for both KCGS (88%) and the FDA-approved inhibitors (78%). LogP is a common measure of lipophilicity and is considered a critical factor in assessing the drug-like properties of small molecules [29]. The SwissADME consensus logP (cLogP), which is the arithmetic mean of five calculated values (XLOGP3, WLOGP, MLOGP, SILICOS-IT, and iLOGP), was used to compare KCGS to the FDA-approved kinase inhibitors. The results showed that KCGS clogP values trended towards lower lipophilicity than the FDA-approved drugs, with 65% of the KCGS inhibitors falling between cLogP 2 and 4 and proportionally fewer inhibitors with cLogP > 4 (Figure 3B). Overall, these calculations support the premise that the inhibitors in KCGS have physical properties that render them well-suited for use in cell-based assays.
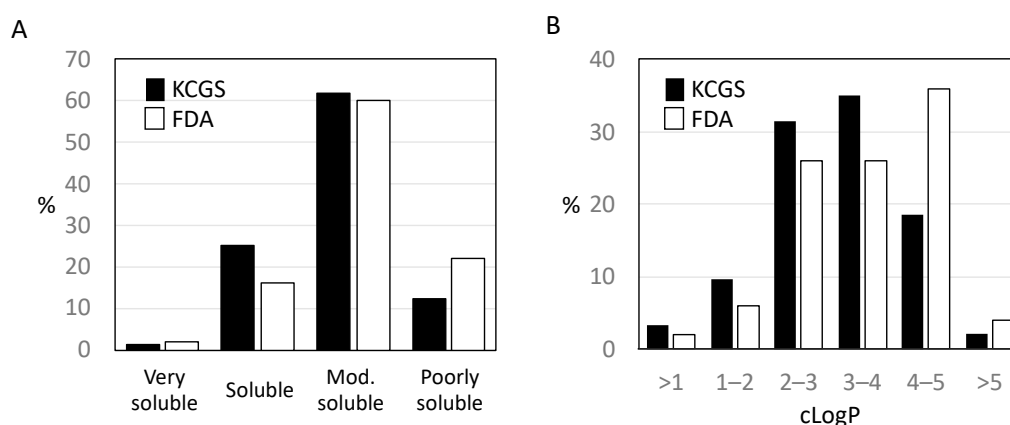
Figure 3. Calculated properties. (**A**) Predicted solubility of the KCGS compounds (black) compared to 52 FDA-approved kinase inhibitors (white) split into four categories and shown as percentage of the set. (**B**) Hydrophobicity analysis of the KCGS compounds (black) using SwissADME compared to the FDA-approved kinase inhibitors (white) split into six ranges of cLogP and shown as percentage of the set.

2.5. Chemogenomic Screening

To format KCGS for distribution to a large number of researchers, 10 mM DMSO stock solutions of the 187 inhibitors were aliquoted into 384-well format plates. Then, 1 μL of each inhibitor was dispensed to each well of the plate using an Echo 550 acoustic dispenser for accurate delivery. This 1 μL/10 mM volume provides sufficient compound to run 100 assays at a 1 μM inhibitor concentration in 96-well format and 200 assays in a 384-well format (assuming 100 and 50 μL working volume, respectively, see Supplementary File S2). KCGS was delivered with a plate map that delineates compound identification numbers as well as the kinase profile for each compound (Table S1). Based on the kinase selectivity profile of the inhibitors, 1 μM is the recommended screening concentration for chemogenomic experiments to support hit identification and target deconvolution. Screening at higher concentrations will likely complicate data interpretation due to additional undocumented off-target activity of the inhibitors. To aid with hit follow-up, additional quantities of each inhibitor were available from the SGC-UNC for full-dose response and secondary assays.

2.6. Cell Toxicity

To facilitate the use of KCGS in cell-based assays, we determined the acute toxicity of the individual inhibitors at a high dose (10 μM) in HeLa cells. After 24 h treatment, high content imaging [30,31] was used to measure healthy cell count as well as the percent of necrotic and apoptotic cells, which identified those inhibitors that exhibited varying degrees of toxicity (Figure 4 and Table S4). In total, 134 of the kinase inhibitors had little or no effect on total cell count. A total of 43 of the inhibitors reduced cell count by 20% or more. The most toxic compounds that decreased cell count by >67% are highlighted in Figure 4A. The cell toxicity displayed by these compounds may be due to their inhibition of kinases that affect cell division or cell viability, either as a primary or secondary target. Among the compounds with the largest effect on cell count were inhibitors of kinases involved in cell cycle progression, checkpoint regulation, and cell division including the CDKs (GW416981X, THZ531, BI00036838), AURKC (GW814408X), ATR (VE-822), and CHK1/2 (CCT244747, CCT241533). Other compounds with significant toxicities in HeLa cells at the 10 μM dose were GW683134A, a type II inhibitor of KDR, KIT and TEK, and PFE-PKIS 29, a very potent (<10 nM) inhibitor of mTOR and several lipid kinases including all isoforms of PI3K.
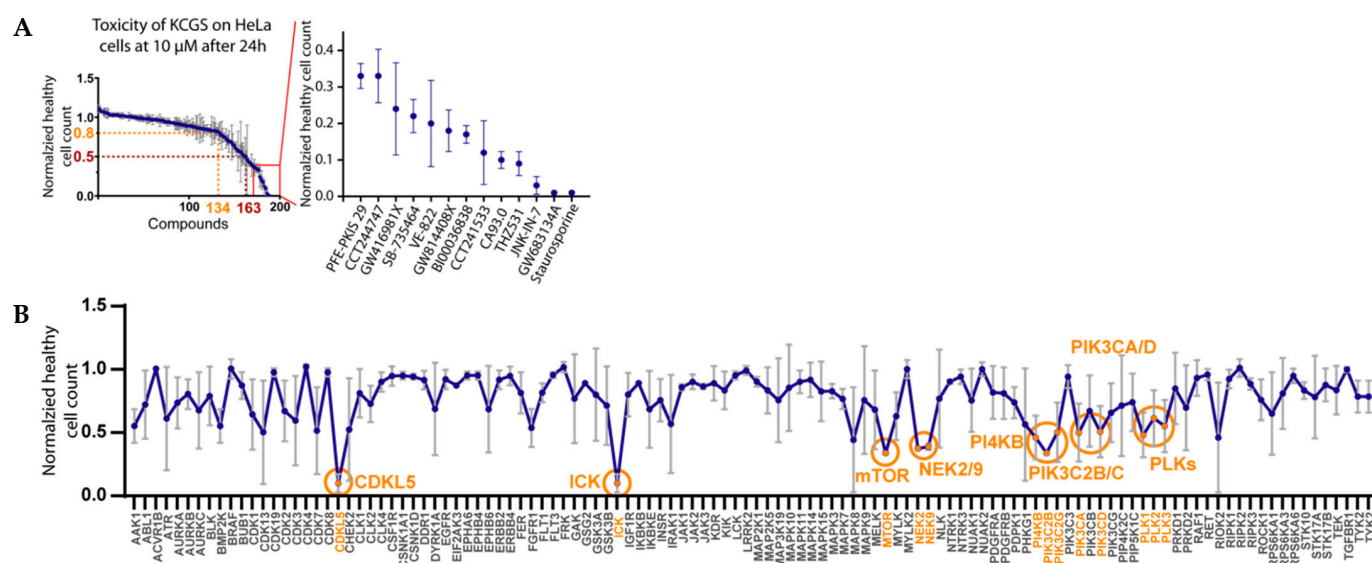
Figure 4. Cell toxicity assessment. (**A**) Effects of KCGS compounds at 10 μM on HeLa cells after 24 h. Measurements were made in triplicate with standard errors shown. Shown is the normalized healthy cell count with highlighted thresholds of 0.8 (80% healthy cells) and 0.5 (50% healthy cells). The panel on the right side displays the compounds with the greatest effect on healthy cell count in HeLa cells. (**B**) Averaged toxicity measured by normalized healthy cell count for every target covered by two or more chemotypes. Highlighted are target kinases that show a significantly lower healthy cell count than the DMSO control.

To gain further insight into kinases associated with cell toxicity, we performed an analysis of every kinase that is covered in KCGS by two or more distinct chemotypes (Figure 4B). Several kinases were identified whose inhibition resulted in a significantly lower healthy cell count. Several inhibitors of the polo-like kinases (PLKs) showed toxicity, as did inhibitors of the PIK3C and PI4KB lipid kinases. The apparent toxicity of NEK2/NEK9 inhibition by GSK579289, GSK461364, GSK579289, and GSK237701 may also be attributed to the collateral PLK inhibition of these compounds at the high concentration that the assay was performed at. The apparent toxicity of inhibition of the dark kinases CDKL5 and ICK by JNK-IN-7 and BI00036838 may also be due to the inhibition of the other kinase targets of these two inhibitors (Table S1).

2.7. Cell Growth

To further document the effect of KGCS on cell viability, we performed assays for cell growth [32] in 16 immortalized cell lines that were selected to cover breast, ovarian, prostate, colorectal, lung, skin, brain, and pancreatic cancers (Table S5). Nonmalignant breast and lung cell lines were included for comparison. Using a 1 μL aliquot of KCGS (10 mM in DMSO), the set was screened in duplicate across the 18 cell lines at a compound concentration of 1 μM. The effects on cell growth, viability and cell cycle were determined after 72 h treatment using high-throughput microscopy [33]. Growth rate (GR) inhibition values, employed to account for variable division times, were computed [34]. GR values below zero are indicative of net cell loss whereas values between zero and one can result from growth arrest or a combination of cell death and proliferation over the assay duration. Therefore, the fraction of dead cells and the cell cycle distribution of the live cells were determined (Table S6). One cell line (SW1783) did not grow under the assay conditions and was excluded from analyses (Table S6). The effect of KCGS across the remaining 17 cell lines is depicted in Figure 5.
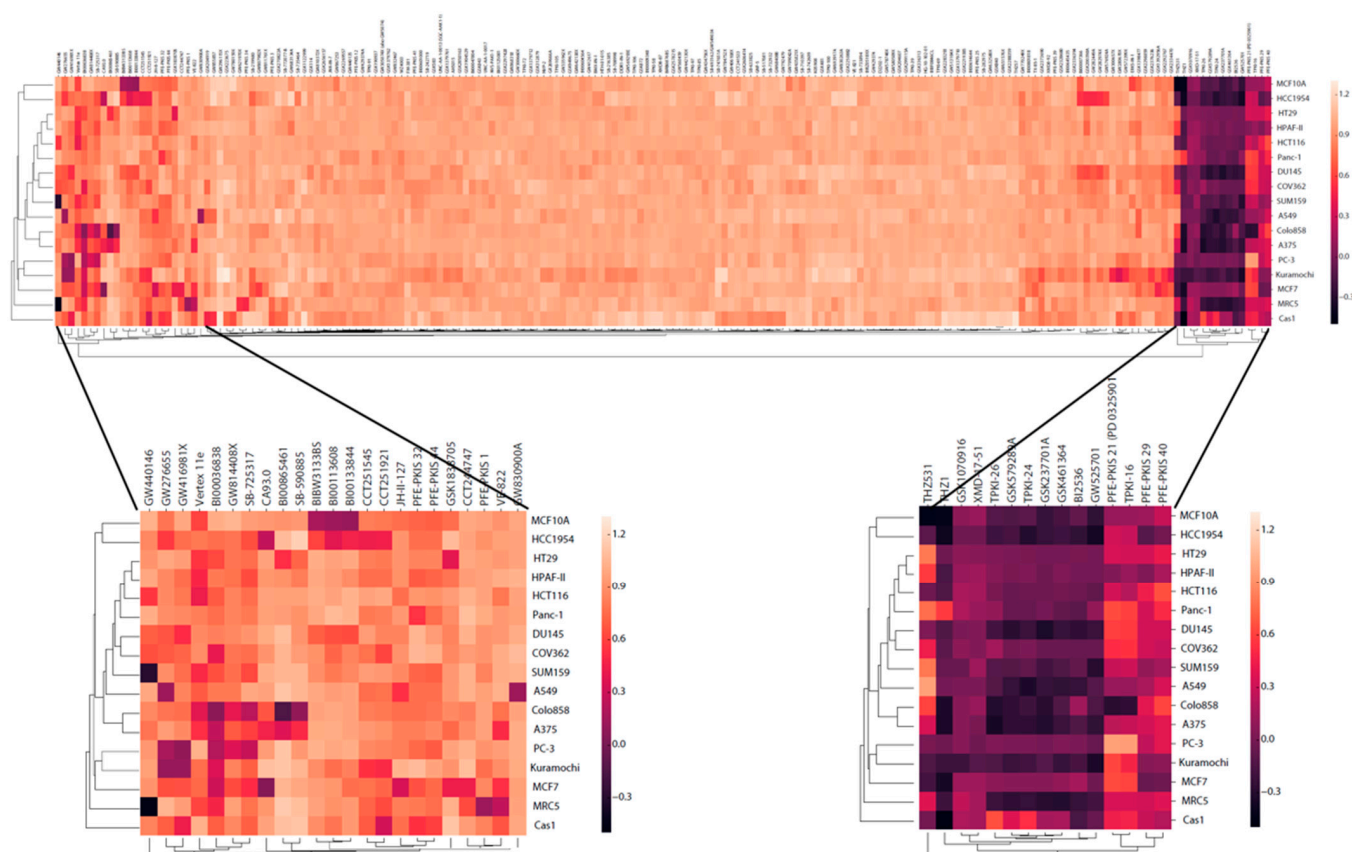
Figure 5. The kinase inhibitors in KCGS have different effects on cell growth across a wide range of lines. Normalized growth rate (GR) inhibition values were determined at 72 h post compound treatment. Each row displays data from a single cell line. Each column displays data from a single compound. GR is colored from −0.5 in black to 1.3 in yellow. The expanded views display data for compounds that showed cell-line selective decrease in GR and relatively cell-line independent effects, respectively.

Analysis of GR across the 17 cell lines identified three categories of kinase inhibitors. The first category included the majority of inhibitors in KCGS that showed no discernable effect on cell growth, with GR values within 10% of the DMSO control. The second category containing 15 inhibitors showed a >30% decrease in GR across most of the cell lines. Six of these compounds (TPKI-24, TPKI-26, GSK461364, GSK579289A, GSK237701A, and BI2536) have PLK inhibitory activity, two are allosteric MEK inhibitors (PFE-PKIS 21 and TPKI-16), and two are inhibitors of aurora kinases (XMD-17-51 and GSK1070916). Notably, only two of these inhibitors (THZ531 and PFE-PKIS 29) were shown to be cytotoxic at a higher concentration in the HeLa cell experiment. The third category contained 23 inhibitors that showed cell line-dependent effects on GR. Six of these compounds (GW416981, BI00036838, GW814408X, SGK-GAK-1 (CA93.0), CCT244747, and VE-882) have been identified as toxic to HeLa cells, but when tested at 1 μM across a wider range of lines their effects were now shown to be dependent on other cellular factors and not intrinsic to the compounds alone. Based on the annotation of these compounds, inhibition of several kinases was highlighted as being responsible for cell line-dependent effects. These kinases include multiple CDK isozymes, GAK, BRAF, and BLK. Determination of whether selective inhibition of these kinases would have potential therapeutic utility in specific cancers will require confirmatory follow-up studies such as CRISPR dropout screens and screening of alternate inhibitors of the same targets. However, these data highlight the power of screening a chemically and biologically diverse chemogenomic set of kinase inhibitors to determine how they perturb a simple cell phenotype.

2.8. Kinases Linked to Autophagy

Autophagy is a central mechanism that helps maintain cellular homeostasis. Autophagy is activated in response to different stress conditions such as starvation, protein aggregation, oxidative stress, bacterial infection, inhibition of the TOR1 pathway, and others [35,36]. To determine the effect of kinases on autophagic flux, the KCGS library was screened at 1 μM concentration in RPE1 cells stably expressing the autophagic flux reporter construct GFP-LC3B-RFP-LC3BΔC [37] (Figure 6). The cells were monitored in a time-dependent manner so that the ratio of GFP/RFP intensity ratio represented the level of autophagic flux. The averaged GFP/RFP ratio was subsequently normalized to time point 0 h in order to facilitate easy visualization of differences to the autophagy control compounds Torin1 (inducer) and Torin1 plus Bafilomycin A (inhibitor and deacidifier of lysosomes) compared to the DMSO vehicle control (Table S7).
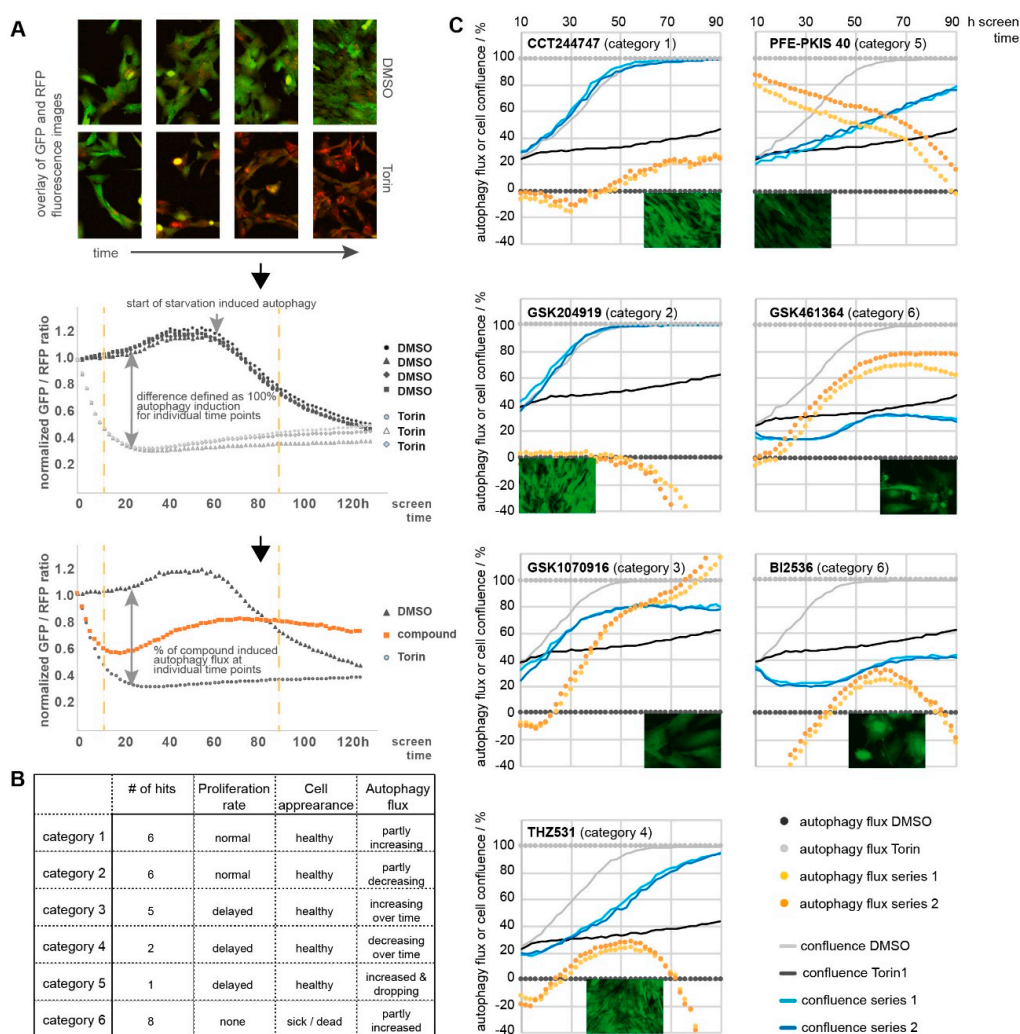

Figure 6. Autophagic flux assay. Compounds (1 μM) were analyzed for their effect on autophagy flux in RPE1 cells stably expressing the general autophagy flux reporter GFP-LC3B-RFP-LC3ΔC. Phase contrast as well as fluorescent images (GFP, RFP) were taken at indicated time points. (**A**) Ratio of the GFP/RFP signal correlating with high (Torin1; defined as 100%) and low (DMSO; defined as 0%) autophagy flux. Compound-induced changes in autophagic flux are represented as percentage of this difference. Small black arrows indicate assay workflow (**B**) Hits are defined as compounds showing > 20% aberration of the GFP/RFP ratio compared in five or more consecutive time points and categorized according to their cell proliferation rate as well as visual appearance. (# = number) (**C**) Examples of compounds with an effect on autophagic flux. Cell confluence is presented as percentage of covered growth area. Visual appearance of cells and cell confluence were ascertained by examining fluorescent images of the GFP channel at 96 h screen time. Graphs contain the individual average of experiments run in triplicate at two different times.

As expected, DMSO-treated cells had a stable level of autophagic flux until nutrients in the media were depleted and they entered a starvation-induced phase of autophagy induction. In contrast, the GFP/RFP ratio of Torin1-treated cells rapidly decreased within the first screening hours and stayed low over the complete time period of the five-day screening. Of note, treatment with Torin I caused an arrest of cell proliferation but no cell death. Confluence analysis was based on phase contrast images corresponding to the cell-covered area of each well. In this assay, cell health can only be assessed based on visual appearance of the cells and cell proliferation.

Hits were defined as compounds that showed >20% aberration of the GFP/RFP ratio in at least five or more consecutive time points, equivalent to a 10 h assay window. Hits were grouped in six categories based on the increase or decrease in proliferation rate, cell appearance and autophagy flux, respectively (detailed in Figure 6). Category 1 hits included GW416981X, a potent CDK1–3 inhibitor. The CDK inhibitors roscovitine and purvalanol have previously been shown to induce autophagy [38]. Likewise, CHK1 inhibition, represented by the category 1 hit CCT244747, has previously been linked to autophagy induction [39]. However, we also identified several new potential kinase targets for autophagy. For example, GSK204919, a potent dual PRKD1/2 inhibitor, caused a reduction in autophagic flux. The role of PRKD in autophagy has not been well-documented. Additional studies are required to link the observed autophagy reduction to PRKD inhibition rather than another kinase target of GSK204919 (e.g., JAK). Categories 3 and 5 compounds contained inhibitors of kinases known to induce autophagy, such as GSK1070916 (an aurora kinase [40] inhibitor) and PFE-PKIS 40 (a PI3K and mTOR [41] inhibitor). Notably, the RPE-1 cells used in the screen did not show any reduction in cell proliferation at 1 μM PFE-PKIS 40, despite its toxicity at 10 μM in HeLa cells (see above). The behavior of the category 4 compounds THZ531 (CDK inhibitor) and PFE-PKIS 29 (mTOR inhibitor) likely resulted from overlap of autophagy induction with cell toxicity as already identified in the cell health and cell growth assays. Most of the compounds in category 6 have also been identified in the cell growth assays, including several inhibitors with activity on PLK (TPKI-24, TPKI-26, GSK461364, GSK579289A, GSK237701A, and BI2536), a kinase known to regulate both autophagy as well as mitosis [42].

3. Discussion

KCGS version 1.0 is currently the best publicly available set of well-annotated potent and selective kinase inhibitors. All of the inhibitors have narrow selectivity profiles as ascertained from screening across an assay panel covering the majority of the human protein kinases. The set can be obtained by any investigator who agrees to the open science principles of not restricting its use by others and also promises to publish the results of their screen (Supplementary File S1). This manuscript describes the chemical structure and kinase annotation of all of the inhibitors in the current set. We recognize that there is additional room for improvement in the breadth (more kinases) and depth (more chemotypes per kinase) of kinase coverage and in the biological annotation of the set. However, initial characterization of KCGS in phenotypic screens confirmed the utility of the set for chemogenomic exploration of kinase signaling. Screening across 18 cell lines identified a subset of compounds that selectively inhibit their growth. Some of these compounds point to dark kinases that have received little attention as potential drug targets. A screen for autophagy uncovered additional kinase pathways that warrant further exploration. The narrow spectrum kinase activity of the individual inhibitors and the accompanying annotation supports rapid identification of target kinases for additional studies. While the compounds are generally nontoxic, we recommend that KGCS is screened at a maximum concentration of 1 μM in cells to minimize the potential for inhibition of additional kinases or off-target toxicity.

Several ongoing activities will support KCGS, which remains as the best publicly available set of kinase inhibitors. One such activity was obtaining screening data on all KCGS compounds in the same assay format. This would ensure that results were

comparable and offers the possibility of providing new kinase coverage. With about a quarter of the set originating in PKIS, which was only screened at Nanosyn, we had an opportunity to further profile these compounds in another 200 kinase assays by utilizing DiscoverX scanMAX. This screening was recently performed at a screening concentration of 1 μM (Table S8) for direct comparison to previously published data [15]. For some compounds, we identified new kinase binding partners in the additional assays while for others we did not. For example, GSK270822A and GSK299115A, both amino indazoles, were previously identified as ROCK1 inhibitors when profiled at Nanosyn [15]. When screened more broadly, these compounds were also found to bind to ROCK2, JAK2, JAK3, TYK2, NUAK2, and LATS2 ≥ 25 PoC. All these results need to be verified as true positives via Kd determination and this work is ongoing. The addition of ROCK2 is perhaps not surprising due to its homology to ROCK1. The inhibition of NUAK2, if confirmed, provides another chemotype to use to study the biology of this understudied kinase. GW814408X is a KCGS compound that based on original PKIS data only demonstrated potent binding to a single kinase (AURKC). Upon further screening, this compound was found to inhibit a number of other kinases. We will determine Kd values for new kinase hits for all KCGS version 1.0 compounds discovered with this new screening. If compounds fall outside our desired selectivity window, they will be replaced in future releases.

Currently, 51% of the screenable kinome, as defined by the DiscoverX scanMAX, is covered by KCGS version 1.0 for a total of 215 human kinases. Over 100 of these kinases were selectively inhibited by two or more chemotypes in the set. Our originally stated goal was to cover all human kinases with two or more chemotypes, so additional inhibitors are still required for those kinases that are covered by only single chemotype. There are an additional 250 "gap kinases" where we are still seeking an inhibitor that meets our minimal potency and selectivity criteria for inclusion in the set. For many of the gap kinases that are routinely screened in the DiscoverX scanMAX, identification of a nonpromiscuous inhibitor is the primary challenge but may be achievable through iterative medicinal chemistry to improve selectivity. Additionally, there are over 50 human kinases for which robust biochemical screening assays are not readily accessible in any format. For these kinases, it is not yet known if useful inhibitors already exist in the current set or among molecules that are in the public domain. Many of these dark kinases are difficult to express and purify or represent pseudokinases with little or no catalytic activity. Development of new screening formats or assay methodologies will be required to identify a complete set of inhibitors for the whole kinome.

One limitation to the design and selection of the inhibitors in KCGS was the use of potency and selectivity data from cell-free biochemical assays. The activity of kinase inhibitors in cells can be affected the binding of other cellular components to the kinase. In addition, some inhibitors may be less potent in cells if they are not efficient at crossing the cell membrane. However, the provenance of compounds included in KCGS, either from lead optimization programs in the pharmaceutical industry or the product of academic chemical probe development projects, suggests that most of them are likely to be cell active. In fact, the profile of physical properties across KCGS is as good if not better than a set of 52 FDA-approved kinase inhibitor drugs. Regardless, it is not uncommon for kinase inhibitors to demonstrate lower potency in cells than in cell-free assays. A recent advance in the application of NanoBRET technology to measure the target engagement of kinase inhibitors in living cells has provided a method to study this issue [43]. NanoBRET assays have now been developed for 133 of the human kinases that are inhibited by the molecules in KCGS version 1.0. By using these NanoBRET assays, we have begun the process of annotating each of the inhibitors in KCGS for its activity against its corresponding target kinase in live cells. These data will aid the deconvolution of phenotypic screening data of KCGS and identify kinases for which inhibitors with improved cell activities will be required in future releases.

The inhibitors in KCGS were sourced from multiple industrial and academic laboratories in a conscientious effort to maximize both the number of chemotypes (chemical

diversity) and the breadth of kinase coverage (biological diversity). While the core of the set is still composed of molecules that were published by GlaxoSmithKline chemists, KCGS version 1.0 contains inhibitors that originated from the laboratories of four pharmaceutical companies and three academic laboratories. We continue to seek new inhibitors to add to KCGS that represent either a new chemotype or an inhibitor of a gap kinase. To this end, we have completed profiling of molecules that have been donated by three additional companies as well as molecules synthesized in our laboratories and by academic collaborators. Inhibitors representing new chemotypes that increase the depth of coverage on many kinases will be made available as a supplemental set (KCGS version 1.1). Identification of potent and selective inhibitors of the gap kinases represents a more formidable yet surmountable challenge. We continue to welcome donations of candidate inhibitors of these kinases from industrial and academic laboratories to support expansion of the KCGS. All donor laboratories, in return, receive copies of the full KCGS set and the satisfaction of contributing to the goal of maintaining the best publicly available set of a high-quality kinase inhibitors.

4. Materials and Methods

4.1. KCGS

The current version of KCGS is available in 1 µL aliquots of a 10 mM DMSO solution at www.sgc-unc.org/request-kcgs/.

4.2. Kinase Assays

Compounds were screened at 1 µM using the KINOMEscan technology in the scanMAX assay panel of 401 wild-type human kinases and S_{10} was calculated as previously described [16]. Compounds with $S_{10} < 0.04$ were submitted for K_D measurement on kinases with POC < 20%. Compounds with $K_D < 100$ nM and S_{10} (1 µM) < 0.025 were selected as candidates for inclusion in KCGS.

4.3. Chemotype Binning

Each molecular substructure or bin representing the desired hinge-binder was manually codified in SMARTS language [26] and were given a priority order. Each molecule in KCGS was represented as a SMILES code. The SMARTS search was performed using Open Babel [44] to generate an .smi file to associate the SMILES code of each molecule with a specific SMARTS bin. All .smi files were processed in MATLAB [45] to create a compound–SMART matrix. Compounds with multiple matches were assigned to bin that corresponded to the highest priority SMARTS.

4.4. Cytotoxicity Assays

A triple staining high content screen was performed as previously described [30,31]. HeLa cells exposed to KCGS compounds at 10 µM for 24 h were stained with the three dyes: Hoechst 33342 (1 µM), Yo-Pro 3 (1 µM) and Annexin V (0.3 µL per well) for 1 h. Cellular fluorescence was measured using the CQ1 high content imaging system (Yokogawa, Sugarland, TX, USA) with the following setup parameters: Brightfield transmitted light at 70% for 50 ms; Hoechst 33342 was excited by 100 ms exposure; Ex 405 nm/Em 447/60 nm, Yo-Pro 3 by 100 ms exposure; Ex 561 nm/Em 617/73 nm and Annexin V (Alexa 488, ThermoFisher, Waltham, MA, USA) by 50 ms exposure; Ex 488 nm/Em 525/50 nm. All data were analyzed by the Pathfinder software and four categories for cells were designated: healthy cells, early apoptosis, late apoptosis, and necrosis. Each category was calculated as a percentage for every inhibitor. Cell nuclei were classified as either healthy, pyknosed, or fragmented.

4.5. Cell Growth Assays

The KCGS library compounds were arrayed in a 384-well plate at a concentration of 1 mM. Four breast cell lines, (SUM159, MCF7, MCF10A (nonmalignant), and HCC1954),

and two each of ovarian (COV362 and KURAMOCHI), prostate (PC-3 and DU145), colorectal (HT29 and HCT116), lung (A549 and MRC-5), melanoma (COLO858 and A375), glioblastoma (Cas1 and SW1783), and pancreatic (Panc-1 and HPAF-II) cancer cell lines were maintained in their recommended growth media at 37 °C in 5% CO_2, and were seeded in 384-well CellCarrier plates (Perkin Elmer, Waltham, MA, USA) at the densities listed in Table S5. Cells were allowed to adhere for 24 h and treated in duplicate with the KCGS library by pin transfer for a final concentration of 1 μM. Cells were stained and fixed at the time of pin transfer and following 72 h of treatment. Cells were pulsed for one hour with EdU (Lumiprobe, Hunt Valley, MD, USA) and stained with 1:2000 LIVE/DEAD Far Red Dead Cell Stain (LDR) (Thermo Fisher Scientific, Waltham, MA, USA). Cells were then fixed with 3.7% formaldehyde (Sigma Aldrich, St. Louis, MO, USA) for 30 min and permeabilized with 0.5% Triton X-100 in PBS. The EdU was labeled with cy3-azide (Lumiprobe, Hunt Valley, MD, USA) for 30 min. The cells were then blocked for one hour with Odyssey blocking buffer (LI-COR, Lincoln, NE, USA), and stained overnight at 4 °C with 2 μg/mL Hoechst 33342 (Sigma Aldrich, St. Louis, MO, USA) and a 1:1000 dilution of anti-phospho-histone H3 (pHH3) Alexa 488 (Ser10, clone D2C8) conjugated antibody (Cell Signaling Technologies, Danvers, MA, USA). Fixed cells were imaged with a 10x objective using an IXM-C microscope and analyzed using MetaXpress software (Molecular Devices, San Jose, CA, USA). Nuclei were segmented based on their Hoechst signals. DNA content, defined by the total Hoechst intensity within the nuclear mask, was used to identify cells in the G1 and G2 phases of the cell cycle. The average LDR, EdU and phospho-histone H3 intensities within the nuclear masks were determined and used to classify cells as dead, in S phase or in M phase, respectively. Cells with intermediate DNA content and no EdU signal were classified as S phase dropout cells. Live cell counts were normalized to DMSO-treated controls on the same plates to yield normalized growth rate inhibition (GR) values as described previously [32].

4.6. Autophagy Assays

RPE1 cells (1500 cells/well in 50 μL DMEM/F12, 10% FBS, and 1% P/S) stably expressing the GFP-LC3-RFP-LC3ΔC autophagy flux reporter [37] were seeded in 384-well plates and grown for approximately 18 h. In total, 50 μL media with 2× compound concentration were added and plates were subsequently placed and monitored in an IncuCyte® (Sartorius, Bohemia, NY, USA) instrument. Cells were scanned at indicated times for phase contrast and fluorescence intensity (GFP and RFP) to obtain information about confluence and autophagic flux, respectively. Hits are defined as compounds showing > 20% aberration of the GFP/RFP ratio compared to the control compounds DMSO (0.1%) and Torin1 (250 nM) in at least 5 or more consecutive time points (equivalent to 10 h screening time). Compounds were tested in triplicate and the complete screen was performed twice.

5. Conclusions and Future Directions

The KCGS is the largest fully annotated set of selective small molecule kinase inhibitors that is accessible to the biomedical scientific community to explore the involvement of kinases in a broad range of human pathologies and cellular pathways. The library is available in an arrayed 384-well format to support phenotypic screening in academic screening facilities and well-equipped laboratories to conduct target identification, mechanistic, synergy, synthetic lethality, and repurposing screens. Biological annotation of a common set of diverse kinase inhibitors will deepen our understanding of the role of kinases in cell signaling and may uncover new targets for drug discovery programs and precursors to new medicines.

Importantly, the set is a key resource supporting the expansion of the druggable genome. For example, kinases have been shown to play a pivotal role in many aspects of cancer physiopathology and have been a highly productive protein family for the treatment of several cancers [46,47]. A highly annotated small molecule library can be employed to comprehensively investigate the role of kinases in cancer biology. Indeed, the

Target Discovery Institute (TDI), a collaborative cell-based phenotypic screening facility established at the University of Oxford, Nuffield Department of Medicine, to identify more tractable biological targets for potential drug development, has used the KCGS in a range of cancer screens, including combinatorial screens with proteins involved in DNA repair including ATM, SPRTN, FancD2, SETD2, and KMT2D, and pathways involved in ubiquitin-mediated proteolysis, and mRNA dysregulation. The TDI also plans to employ the KCGS library in future combinatorial screens with temazolamide and radiotherapy (ionizing radiation) in glioblastomas. This research has generated its first manuscript from a screen which revealed a striking synthetic lethality between Chk1 inhibition and cyclin F loss [48]. Additionally, several of these ongoing projects have generated very encouraging validated primary hits and, although they will require vigorous follow-up validation, the results highlight the great utility and potential of the KCGC library to uncover novel anticancer targets.

Finally, it is important to acknowledge the potential for employing the KCGS in even more diverse disease-relevant phenotypic screening campaigns across additional human pathologies. Although kinases are heavily targeted in cancer treatment, kinases have also been implicated as causative genes in amyotrophic lateral sclerosis [49], the pathogenesis of Parkinson's Disease [50], and cardiac disfunction [51], to name a few. By providing open access to the KCGS to a diverse range of biomedical research scientists, the potential to accelerate drug target discovery, identify novel kinase mechanisms, and identify kinase vulnerabilities beyond cancer therapeutics is greatly increased.

of our chemogenomic sets PKIS and PKIS2. These end users have provided valuable feedback that guides our work. Their creative use of the sets provides inspiration to continue down this path so that with ever improving tools the scientific community can link targets to phenotypes and to disease, and through these collaborative efforts identify new targets that will lead to medicines for patients.

References

1. Roskoski, R., Jr. FDA-Approved Small Molecule Protein Kinase Inhibitors. Available online: http://www.brimr.org/PKI/PKIs.htm (accessed on 1 December 2020).
2. Morphy, R. Selectively nonselective kinase inhibition: Striking the right balance. *J. Med. Chem.* **2010**, *53*, 1413–1437. [CrossRef] [PubMed]
3. Ferguson, F.M.; Gray, N.S. Kinase inhibitors: The road ahead. *Nat. Rev. Drug Discov.* **2018**, *17*, 353–377. [CrossRef] [PubMed]
4. Knapp, S.; Arruda, P.; Blagg, J.; Burley, S.; Drewry, D.H.; Edwards, A.; Fabbro, D.; Gillespie, P.; Gray, N.S.; Kuster, B.; et al. A public-private partnership to unlock the untargeted kinome. *Nat. Chem. Biol.* **2013**, *9*, 3–6. [CrossRef] [PubMed]
5. Fedorov, O.; Muller, S.; Knapp, S. The (un)targeted cancer kinome. *Nat. Chem. Biol.* **2010**, *6*, 166–169. [CrossRef]
6. Edwards, A.M.; Isserlin, R.; Bader, G.D.; Frye, S.V.; Willson, T.M.; Yu, F.H. Too many roads not taken. *Nature* **2011**, *470*, 163–165. [CrossRef]
7. Oprea, T.I.; Bologa, C.G.; Brunak, S.; Campbell, A.; Gan, G.N.; Gaulton, A.; Gomez, S.M.; Guha, R.; Hersey, A.; Holmes, J.; et al. Unexplored therapeutic opportunities in the human genome. *Nat. Rev. Drug Discov.* **2018**, *17*, 377. [CrossRef]
8. Klaeger, S.; Heinzlmeir, S.; Wilhelm, M.; Polzer, H.; Vick, B.; Koenig, P.A.; Reinecke, M.; Ruprecht, B.; Petzoldt, S.; Meng, C.; et al. The target landscape of clinical kinase drugs. *Science* **2017**, *358*. [CrossRef]
9. Christmann-Franck, S.; van Westen, G.J.; Papadatos, G.; Beltran Escudie, F.; Roberts, A.; Overington, J.P.; Domine, D. Unprecedently Large-Scale Kinase Inhibitor Set Enabling the Accurate Prediction of Compound-Kinase Activities: A Way toward Selective Promiscuity by Design? *J. Chem. Inf. Model.* **2016**, *56*, 1654–1675. [CrossRef]
10. Arrowsmith, C.H.; Audia, J.E.; Austin, C.; Baell, J.; Bennett, J.; Blagg, J.; Bountra, C.; Brennan, P.E.; Brown, P.J.; Bunnage, M.E.; et al. The promise and peril of chemical probes. *Nat. Chem. Biol.* **2015**, *11*, 536–541. [CrossRef]
11. Jones, L.H.; Bunnage, M.E. Applications of chemogenomic library screening in drug discovery. *Nat. Rev. Drug Discov.* **2017**, *16*, 285–296. [CrossRef]
12. Gautam, P.; Jaiswal, A.; Aittokallio, T.; Al-Ali, H.; Wennerberg, K. Phenotypic Screening Combined with Machine Learning for Efficient Identification of Breast Cancer-Selective Therapeutic Targets. *Cell Chem. Biol.* **2019**, *26*, 970–979.e974. [CrossRef] [PubMed]
13. Bamborough, P.; Drewry, D.; Harper, G.; Smith, G.K.; Schneider, K. Assessment of chemical coverage of kinome space and its implications for kinase drug discovery. *J. Med. Chem.* **2008**, *51*, 7898–7914. [CrossRef] [PubMed]
14. Posy, S.L.; Hermsmeier, M.A.; Vaccaro, W.; Ott, K.H.; Todderud, G.; Lippy, J.S.; Trainor, G.L.; Loughney, D.A.; Johnson, S.R. Trends in Kinase Selectivity: Insights for Target Class-Focused Library Screening. *J. Med. Chem.* **2011**, *54*, 54–66. [CrossRef] [PubMed]
15. Elkins, J.M.; Fedele, V.; Szklarz, M.; Abdul Azeez, K.R.; Salah, E.; Mikolajczyk, J.; Romanov, S.; Sepetov, N.; Huang, X.-P.; Roth, B.L.; et al. Comprehensive characterization of the Published Kinase Inhibitor Set. *Nat. Biotech.* **2016**, *34*, 95–103. [CrossRef] [PubMed]
16. Drewry, D.H.; Wells, C.I.; Andrews, D.M.; Angell, R.; Al-Ali, H.; Axtman, A.D.; Capuzzi, S.J.; Elkins, J.M.; Ettmayer, P.; Frederiksen, M.; et al. Progress towards a public chemogenomic set for protein kinases and a call for contributions. *PLoS ONE* **2017**, *12*, e0181585. [CrossRef]
17. Drewry, D.H.; Wells, C.I.; Zuercher, W.J.; Willson, T.M. A Perspective on Extreme Open Science: Companies Sharing Compounds without Restriction. *SLAS Discov.* **2019**, *24*, 505–514. [CrossRef]
18. Moret, N.; Clark, N.A.; Hafner, M.; Wang, Y.; Lounkine, E.; Medvedovic, M.; Wang, J.; Gray, N.; Jenkins, J.; Sorger, P.K. Cheminformatics Tools for Analyzing and Designing Optimized Small-Molecule Collections and Libraries. *Cell Chem. Biol.* **2019**, *26*, 765–777.e763. [CrossRef]
19. Edwards, A.; Morgan, M.; Al Chawaf, A.; Andrusiak, K.; Charney, R.; Cynader, Z.; ElDessouki, A.; Lee, Y.; Moeser, A.; Stern, S.; et al. A trust approach for sharing research reagents. *Sci. Transl. Med.* **2017**, *9*. [CrossRef]
20. The Structural Genomics Consortium. Available online: www.thesgc.org (accessed on 1 December 2019).

21. Fabian, M.A.; Biggs, W.H., 3rd; Treiber, D.K.; Atteridge, C.E.; Azimioara, M.D.; Benedetti, M.G.; Carter, T.A.; Ciceri, P.; Edeen, P.T.; Floyd, M.; et al. A small molecule-kinase interaction map for clinical kinase inhibitors. *Nat. Biotechnol.* **2005**, *23*, 329–336. [CrossRef]

22. DiscoverX. scanMAX. Available online: https://www.discoverx.com/services/drug-discovery-development-services/kinase-profiling/kinomescan/scanmax (accessed on 1 December 2019).

23. Manning, G.; Whyte, D.B.; Martinez, R.; Hunter, T.; Sudarsanam, S. The Protein Kinase Complement of the Human Genome. *Science* **2002**, *298*, 1912–1934. [CrossRef]

24. Zwick, M.; Kraemer, O.; Carter, A.J. Dataset of the frequency patterns of publications annotated to human protein-coding genes, their protein products and genetic relevance. *Data Brief* **2019**, *25*, 104284. [CrossRef] [PubMed]

25. Carter, A.J.; Kraemer, O.; Zwick, M.; Mueller-Fahrnow, A.; Arrowsmith, C.H.; Edwards, A.M. Target 2035: Probing the human proteome. *Drug Discov. Today* **2019**, *24*, 2111–2115. [CrossRef] [PubMed]

26. DAYLIGHT Chemical Information Systems. Available online: www.daylight.com/dayhtml/doc/theory/theory.smarts.html (accessed on 1 December 2019).

27. Daina, A.; Michielin, O.; Zoete, V. SwissADME: A free web tool to evaluate pharmacokinetics, drug-likeness and medicinal chemistry friendliness of small molecules. *Sci. Rep.* **2017**, *7*, 42717. [CrossRef] [PubMed]

28. Roskoski, R., Jr. Properties of FDA-approved small molecule protein kinase inhibitors. *Pharmacol. Res.* **2019**, *144*, 19–50. [CrossRef]

29. Varma, M.V.; Obach, R.S.; Rotter, C.; Miller, H.R.; Chang, G.; Steyn, S.J.; El-Kattan, A.; Troutman, M.D. Physicochemical space for optimum oral bioavailability: Contribution of human intestinal absorption and first-pass elimination. *J. Med. Chem.* **2010**, *53*, 1098–1108. [CrossRef]

30. Montenegro, R.C.; Clark, P.G.; Howarth, A.; Wan, X.; Ceroni, A.; Siejka, P.; Nunez-Alonso, G.A.; Monteiro, O.; Rogers, C.; Gamble, V.; et al. BET inhibition as a new strategy for the treatment of gastric cancer. *Oncotarget* **2016**, *7*, 43997–44012. [CrossRef]

31. Howarth, A.; Schroder, M.; Montenegro, R.C.; Drewry, D.H.; Sailem, H.; Millar, V.; Muller, S.; Ebner, D.V. HighVia—A Flexible Live-Cell High-Content Screening Pipeline to Assess Cellular Toxicity. *SLAS Discov.* **2020**, *25*, 801–811. [CrossRef]

32. Hafner, M.; Niepel, M.; Chung, M.; Sorger, P.K. Growth rate inhibition metrics correct for confounders in measuring sensitivity to cancer drugs. *Nat. Methods* **2016**, *13*, 521–527. [CrossRef]

33. Mills, C.; Gerosa, L. Optimized Experimental and Analytical Tools for Reproducible Drug-Response Studies. Available online: http://lincs.hms.harvard.edu/wordpress/wp-content/uploads/2018/06/DoseResponseNanocourse_2018_Final.pdf (accessed on 1 December 2019).

34. Hafner, M.; Niepel, M.; Subramanian, K.; Sorger, P.K. Designing Drug-Response Experiments and Quantifying their Results. *Curr. Protoc. Chem. Biol.* **2017**, *9*, 96–116. [CrossRef]

35. Stolz, A.; Putyrski, M.; Kutle, I.; Huber, J.; Wang, C.; Major, V.; Sidhu, S.S.; Youle, R.J.; Rogov, V.V.; Dotsch, V.; et al. Fluorescence-based ATG8 sensors monitor localization and function of LC3/GABARAP proteins. *EMBO J.* **2017**, *36*, 549–564. [CrossRef]

36. Dikic, I.; Elazar, Z. Mechanism and medical implications of mammalian autophagy. *Nat. Rev. Mol. Cell Biol.* **2018**, *19*, 349–364. [CrossRef] [PubMed]

37. Kaizuka, T.; Morishita, H.; Hama, Y.; Tsukamoto, S.; Matsui, T.; Toyota, Y.; Kodama, A.; Ishihara, T.; Mizushima, T.; Mizushima, N. An Autophagic Flux Probe That Releases an Internal Control. *Mol. Cell* **2016**, *64*, 835–849. [CrossRef] [PubMed]

38. Ozfiliz-Kilbas, P.; Sarikaya, B.; Obakan-Yerlikaya, P.; Coker-Gurkan, A.; Arisan, E.D.; Temizci, B.; Palavan-Unsal, N. Cyclin-dependent kinase inhibitors, roscovitine and purvalanol, induce apoptosis and autophagy related to unfolded protein response in HeLa cervical cancer cells. *Mol. Biol. Rep.* **2018**, *45*, 815–828. [CrossRef] [PubMed]

39. Zhou, Z.R.; Yang, Z.Z.; Wang, S.J.; Zhang, L.; Luo, J.R.; Feng, Y.; Yu, X.L.; Chen, X.X.; Guo, X.M. The Chk1 inhibitor MK-8776 increases the radiosensitivity of human triple-negative breast cancer by inhibiting autophagy. *Acta Pharmacol. Sin.* **2017**, *38*, 513–523. [CrossRef]

40. Liu, Z.; Wang, F.; Zhou, Z.W.; Xia, H.C.; Wang, X.Y.; Yang, Y.X.; He, Z.X.; Sun, T.; Zhou, S.F. Alisertib induces G2/M arrest, apoptosis, and autophagy via PI3K/Akt/mTOR- and p38 MAPK-mediated pathways in human glioblastoma cells. *Am. J. Transl. Res.* **2017**, *9*, 845–873. [PubMed]

41. Wang, Y.; Zhang, H. Regulation of Autophagy by mTOR Signaling Pathway. *Adv. Exp. Med. Biol.* **2019**, *1206*, 67–83. [CrossRef]

42. Li, Z.Y.; Zhang, X. Kinases Involved in Both Autophagy and Mitosis. *Int. J. Mol. Sci.* **2017**, *18*, 1884. [CrossRef]

43. Vasta, J.D.; Corona, C.R.; Wilkinson, J.; Zimprich, C.A.; Hartnett, J.R.; Ingold, M.R.; Zimmerman, K.; Machleidt, T.; Kirkland, T.A.; Huwiler, K.G.; et al. Quantitative, Wide-Spectrum Kinase Profiling in Live Cells for Assessing the Effect of Cellular ATP on Target Engagement. *Cell Chem. Biol.* **2018**, *25*, 206–214.e211. [CrossRef]

44. Open Babel: The Open Source Chemistry Toolbox. Available online: http://openbabel.org/ (accessed on 1 December 2019).

45. MATLAB. Available online: https://www.mathworks.com/products/matlab.html (accessed on 1 December 2019).

46. Bhullar, K.S.; Lagaron, N.O.; McGowan, E.M.; Parmar, I.; Jha, A.; Hubbard, B.P.; Rupasinghe, H.P.V. Kinase-Targeted cancer therapies: Progress, challenges and future directions. *Mol. Cancer* **2018**, *17*, 48. [CrossRef]

47. Kannaiyan, R.; Mahadevan, D. A comprehensive review of protein kinase inhibitors for cancer therapy. *Expert. Rev. Anticancer Ther.* **2018**, *18*, 1249–1270. [CrossRef]

48. Burdova, K.; Yang, H.B.; Faedda, R.; Hume, S.; Chauhan, J.; Ebner, D.; Kessler, B.M.; Vendrell, I.; Drewry, D.H.; Wells, C.I.; et al. E2F1 proteolysis via SCF-cyclin F underlies synthetic lethality between cyclin F loss and Chk1 inhibition. *EMBO J.* **2019**, *38*. [CrossRef] [PubMed]

49. Guo, W.; Vandoorne, T.; Steyaert, J.; Staats, K.A.; Van Den Bosch, L. The multifaceted role of kinases in amyotrophic lateral sclerosis: Genetic, pathological and therapeutic implications. *Brain* **2020**, *143*, 1651–1673. [CrossRef] [PubMed]

50. Guttuso, T., Jr.; Andrzejewski, K.L.; Lichter, D.G.; Andersen, J.K. Targeting kinases in Parkinson's disease: A mechanism shared by LRRK2, neurotrophins, exenatide, urate, nilotinib and lithium. *J. Neurol. Sci.* **2019**, *402*, 121–130. [CrossRef] [PubMed]

51. Singh, R.M.; Cummings, E.; Pantos, C.; Singh, J. Protein kinase C and cardiac dysfunction: A review. *Heart Fail. Rev.* **2017**, *22*, 843–859. [CrossRef]

Strategy for Lead Identification for Understudied Kinases

David Drewry, Joel K. Annor-Gyamfi, Carrow Wells, Julie E. Pickett, Alison Axtman

In our manuscript we outline an approach in which we convert a promiscuous pyrimidine scaffold into narrowly selective, cell-active chemical leads for several understudied kinases, including DRAK1, BMP2K, and MARK4. These chemical tools will allow illumination of the function(s) of these poorly characterized kinases for the first time. Several of the understudied kinases that we inhibit with our pyrimidine-based compounds are also implicated in neurodegenerative disease, pushing the utility of kinase inhibitors outside of the oncology space and offering opportunities for the validation of therapeutic hypotheses attributed to these kinases.

File list (2)

Strategy for lead identification for understudied kinases Ch... (4.54 MiB)	view on ChemRxiv • download file
ChemRxiv pyrimidine SI.pdf (14.65 MiB)	view on ChemRxiv • download file

Strategy for lead identification for understudied kinases

David H. Drewry[1,2,3], Joel K. Annor-Gyamfi[1,2], Carrow I. Wells[1,2], Julie E. Pickett[1,2], Alison D. Axtman[*,1,2]

[1]Structural Genomics Consortium, UNC Eshelman School of Pharmacy, University of North Carolina at Chapel Hill, Chapel Hill, NC, 27599, USA

[2]Division of Chemical Biology and Medicinal Chemistry, UNC Eshelman School of Pharmacy, University of North Carolina at Chapel Hill, Chapel Hill, NC, 27599, USA

[3]UNC Lineberger Comprehensive Cancer Center, UNC Eshelman School of Pharmacy, University of North Carolina at Chapel Hill, Chapel Hill, NC, 27599, USA

ABSTRACT

The pyrimidine core has been utilized extensively to construct kinase inhibitors. In fact, 8 FDA-approved drugs targeting kinases bear a pyrimidine core that makes key hydrogen bond interactions with the crucial hinge region shared by most human kinases. Because the pyrimidine hinge-binding motif is accommodated by many kinases within the larger kinome, kinome-wide selectivity of resultant molecules can be poor. In our quest to create useful inhibitors for all human kinases, this liability was seen as an advantage since it is well tolerated by many understudied kinases. We hypothesized that small sets of non-exemplified pyrimidines based on selected literature examples would provide us with useful inhibitors of these lesser studied kinases. As proof of concept, we designed a small library of inhibitors that incorporated the side chains from some well-annotated pyrimidine-based kinase inhibitors of TBK1 that also displayed activity on understudied kinases of interest. Our strategy paired mixing and matching the side chains from the 2- and 4-positions of the parent compounds with modifications at the 5-position of the pyrimidine core, which is situated near the gatekeeper residue of the binding pocket. We reasoned that these targeted changes in three positions would provide sufficient structural diversity to uncover useful structure–activity relationships (SAR) for understudied kinases. Utilizing this approach, we imparted improved kinome-wide selectivity to most members of the resultant library. Importantly, we also identified potent biochemical and cell-active lead compounds that can be further developed into chemical probes for understudied kinases like DRAK1 and MARK3/4. Our studies demonstrate that pyrimidine-based kinase inhibitors can be converted to selective, cell-active inhibitors for lesser studied kinases. Furthermore, we provide a simple strategy that can be employed with other kinase scaffolds to identify tools for understudied kinases.

INTRODUCTION

Pyrimidines represent an important building block in the medicinal chemistry arsenal. Compounds bearing a pyrimidine core have proven to be bioactive and exhibit diverse pharmacology, including anti-convulsant, analgesic, sedative, anti-depressive, anti-pyretic, anti-inflammatory, anti-viral, anti-HIV, anti-microbial, and anti-tumor activities.[1] Pyrimidines are very useful as kinase scaffolds because the pyrimidine nitrogen and an NH in the 2-position make key hydrogen bonds with the conserved hinge region found in nearly all human kinases. To date, 8 FDA-approved kinase inhibitors employ a pyrimidine as the key kinase hinge-binding motif.[2]

The work we describe here stems from the synergistic convergence of two separate interests that were satisfied through diversification of the pyrimidine scaffold. The first of these interests centers around the generation and use of kinase inhibitors as tools to build deeper understanding of signaling in neurodegenerative disease. TBK1, a kinase with links to amyotrophic lateral sclerosis (ALS), frontotemporal dementia (FTD), Huntington's disease, and Alzheimer's disease (AD), is potently inhibited by a number of pyrimidine-bearing compounds.[3-12] A second interest of ours is identification of high-quality tool molecules for understudied kinase targets. Our pursuit of this interest relies on parallel chemical tool and kinase assay development, efforts that are supported in part by the NIH Illuminating the Druggable Genome (IDG) program. The IDG program aims to catalyze the characterization of all proteins through stimulating research around those that are most poorly studied.[13] One arm of the IDG program supports illumination of the dark kinome, which includes development of high-quality chemical tools for these understudied kinases. As we examined the data available for literature pyrimidine-based TBK1 inhibitors, we noticed a range of understudied kinases that were also inhibited by these compounds.

Several of the understudied kinases inhibited by pyrimidines also have been genetically implicated in driving neurodegenerative diseases. The MARK family of kinases, for example, phosphorylate tau protein in its repeat domain and thereby regulate its affinity for microtubules, affecting the aggregation of tau into neurofibrillary tangles. Observations of AD brains show a strong correlation between cognitive dysfunction and cortical neurofibrillary tangle density.[14-16] Mutations in tau have also been shown to cause a form of FTD.[16] Furthermore, with a characterized role in dendrite branching and spine development, understudied kinase AAK1 plays a role in several neurodegenerative disorders, including AD and
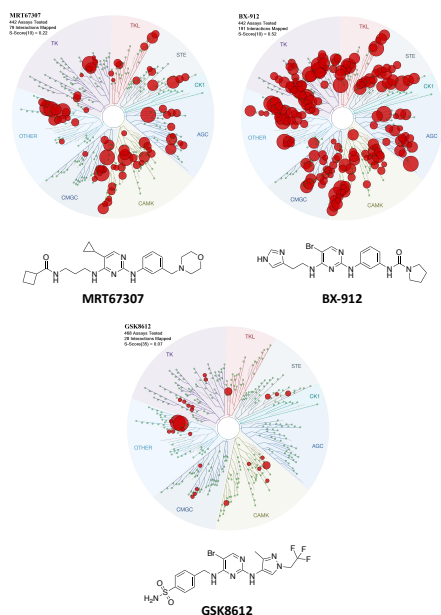
Figure 1. Structures and broad selectivity profiling of pyrimidine-based inhibitors that served as the basis for library design. All wild-type kinases inhibited >90% at 10 μM by MRT67307 and BX-912 and all wild-type kinases inhibited >65% at 1 μM by GSK8612 are shown.

Figure 1 shows the structures and kinome-wide profiling data generated at DiscoverX (*scan*MAX or KINOMEscan) for three TBK1-targeting pyrimidines.[19] The data for TBK1 inhibitors MRT67307 and BX-912 (designed for PDK1 but potent inhibitor of TBK1) is already in the literature (LINCS database).[20-24] These two compounds were screened at 10 μM (Figure 1). GSK8612 was recently disclosed by GlaxoSmithKline as a potent and selective TBK1 inhibitor.[25] We opted to survey the kinome-wise selectivity of GSK8612 at DiscoverX at 1 μM (Figure 1). While the screening concentrations are different, it is apparent that these scaffolds differentially and potently inhibit many kinases across the kinome, and that selectivity can be augmented through structural changes.

Several kinases potently inhibited by pyrimidines like BX-912, MRT67307, and/or GSK8612 are members of the IDG nominated list of dark kinases. Thus, this scaffold was considered an excellent starting point from which to design high-quality chemical tools. Development of these tools will enable elucidation of the function of those kinases that have suffered from a dearth of characterization, including those on the IDG list. Our high-quality chemical tools will also enable further characterization of kinase-mediated signaling in neurodegenerative disease and facilitate the validation of therapeutic hypotheses.

Table 1. Selectivity profiling data for pyrimidine library

| Cmpd | % control at 1 μM[b] | | | | | | | | | | | | | | | | # kinases ≤10% | S_{10}(1 μM)[d] | # kinases with PoC <10)[e] |
	AAK1	AURKB	BMP2K	DRAK1[c]	DRAK2[c]	IKKε	JAK2	MARK1[c]	MARK2	MARK3[c]	MARK4[c]	MLK1	MLK3	NUAK1	TBK1	ULK1			
3	90	82	96	107	59	95	123	71	90	96	88	72	91	73	81	78	0	0.005	2
4	61	102	73	25	13	12	99	79	93	96	100	78	94	82	4	58	1	0.027	11
5	101	102	94	105	88	43	100	108	100	111	110	90	89	97	10	106	1	0.005	2
6	12	7	7	58	39	32	3	66	65	68	61	25	34	23	4	50	4	0.047	19
7	7	38	19	5	5	1	67	8	19	35	27	21	36	22	-1	3	7	0.154	62
8	81	90	101	106	60	63	114	108	103	126	113	85	106	86	61	96	0	0.002	1
9	4	1	1	8	4	36	6	-3	5	16	3	-1	2	1	21	3	13	0.233	94
10	54	22	47	63	12	55	106	49	55	68	49	30	60	13	21	20	0	0.069	28
11	70	51	68	108	84	43	87	100	98	109	98	72	68	83	10	88	1	0.007	3
12	82	82	86	103	92	73	95	107	108	122	101	97	95	94	49	99	0	0.002	1
13	8	6	1	41	23	35	12	57	57	63	42	30	24	11	1	66	4	0.03	12
14	49	2	18	50	14	55	82	1	14	0	4	7	27	6	43	24	6	0.067	27
15	82	71	104	99	91	83	89	109	104	126	99	77	94	90	87	88	0	0	0
16	73	53	80	82	96	79	62	104	115	115	99	86	89	78	68	97	0	0.002	1
17	33	56	56	18	17	33	88	72	82	92	85	79	86	87	36	75	0	0.007	3
18	1	5	-1	0	0	-2	10	-6	2	-3	-1	0	-3	0	-2	2	16	0.223	90
19	61	48	51	93	96	78	54	102	102	113	98	81	95	79	33	92	0	0.007	3
20	59	5	58	78	65	80	81	75	93	78	68	73	82	14	50	85	1	0.022	9
21	73	61	64	79	77	52	107	94	93	112	89	89	72	89	6	82	1	0.002	1
22	12	11	8	2	3	3	68	-4	6	0	7	31	27	51	-4	17	9	0.074	30
MRT67307	6	5	3	3	7	4	46	-5	4	-1	5	19	38	31	-1	9	12	N.T.[a]	N.T.[a]
MRT68921	4	8	3	3	4	4	44	-1	3	-4	3	14	44	6	1	1	13	N.T.[a]	N.T.[a]
BX-795	2	3	1	2	4	2	6	-5	3	-4	2	4	1	2	-3	4	16	N.T.[a]	N.T.[a]
BX-912	5	2	2	6	1	44	24	-4	5	-1	2	5	2	1	10	6	14	N.T.[a]	N.T.[a]
GSK8612	37	87	30	93	47	23	70	90	89	105	79	80	82	58	5	77	1	0.02	8

[a]N.T.: not tested. [b]Compounds tested at a single concentration (1 μM) in duplicate. [c]IDG kinase; DRAK1 = STK17A and DRAK2 = STK17B. [d]S_{10}(1 μM): percentage of screened kinases with percent of control (PoC) values <10 at 1 μM. [e]Number of kinases with PoC values <10 at 1 μM.

RESULTS AND DISCUSSION

Compound Design and Synthesis. Our library design involved mixing and matching the side chains and cores from published pyrimidine-based inhibitors MRT67307, BX-912, and GSK8612 to furnish 21 total analogs. Specifically, we paired mixing and matching the side chains from the 2- and 4-positions of the parent compounds with modifications at the 5-position of the pyrimidine core as shown in the box in Scheme 1. Seven final compounds were prepared with X = H, seven with X = Br, and seven with X = cyclopropyl (Figure 2). Analogs of BX-912 and MRT67307 (and the parent compounds themselves) that varied only at the 5-position (box in Scheme 1) were not prepared. A great deal of effort has been dedicated to making close structural analogs of these two compounds and we did not want our work to be redundant. Since it was not commercially available at the time and the most selective of the parent scaffolds, GSK8612 and variants with X = H and cyclopropyl were all synthesized. The method used to prepare these analogs is outlined in Scheme 1. Briefly, taking advantage of the inherent reactivity of 2,4-dichloropyrimidines, iterative amine couplings were executed, and specific brominated compounds (GSK8612, **6**, **9**, **10**, and **13**) were subsequently dehalogenated to furnish all final compounds.

We had several expected outcomes from our strategy of mixing and matching the side chains and cores from well exemplified pyrimidine-based inhibitors. Firstly, we intended to develop more narrowly selective compounds by incorporating these distinct side chains and 5-position modifications into new compounds. Next, we wanted to generate preliminary SAR for several understudied kinases. In doing so we aimed to leverage these scaffolds with known inhibitory activity of dark kinases to identify more optimal chemical starting points for development of high-quality chemical tools. Finally, we wanted to develop focused SAR around the 5-position (box in Scheme 1), which has not been systematically investigated in the literature yet is proposed to play a key role in dictating both potency and selectivity due to its proximity to the kinase gatekeeper residue.

Scheme 1. Library design and preparation strategy. *Step A*: Pyrimidine 1, Amine 1, DIPEA, ethanol, -10°C to 50°C; *Step B*: Pyrimidine 2, Amine 2, Dioxane×HCl, butanol, 80°C; *Step C*: Pyrimidine 3, 5% Pd/C, H_2, TEA, methanol, r.t.
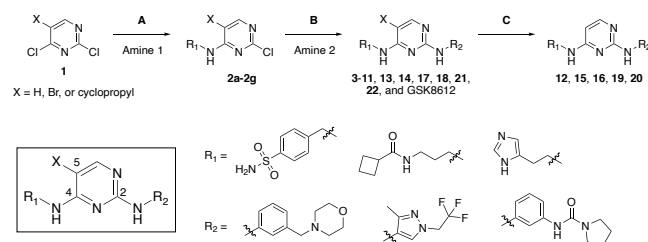
Targeted Kinase Selectivity Profiling. We selected a small panel of representative kinases against which to profile our library of 21 pyrimidine analogs. These kinases include some of the original targets for which pyrimidine-based inhibitors were prepared (JAK2, IKKε, TBK1, and ULK1), a more well-studied kinase that is potently inhibited by many analogs within this structural class (AURKB), and several understudied kinases, many of which are both on the IDG list (AAK1, BMP2K, DRAK1–2, MARK1–4, MLK1, MLK3, and NUAK1) and of interest in the neuroscience space.[14, 15, 17, 26-29] We profiled our pyrimidine series and the parent pyrimidines that influenced our design against this kinase panel at a single

concentration (1 μM) in radiometric enzymatic assays at Eurofins at the Km = ATP for each kinase. Table 1 shows the results of this study, where % control is reported for each compound for each kinase and lower values indicate greater inhibition. The column labeled "# ≤10%" captures the number of kinases in this 16-member panel inhibited ≥90% by each compound.

We found that, with the exception of 2 analogs, all compounds in our library were more selective in this custom kinase panel than published compounds BX-912, BX-795, MRT67307, and MRT68921.[20-23] In most cases we demonstrated a significant increase in selectivity. Gratifyingly, unlike the published compounds from the BX and MRT series that elicited potent inhibition of nearly all kinases in the panel, our compounds have cleaned-up profiles and we were able to dial out inhibition of certain kinases through structural modification. We were pleased to observe potent inhibition of several understudied kinases by some of our more selective analogs, including BMP2K by **6**; AAK1, DRAK1, DRAK2, and MARK1 by **7**; AAK1 and BMP2K by **13**; and MARK1, MARK3, MARK4, MLK1, and NUAK1 by **14**.
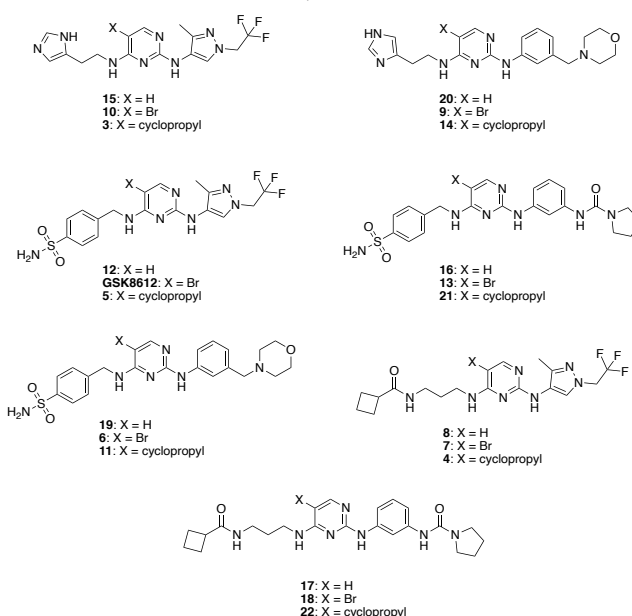
Figure 2. Library of pyrimidine analogs prepared.

When we examined the data generated via screening in the Eurofins kinase panel versus compound structures for our synthetic library, we noticed some predominating trends. When varying the 5-position (X in Figure 2), the greatest number of kinases were tolerant of the bromo substituent and thus those analogs bearing X = Br inhibited the most kinases. When X = Br, an average of 6.4 kinases were inhibited ≥90% (range of 0–16 kinases). Switching to X = H resulted in the most selective compounds in the series, with an average of only 0.1 kinases demonstrating ≥90% inhibition in the Eurofins panel at 1 μM (range of 0–1 kinase). Finally, cyclopropyl at position X was somewhere between H and Br in terms of selectivity, with an average of 2.7 kinases inhibited ≥90% (range of 0–9 kinases). When considering the amine side chains in the 2- and 4-positions, some general selectivity trends were also observed. Incorporation of the sulfonamide-bearing side chain in the pyrimidine 4-position (R_1 position, Scheme 1) resulted in the most selective compounds, inhibiting an average of 1.3 kinases ≥90% at 1 μM (range of 0–4 kinases). In the pyrimidine 2-position, the R_2 substituent that yielded the most selectivity within the panel is the substituted

pyrazole, which inhibited an average of 1.1 kinases ≥90% (range of 0–7 kinases). The ortho-methyl group on the pyrazole ring likely contributes to this enhanced selectivity when compared to other side chains at the R_2 position.

Library-wide Cellular Target Engagement Studies. The data generated by screening our pyrimidine analogs in the panel of kinases at Eurofins motivated follow-up cell-based studies. We used cellular target engagement assays to determine whether potent enzyme inhibition corresponded with potent binding in cells. The NanoBRET assay offers a method through which cellular penetrance and binding of a compound to its kinase target in cells can be simultaneously assessed.[30] Given the consistently potent inhibition of TBK1 by nearly all compounds in our library (Table 1) and our interest in this kinase, we profiled the entire library using the TBK1 NanoBRET assay in dose–response format (Table 2). We found that potent enzymatic inhibition of TBK1 did not always translate to potent engagement of TBK1 in cells. All compounds that demonstrated 50% inhibition at 10 μM when tested using the TBK1 NanoBRET assay in the first dose–response experiment were followed up with two additional replicates. Two members of our library, 7 and 18, and GSK8612 demonstrated sub-micromolar IC_{50} values in the TBK1 NanoBRET assay. The validation of GSK8612 as a potent, cell-active compound targeting TBK1 aligns well with the recent publication that described its development and characterization.[25]

Shifting our attention to understudied kinases, we also observed that some of our compounds potently inhibited DRAK1, MARK3, and MARK4. As part of the IDG program, we have interest in developing high-quality chemical tools to help elucidate the function of these poorly characterized kinases. For our pyrimidine series, dose–response NanoBRET analysis yielded 5 analogs (4, 7, 9, 18, and 22) and MRT67307 with sub-micromolar activity in the DRAK1 NanoBRET assay. We repeated NanoBRET dose–response on these six compounds and found all to maintain activity over three replicates. Finally, the entire series was tested in the MARK3 and MARK4 NanoBRET assays. We found 4 compounds (9, 14, 18, and 22) with sub-micromolar IC_{50} values in the MARK4 NanoBRET assay, 2 of which (9 and 18) also demonstrated sub-micromolar IC_{50} values in the MARK3 NanoBRET assay. Several of the parent compounds also had sub-micromolar IC_{50} values in the MARK3/4 NanoBRET assays. Based on our 16-kinase enzyme inhibition panel (Table 1), we felt confident that some of these understudied kinase chemical leads were more selective than their parent compounds, and we chose to assess their kinome-wide selectivities to determine whether they require further optimization in our pursuit of high-quality chemical tools.

Table 2. NanoBRET profiling of entire pyrimidine library

| | IC_{50} values (nM) | | | |
Cmpd	DRAK1[b]	MARK3[c]	MARK4[c]	TBK1[b]
3	>10000	>10000	>10000	>10000
4	874 ± 103	>10000	>10000	2680 ± 230
5	>10000	>10000	>10000	7456
6	>10000	>10000	>10000	>10000
7	126 ± 27.6	>10000	3537	321 ± 2.49
8	>10000	>10000	>10000	>10000
9	638 ± 91.1	872	214	>10000
10	>10000	>10000	8445	>10000
11	>10000	>10000	>10000	2050 ± 196
12	>10000	>10000	>10000	>10000
13	>10000	>10000	>10000	6170 ± 2190
14	3622	4015	808	>10000
15	>10000	>10000	>10000	>10000
16	>10000	>10000	>10000	>10000
17	2311	>10000	>10000	>10000
18	4.47 ± 0.406	137	72	338 ± 22.5
19	>10000	>10000	>10000	>10000
20	>10000	>10000	>10000	>10000
21	>10000	>10000	>10000	>10000
22	58.2 ± 3.21	2001	509	2580 ± 215
MRT67307	43.2 ± 2.69	328 ± 38.5	319	N.T.[a]
MRT68921	N.T.[a]	95	N.T.[a]	N.T.[a]
BX-795	N.T.[a]	515	N.T.[a]	N.T.[a]
BX-912	N.T.[a]	3333	338 ± 4.5	2327
GSK8612	>10000	>10000	>10000	339 ± 39.5

[a]N.T.: not tested. [b]Compounds tested in singlicate (n =1) in dose–response where error not shown, compounds with SEM tested in triplicate (n = 3) in dose–response. [c]Compounds tested in singlicate (n =1) in dose–response where error not shown, compounds with SEM tested in duplicate (n = 2) in dose–response.

Assessment of Kinome-wide Selectivity. The promising selectivity of our pyrimidine series in the custom enzymatic assay panel motivated a broader survey to ascertain the kinome-wide selectivity of our library. All 21 novel analogs were screened at 1 μM via the DiscoverX scanMAX platform, which includes 403 wild-type human kinases. A selectivity score (S_{10}) for each compound is included in Table 1, representative of the percentage of kinases that exhibit binding with a percent of control (PoC) <10 at 1 μM. A final column is included that converts this $S_{10}(1 \mu M)$ value into the number of kinases bound with a PoC <10 in the DiscoverX panel. Figure S1 details the specific wild-type kinases that bound with a PoC <10 at 1 μM in the DiscoverX scanMAX panel.

This more comprehensive analysis of selectivity surfaced many findings. We learned that trends within our smaller curated enzymatic kinase panel were generally maintained in this larger profiling effort. Compounds that were the most selective in the Eurofins enzymatic panel were largely those that demonstrated the most favorable selectivity profile in the DiscoverX scanMAX screening. We identified a number of pyrimidine-based kinase inhibitors with useful selectivity. To provide some context on a useful selectivity threshold for tool compounds, we include kinase inhibitors with an $S_{10}(1 \mu M)$ <0.04 in our kinase chemogenomic set (KCGS) since they are the compounds that when screened can be more easily used to correlate phenotype with kinase target.[31, 32] 14 of 21, or 67%, of our novel inhibitors were found to be KCGS eligible based on their selectivity scores. We confirmed that kinases potently inhibited in the smaller enzymatic panel were also inhibited in the DiscoverX profiling and identified additional kinases that were differentially inhibited by certain analogs, providing fodder for future projects.

Taken together, our NanoBRET profiling (Table 2) and kinome-wide screening (Table 1) enabled us to confirm that GSK8612 is the most potent in cells, selective $(S_{10}(1 \mu M) = 0.02)$, and the most useful TBK1 inhibitor from all that we tested. We were not able to improve upon the activity of this published compound through our

synthetic efforts. Next, of the DRAK1 active compounds in the NanoBRET assay, only **4** was selective enough to be considered a valuable tool molecule. Given its $S_{10}(1\ \mu M) = 0.027$ and sub-micromolar IC_{50} value in the DRAK1 NanoBRET assay, compound **4** was nominated as a dark kinase tool that can be used to illuminate the function of DRAK1. Information for compound **4** has been posted on the Dark Kinase Knowledgebase.[33] Finally, selectivity profiling shows that all compounds with sub-micromolar IC_{50} values in the MARK3/4 NanoBRET assays require further optimization to reduce the number of off-target kinases that are potently inhibited in addition to MARK3/4 ($S_{10}(1\ \mu M) = 0.067$–0.233). Efforts are ongoing to improve the selectivity of analogs we identified as cell-active in the MARK3/4 NanoBRET assays.

Table 3. Combined enzymatic data

Cmpd	Potently active[a]	Moderately active[b]	Weakly active[c]
15		MYLK2 = 479 nM	DRAK2: 91%
8			MKNK2 = 2866 nM, DRAK2: 60%, YANK2 >10000 nM
12		CSF1R = 233 nM	
16	TYK2 = 33 nM	CSF1R = 305 nM	JAK2: 62%
21		TBK1 = 128 nM, TRKA = 477 nM	BMPR2 = 2918 nM, AURKB: 61%, JAK2: 107%
3	LRRK2 = 89 nM		DRAK2: 59%, NIM1 = 4398 nM, MYLK2 = 1119 nM
5		TBK1 = 149 nM	IKKε = 1199 nM
11		TBK1 = 187 nM, TRKA = 153 nM	JAK2: 87%, IKKε = 1314 nM, AURKB: 51%
17		DRAK1 = 325 nM, DRAK2 = 161 nM, AAK1 = 390 nM, SIK2 = 481 nM	MKNK2 = 769 nM, TYK2 = 720 nM, JAK2 >10000 nM, BMP2K: 56%
19	CSF1R = 91 nM	TYK2 = 276 nM	JAK2: 54%, ERBB2 >10000 nM, TBK1 = 2737 nM
GSK8612	TBK1 = 37 nM	LRRK2 = 159 nM, MAP2K5: 11%, CSF1R = 264 nM	IKKε = 552 nM, DAPK3 >10000 nM, NUAK2 = 1151 nM, ULK3 = 946 nM, MKNK2 = 1369 nM
20	AURKB: 5%	NUAK1 = 176 nM, SIK2 = 185 nM	BMP2K: 58%, DRAK1: 78%, DRAK2: 65%, JAK2: 81%, ACVR1 = 537 nM, BMPR1B = 9028 nM
4	LRRK2 = 19 nM, DRAK2 = 62 nM	IKKε = 216 nM, DRAK1 = 202 nM, ULK3 = 343 nM, MKNK2 =	ULK2 = 1742 nM, ULK1: 58%
13	AURKB: 6%, BMP2K = 40 nM, AAK1 = 74 nM, TYK2 = 48 nM, STK16 = 82 nM	380 nM, TBK1 = 192 nM, MAP2K5: 12% TBK1 = 192 nM, JAK2: 12%, BMPR2 = 488 nM, TRKA = 283 nM, NUAK1 = 317 nM	NUAK2 = 900 nM, CSNK2A2 = 2269 nM, PIP5K1A >10000 nM, MKNK2 = 1009 nM
6	TBK1 = 66 nM, JAK2: 3%, BMP2K = 38 nM, STK16 = 88 nM, TYK2 = 67 nM, AURKB: 7%, AAK1 = 80 nM	CSF1R = 192 nM, TRKA = 158 nM, NUAK1 = 171 nM	PRP4 >10000 nM, PIP5K1A >10000 nM, CSNK2A2 = 2304 nM, CSNK2A1 >10000 nM, ULK3 = 1371 nM

[a]Potently active: IC_{50} value <100 nM or <10% control at 1 μM (Table 1).
[b]Moderately active: IC_{50} value 200–500 nM or 10-49% control at 1 μM (Table 1). [c]Weakly active: IC_{50} value >500 nM or >49% control at 1 μM (Table 1). [a,b,c]All IC_{50} values determined in duplicate.

Orthogonal Validation of *scan*MAX Results. The *scan*MAX assay identifies potential targets for our compounds across the kinome. We chose to follow up and validate the *scan*MAX kinase binding results by further testing of actives in enzyme inhibition assays. Our choice of kinases for follow-up varied depending on the selectivity of the compound in question, as measured by $S_{10}(1\ \mu M)$. Highly selective compounds have the potential to be chemical probe candidates, and, as such, we chose to execute thorough enzyme profiling to validate or invalidate potential off-targets. Thus, for the 5 compounds in our library with an $S_{10}(1\ \mu M) <0.002$ (**15**, **8**, **12**, **16**, and **21**) we followed-up on all kinases inhibited >65% at 1 μM in the *scan*MAX platform and/or inhibited >50% in our initial custom enzymatic profiling panel at Eurofins (Table 1). One exception to this was exclusion of AURKA follow-up for **21**. For the 6 compounds in our library with an $S_{10}(1\ \mu M) = 0.005$–0.02 (**3**, **5**, **11**, **17**, **19**, and GSK8612), we carried out enzymatic assays on all kinases inhibited >80% at 1 μM in the *scan*MAX platform and/or inhibited >50% in our initial enzymatic profiling at Eurofins (Table 1). Given our interest in identifying chemical leads, a few additional understudied kinases inhibited >65% at 1 μM in the *scan*MAX platform by these 6 compounds were also selected for follow-up. Lastly, for a final 4 compounds (**20**, **4**, **13**, and **6**) with $S_{10}(1\ \mu M) = 0.022$–0.047, we selected only certain kinases inhibited >80% at 1 μM in the *scan*MAX platform and/or inhibited >50% in our initial profiling at Eurofins (Table 1) for targeted follow-up, with a bias toward kinases that were frequently inhibited by other analogs in the series as well as understudied kinases of interest. All follow-up enzymatic assays were executed at the K_m = ATP for each respective kinase. Results from these studies combined with the single-concentration enzymatic results from Table 1 are displayed in Table 3. Compounds in Table 3 are listed in order of their kinome-wide selectivity scores from most (**15**) to least (**6**) selective.

In examining the data generated and collected in Table 3 some interesting trends emerge. The most selective compounds ($S_{10}(1\ \mu M) <0.02$: **15**, **8**, **12**, **16**, and **21**) that were comprehensively profiled via enzymatic assays potently inhibited 0–1 kinases (Potently active, Table 3). We classify the kinases potently inhibited by these compounds as more well-studied. With the exception of **17** and GSK8612, the same group of most selective compounds ($S_{10}(1\ \mu M) <0.02$) inhibited 0–2 kinases with moderate potency (Table 3).

Some less selective compounds (**13** and **6**) for which we did selective enzymatic follow-up were found to be potent inhibitors of 5–7 kinases, including several from the understudied NAK family (AAK1, BMP2K, STK16).[17] Several of the pyrimidines tested were found to demonstrate IC_{50} values of 200–500 nM or inhibition equal to 10-49% control at 1 µM for understudied kinases. Given their kinome-wide selectivity scores and modest potency, these compounds represent good chemical leads for the development of chemical tools to study these poorly characterized kinases. Many kinases were assigned the weakly active designation based on weak potency in the respective enzymatic assays. In some cases, such as with compounds **5** and **13**, two kinases that share high structural homology were inhibited with differential potencies. For compound **5**, there is an 8-fold difference in potency for TBK1 and IKKε, and for compound **13** there is a nearly 3-fold difference between NUAK1 and NUAK2.

Importantly, we see that the compounds with sub-micromolar IC_{50} values in the respective NanoBRET assays corresponded with enzymatic inhibition IC_{50} values <250 nM for GSK8612 (TBK1 = 37 nM) and compound **4** (DRAK1 = 202 nM). TBK1, LRRK2, DRAK1/2, CSF1R, TYK2, and TRKA were identified as frequently inhibited kinases by our pyrimidine series. This list is comprised of some kinases that pyrimidines are known to potently inhibit (TBK1 and TYK2[34, 35]) as well as kinases that represent new targets for optimization. Analysis of the compounds that inhibit these kinases could inform next steps in new chemistry to develop specific SAR for these kinases. Before embarking on next synthetic steps, the narrow selectivity profiles of exemplars within our series coupled with potent enzymatic data motivated interrogation of the cell-based activity of some of these compounds in the respective NanoBRET assays.

Table 4. Selected NanoBRET follow-up

	IC_{50} values (nM)[a]					
Cmpd	BMP2K	CSF1R	LRRK2	MYLK2	NUAK1	TYK2
3			>10000			
6	1020				7010	
12		>10000				
13	3000				>10000	
15				3670		
16		>10000				>10000
19		5060				>10000
GSK8612		>10000	>10000			

[a]Compounds tested in singlicate (n =1) in dose–response.

Selective NanoBRET Assay Follow-up. For compounds in Table 3 that inhibited kinases with potency <500 nM we elected to determine their cellular target engagement via the NanoBRET assay. No more than 2 kinases were evaluated per compound. Several single digit micromolar inhibitors of specific kinases were identified amongst these selective pyrimidine compounds. Table 4 shows that these compounds were most cell-active in the BMP2K NanoBRET assay. We were excited to identify that weaker inhibition of MYLK2 in the enzymatic assay (IC_{50} value = 479 nM) translated to single digit micromolar activity in the MYLK2 NanoBRET assay. Compound **15** is the most selective of the compounds that we synthesized (Tables 1 and 3) and represents a high-quality chemical

starting point for MYLK2 chemical probe development. We also observed that compounds that exhibited potent activity in the LRRK2 enzyme assay (**3** and GSK8612, IC_{50} values <160 nM) and in the TYK2 enzyme assay (**16** and **19**, IC_{50} values <280 nM) did not have any activity in the respective NanoBRET assays when tested at concentrations up to 10 µM. The disparity between our enzymatic potencies and NanoBRET IC_{50} values prompted us to further investigate compound properties that might impact cell permeability.

Assessment of Compound Properties. With exceptions, we observed >30–300-fold losses in potency when considering enzymatic versus NanoBRET activities. This was true for NanoBRET values reported both in Tables 2 and 4. A <10-fold loss in potency was only observed in 4 cases: GSK8612 for TBK1, **15** for MYLK2, and **4** and **17** for DRAK1. The overall trend of biochemical activity not translating to cellular potency made us curious about the physicochemical properties of our pyrimidines. To address this, we evaluated the kinetic solubility and permeability (PAMPA) of our library of compounds and included the parent compounds as well (Table 5).

Table 5. Kinetic solubility and PAMPA assay results.

Cmpd	Kinetic solubility (µM)	P_e (cm/s)
3	171.0	3.89E-07
4	190.1	5.08E-06
5	33.2	<LOQ[a]
6	4.7	<LOQ[a]
7	40.3	3.73E-06
8	174.6	2.39E-06
9	159.0	1.30E-06
10	195.2	1.51E-06
11	118.7	7.09E-07
12	167.7	<LOQ[a]
13	20.0	<LOQ[a]
14	173.6	5.61E-07
15	176.9	6.23E-08
16	147.0	<LOQ[a]
17	169.3	8.24E-08
18	135.6	8.85E-07
19	176.5	4.56E-07
20	199.7	1.66E-07
21	85.6	2.60E-06
22	164.0	5.97E-07
MRT67307	164.6	2.60E-06
BX-912	155.5	1.39E-07
GSK8612	173.1	<LOQ[a]

[a]<LOQ: Below limit of quantitation.

Results in Table 5 demonstrated that our compounds were generally very soluble. With the exception of **5**, **6**, **7**, **11**, **13**, **16**, **18**, and **21**, the measured solubility was estimated to be greater than 75% of the dose concentration and thus the actual solubility may be higher than Table 5 reflects. As nearly all compounds demonstrated solubility >10 µM, they were not considered poorly soluble, and this was eliminated from consideration as driving their poor cellular potency. The permeability data, however, was a bit more varied for

this pyrimidine library. Six compounds (**5**, **6**, **12**, **13**, **16**, and GSK8612) were below the limit of quantitation (LOQ) and/or precipitated in the assay media, making it impossible to determine their permeability. Several of these compounds were amongst the analogs with the lowest kinetic solubility concentrations as well. For reference, P_e (permeability coefficient) values <1.50E-06 cm/s correlate with human fraction absorbed <80% and is a generally accepted cutoff for low permeability. In addition to the compounds already mentioned that were below the LOQ, this cutoff adds the majority of our library as well as some parent compounds to a low permeability category: **3**, **9**, **11**, **14**, **15**, **17–20**, **22**, and BX-912.

If we start to consider which structural elements could be compromising the solubility and/or permeability of our compounds, some trends emerge. The sulfonamide side chain is present in the majority of the least soluble compounds (**5**, **6**, **11**, **13**, **16**, and **21**) and all poorly permeable compounds (**5**, **6**, **12**, **13**, **16**, and GSK8612). As compounds with suboptimal solubility (**7**) or poor permeability (GSK8612) still proved active in our NanoBRET assays, just looking at half of the data is not sufficient. None of the compounds with both problematic solubility and permeability (**5**, **6**, **13**, and **16**) were active in our NanoBRET assays, leading us to conclude that these two factors together point to compounds that are poorly cell permeable. Since the majority of compounds did not fall into this final category, consideration of physicochemical properties did not explain our cell-based results.

It is worth noting for compounds/kinases where enzymatic data has been published, the control compounds used in the NanoBRET assays can be considered as a benchmark. For CSF1R, dasatinib has a published enzymatic IC_{50} = 0.57 nM and we determined its NanoBRET IC_{50} to be 18.3 nM. For NUAK1, BX-795 has a published IC_{50} = 5 nM and we determined its NanoBRET IC_{50} to be 187 nM.[19] In both cases, single-digit or sub-nanomolar enzymatic IC_{50} values translated to sub-micromolar NanoBRET IC_{50} values and a ~34-fold loss in potency was observed when moving to the cell-based assay. While not universal, it appears that for this set of compounds and kinase targets exceptional enzymatic potency is key to achieving cellular potency to overcome the more than 30-fold drop-off in cellular potency.
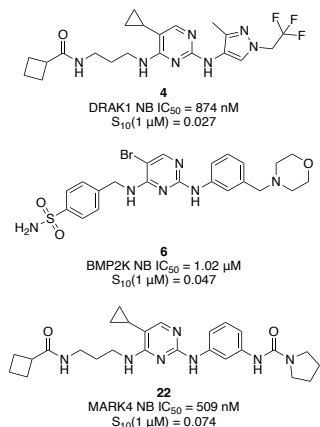

4
DRAK1 NB IC_{50} = 874 nM
S_{10}(1 μM) = 0.027

6
BMP2K NB IC_{50} = 1.02 μM
S_{10}(1 μM) = 0.047

22
MARK4 NB IC_{50} = 509 nM
S_{10}(1 μM) = 0.074

Figure 3. Promising chemical leads for understudied kinases.

CONCLUSIONS

In summary, we provide details related to the synthesis and extensive biological evaluation of a library of pyrimidines. We have shown that selectivity can be built into the pyrimidine scaffold through medicinal chemistry optimization. Several cell-active compounds

were discovered that exhibit sub-micromolar NanoBRET cellular target engagement IC_{50} values against kinases including TBK1, DRAK1, MARK3, and MARK4. Three of these kinases (DRAK1, MARK3, and MARK4) are understudied, IDG kinases that are in need of high-quality chemical tools to be able to characterize their function. Examples of compounds with sub-micromolar activities for understudied kinases and modest kinome-wide selectivity are included in Figure 3. These pyrimidines represent high-quality chemical starting points in our campaign to identify chemical probes to enable elucidation of the biological function(s) of lesser studied kinases. Results here reiterate the need to employ orthogonal biochemical and cell-based assays in order to more fully understand the actual selectivity and potency of kinase inhibitors. The methods described herein offer a path for others to identify and develop high-quality inhibitors for understudied kinases to facilitate illumination of the entire druggable kinome.

EXPERIMENTAL SECTION

Chemistry. General Information. Reagents were purchased from commercial suppliers and used without further characterization or purification. Temperatures are given in degrees Celsius (°C); unless otherwise stated, operations were carried out at room or ambient temperature (r.t.), typically around 25°C; evaporation of solvent was carried out using a rotary evaporator under reduced pressure with a bath temperature not exceeding 60 °C; thin layer chromatography (TLC) was used to follow the course of reactions; intermediates and products exhibited satisfactory ^{1}H-NMR and/or microanalytical data; and the following conventional abbreviations are also used: equivalents (eq), mL (milliliters), mmol (millimoles), g (grams), mg (milligrams), min (minutes), and h (hours). Reactions were carried out under a blanket of nitrogen unless otherwise stated. Compounds were visualized using a UV (ultraviolet) lamp (254 nM). ^{1}H and ^{13}C NMR spectra were collected in DMSO-d_6, acetonitrile-d_4, chloroform-d, or methanol-d_4 and recorded on Varian Inova 400 Megahertz (MHz), Bruker DRX 500 MHz, Bruker Avance III 400 MHz, Varian VNMRS 500 MHz, or Agilent ProPulse 600 MHz spectrometers, noting the magnet strength in all cases. Peak positions are given in parts per million (ppm) and calibrated based upon the shift of the indicated solvent; coupling constants (J values) are expressed in hertz (Hz); multiplicities are reported as follows: singlet (s), doublet (d), doublet of doublets (dd), doublet of doublet of doublets (ddd), triplet (t), triplet of doublets (td), triplet of triplet of doublets (ttd), doublet of triplets (dt), quartet (q), doublet of quartets (dq), quartet of doublets (qd), pentet (p), pentet of doublets (pd), heptet (h), and multiplet (m). Purity was assessed via LC–MS using an Agilent mass spectrometer (column: Agilent Poroshell 120 SB-C18, 4.6 mm X 30 mm, 2.7 μm with UHPLC Guard Infinity Lab Poroshell 120 SB-C18, 4.6 mm X 5 mm, 2.7 μm).

General Procedure for the Synthesis of Compound 2: Procedure A. To a solution of **compound 1** (1 eq) in ethanol (10–20 mL) were added dropwise DIPEA (2 mL) and **amine 1** (1 eq) at -10°C. The resulting mixture was heated to r.t. then stirred at 50°C for 16 h. Solvent was next evaporated from the reaction mixture and to the resulting material was added water (30 mL). The obtained precipitate was filtered, washed with water, isopropanol, and hexane, and dried under vacuum at 50°C to give **compounds 2a–2g** (*amount, yield, purity*), which were used in the next step without further purification.

N-(3-((2-chloropyrimidin-4-yl)amino)propyl)cyclobutanecarboxamide (2a): 330 mg, 50% yield, 95% purity by LC–MS.

N-(3-((5-bromo-2-chloropyrimidin-4-yl)amino)propyl)cyclobutanecarboxamide (2b): 2.20 g, 50% yield, 95% purity by LC–MS.

N-(3-((2-chloro-5-cyclopropylpyrimidin-4-yl)amino)propyl) cyclobutanecarboxamide (2c): 570 mg, 67% yield, 95% purity by LC–MS.

4-(((5-bromo-2-chloropyrimidin-4-yl)amino)methyl)benzenesulfonamide (2d): 6.40 g, 55% yield, 95% purity by LC–MS.

4-(((2-chloro-5-cyclopropylpyrimidin-4-yl)amino)methyl)benzenesulfonamide (2e): 850 mg, 50% yield, 95% purity by LC–MS.

N-(2-(1H-imidazol-4-yl)ethyl)-5-bromo-2-chloropyrimidin-4-amine (2f): 2.50 g, 25% yield, 95% purity by LC–MS.

N-(2-(1H-imidazol-4-yl)ethyl)-2-chloro-5-cyclopropylpyrimidin-4-amine (2g): 420 mg, 50% yield, 95% purity by LC–MS.

General Procedure for the Synthesis of Compounds 3–11, 13, 14, 17, 18, 21, 22, and GSK8612: Procedure B. To a solution of *compound 2* (1 eq) and *amine 2* (1 eq) in butanol (2–5mL) was added Dioxane×HCl (10%w/w) (0.5–2 mL) and the resulting mixture was stirred at 80°C for 16 h. The reaction mixture was next neutralized with aqueous ammonia and concentrated under vacuum. The resulting material was purified by preparative HPLC (2–7 min, 35–70% methanol (0.1% ammonium hydroxide), 30 mL/min; column: YMC-ACTUS TRIART C18, 20 mm X 100 mm, 5 μm) to give *final compounds 3–11, 13, 14, 17, 18, 21, 22, and GSK8612 (amount, yield).*

N^4-(2-(1H-imidazol-4-yl)ethyl)-5-cyclopropyl-N^2-(3-methyl-1-(2,2,2-trifluoroethyl)-1H-pyrazol-4-yl)pyrimidine-2,4-diamine (3): 71.0 mg, 36% yield. ^{1}H NMR (400 MHz, DMSO-d_6) δ 11.86 (s, 1H), 8.11 (s, 2H), 7.56 (s, 2H), 6.84 (d, J = 16.5 Hz, 2H), 5.02–4.91 (m, 2H), 3.63 (q, J = 6.8 Hz, 2H), 2.81 (t, J = 7.4 Hz, 2H), 2.16 (s, 3H), 1.41 (td, J = 10.7, 8.6, 5.9 Hz, 1H), 0.78 (d, J = 8.0 Hz, 2H), 0.40 (t, J = 5.1 Hz, 2H). ^{13}C NMR (151 MHz, Acetonitrile-d_3) δ 160.51, 156.33, 150.93, 138.16, 134.55, 132.59, 121.60 (q, J = 280.0 Hz), 120.39, 120.11, 113.02, 107.40, 49.73 (q, J = 33.9 Hz), 38.56, 24.68, 8.17, 5.05, 1.84. HPLC purity: 95.0%. HRMS (ESI) ([M+H]$^+$) Calcd. for C$_{18}$H$_{22}$F$_3$N$_8$: 407.1920, found: 407.1918.

N-(3-((5-cyclopropyl-2-((3-methyl-1-(2,2,2-trifluoroethyl)-1H-pyrazol-4-yl)amino)pyrimidin-4-yl)amino)propyl)cyclobutanecarboxamide (4): 57.0 mg, 11% yield. ^{1}H NMR (400 MHz, Chloroform-d) δ 8.01 (s, 1H), 7.70 (s, 1H), 6.21 (s, 1H), 5.94 (s, 1H), 5.59 (s, 1H), 4.62 (q, J = 8.5 Hz, 2H), 3.53 (q, J = 5.9 Hz, 2H), 3.36 (q, J = 6.3 Hz, 2H), 2.96 (p, J = 8.2 Hz, 1H), 2.31–2.19 (m, 5H), 2.18–2.10 (m, 2H), 2.03–1.82 (m, 2H), 1.77 (p, J = 6.7 Hz, 2H), 1.51–1.40 (m, 1H), 1.25 (s, 1H), 0.91 (dq, J = 5.7, 3.9 Hz, 2H), 0.53–0.45 (m, 2H). ^{13}C NMR (101 MHz, Chloroform-d) δ 175.72, 162.75, 157.86, 152.71, 140.54, 123.13 (q, J = 280 Hz), 122.38, 121.92, 110.04, 52.97 (q, J = 34.7 Hz), 39.91, 37.24, 36.04, 29.84, 25.43, 18.09, 10.99, 7.41, 4.56. HPLC purity: 100%. HRMS (ESI) ([M+H]$^+$) Calcd. for C$_{21}$H$_{29}$F$_3$N$_7$O: 452.2386, found: 452.2385.

4-(((5-cyclopropyl-2-((3-methyl-1-(2,2,2-trifluoroethyl)-1H-pyrazol-4-yl)amino)pyrimidin-4-yl)amino)methyl)benzenesulfonamide (5): 74.0 mg, 15% yield. ^{1}H NMR (400 MHz, DMSO-d_6) δ 8.01 (s, 1H), 7.79–7.70 (m, 3H), 7.59 (s, 1H), 7.46 (d, J = 8.0 Hz, 2H), 7.38–7.33 (m, 1H), 7.26 (s, 2H), 4.87 (q, J = 9.2 Hz, 2H), 4.68 (d, J = 6.1 Hz, 2H), 2.08 (s, 3H), 1.52 (s, 1H), 0.83 (d, J = 8.0 Hz, 2H), 0.48 (d, J = 5.0 Hz, 2H). ^{13}C NMR (151 MHz, Acetonitrile-d_3) δ 160.37, 156.47, 151.51, 143.05, 139.49, 138.98, 125.27, 123.81, 123.0 (q, J = 279 Hz), 120.72, 119.89, 107.57, 49.90 (q, J = 34.0 Hz), 41.03, 8.12, 5.08, 1.98. HPLC purity: 100%. HRMS (ESI) ([M+H]$^+$) Calcd. for C$_{20}$H$_{23}$F$_3$N$_7$O$_2$S: 482.1588, found: 482.1582.

4-(((5-bromo-2-((3-(morpholinomethyl)phenyl)amino)pyrimidin-4-yl)amino)methyl)benzenesulfonamide (6): 128 mg, 24% yield. ^{1}H NMR (400 MHz, DMSO-d_6) δ 9.19 (s, 1H), 8.06 (s, 1H), 7.73 (dd, J = 15.3, 7.0 Hz, 4H), 7.60 (s, 1H), 7.50 (d, J = 8.0 Hz, 2H), 7.43 (d, J = 8.2 Hz, 1H), 7.26 (s, 2H), 7.10 (t, J = 7.8 Hz, 1H), 6.81 (d, J = 7.4 Hz, 1H), 4.70 (d, J = 6.1 Hz, 2H), 3.52 (d, J = 4.8 Hz, 4H), 3.17 (d, J = 5.2 Hz, 2H), 2.28 (s, 4H). ^{13}C NMR (126 MHz, Acetonitrile-d_3) δ 158.62, 156.44, 145.31, 144.49, 141.94, 140.19, 133.48, 128.40, 127.58, 126.11, 122.69, 121.42, 119.70, 93.02, 66.45, 62.66, 60.58, 53.35, 43.67, 24.27. HPLC purity: 98.4%. HRMS (ESI) ([M+H]$^+$) Calcd. for C$_{22}$H$_{26}$BrN$_6$O$_3$S: 533.0970, found: 534.11.

N-(3-((5-bromo-2-((3-methyl-1-(2,2,2-trifluoroethyl)-1H-pyrazol-4-yl)amino)pyrimidin-4-yl)amino)propyl)cyclobutanecarboxamide (7): 83.0 mg, 17% yield. ^{1}H NMR (400 MHz, Chloroform-d) δ 7.95 (s, 2H), 6.34 (s, 1H), 6.04–5.99 (m, 1H), 5.58–5.53 (m, 1H), 4.64 (q, J = 8.5 Hz, 2H), 3.49 (q, J = 6.2 Hz, 2H), 3.35 (q, J = 6.4 Hz, 2H), 2.98 (p, J = 8.5 Hz, 1H), 2.33–2.20 (m, 5H), 2.19–2.08 (m, 2H), 2.04–1.80 (m, 2H), 1.76 (p, J = 6.3 Hz, 2H). ^{13}C NMR (151 MHz, Acetonitrile-d_3) δ 173.06, 156.65, 156.48, 153.76, 138.90, 121.5 (q, J = 279.8), 120.99, 119.51, 119.43, 49.88 (q, J = 34.2 Hz), 37.32, 35.47, 33.62, 26.93, 22.78, 15.55, 8.19. HPLC purity: 97.8%. HRMS (ESI) ([M+H]$^+$) Calcd. for C$_{18}$H$_{24}$BrF$_3$N$_7$O: 490.1178, found: 490.1176.

N-(3-((2-((3-methyl-1-(2,2,2-trifluoroethyl)-1H-pyrazol-4-yl)amino)pyrimidin-4-yl)amino)propyl)cyclobutanecarboxamide (8): 75.0 mg, 15% yield. ^{1}H NMR (400 MHz, Chloroform-d) δ 7.98 (s, 1H), 7.83 (d, J = 5.9 Hz, 1H), 6.33 (s, 1H), 5.82 (d, J = 5.6 Hz, 1H), 5.56 (s, 2H), 4.59 (q, J = 8.5 Hz, 2H), 3.41–3.25 (m, 4H), 2.95 (p, J = 8.6 Hz, 1H), 2.31–2.18 (m, 5H), 2.13 (q, J = 9.1, 8.3 Hz, 2H), 2.01–1.79 (m, 3H), 1.72 (p, J = 6.3 Hz, 2H). ^{13}C NMR (151 MHz, Acetonitrile-d_3) δ 172.67, 161.10, 157.78, 153.04, 138.64, 125.45, 121.63 (q, J = 280), 120.78, 119.87, 118.98, 49.87 (q, J = 34.0 Hz), 37.31, 33.92, 26.98, 22.74, 15.56, 8.19. HPLC purity: 100%. HRMS (ESI) ([M+H]$^+$) Calcd. for C$_{18}$H$_{25}$F$_3$N$_7$O: 412.2073, found: 412.2069.

N^4-(2-(1H-imidazol-4-yl)ethyl)-5-bromo-N^2-(3-(morpholinomethyl)phenyl)pyrimidine-2,4-diamine (9): 190 mg, 11% yield. ^{1}H NMR (400 MHz, DMSO-d_6) δ 11.83 (s, 1H), 9.21 (s, 1H), 8.01 (s, 1H), 7.75 (s, 1H), 7.63–7.54 (m, 2H), 7.14 (t, J = 7.8 Hz, 2H), 6.83 (d, J = 7.5 Hz, 2H), 3.68 (q, J = 6.9 Hz, 2H), 3.54 (t, J = 4.6 Hz, 4H), 3.31 (s, 2H), 2.87–2.78 (m, 2H), 2.29 (s, 4H). ^{13}C NMR (101 MHz, Methanol-d_4) δ 163.42, 158.65, 158.56, 155.08, 140.37, 137.30, 134.65, 128.08, 122.67, 120.21, 118.15, 116.24, 92.60, 66.28, 63.13, 53.22, 40.58, 26.34. HPLC purity: 95.9%. HRMS (ESI) ([M+H]$^+$) Calcd. for C$_{20}$H$_{25}$BrN$_7$O: 458.1304, found: 458.1300.

N^4-(2-(1H-imidazol-5-yl)ethyl)-5-bromo-N^2-(3-methyl-1-(2,2,2-trifluoroethyl)-1H-pyrazol-4-yl)pyrimidine-2,4-diamine (10): 325 mg, 17% yield. ^{1}H NMR (400 MHz, DMSO-d_6) δ 11.84 (s, 1H), 8.55 (s, 1H), 8.09 (s, 1H), 7.95 (s, 1H), 7.55 (s, 1H), 7.08 (s, 1H), 6.87 (s, 1H), 4.98 (s, 2H), 3.60 (q, J = 6.9, 6.5 Hz, 2H), 2.78 (t, J = 7.1 Hz, 2H), 2.16 (s, 3H). ^{13}C NMR (151 MHz, Acetonitrile-d_3) δ 156.58, 156.46, 153.77, 144.88, 143.51, 138.62, 132.63, 121.54 (q, J = 279.9 Hz), 120.99, 119.43, 117.93, 49.74 (q, J = 34.1 Hz), 38.91, 24.47, 8.21. HPLC purity: 96.6%. HRMS (ESI) ([M+H]$^+$) Calcd. for $C_{15}H_{17}BrF_3N_8$: 445.0712, found: 445.0709.

4-(((5-cyclopropyl-2-((3-(morpholinomethyl)phenyl)amino)pyrimidin-4-yl)amino)methyl)-benzenesulfonamide (11): 18.0 mg, 4% yield. ^{1}H NMR (400 MHz, DMSO-d_6) δ 8.83 (s, 1H), 7.75 (d, J = 8.1 Hz, 2H), 7.66 (s, 2H), 7.52 (d, J = 8.0 Hz, 2H), 7.50–7.42 (m, 3H), 7.25 (s, 2H), 7.06 (t, J = 7.9 Hz, 1H), 6.75 (d, J = 7.7 Hz, 1H), 4.75 (d, J = 5.9 Hz, 2H), 3.57–3.50 (m, 5H), 3.17 (d, J = 5.5 Hz, 2H), 2.32–2.25 (m, 4H), 1.61–1.50 (m, 1H), 0.88–0.83 (m, 2H), 0.52 (d, J = 4.7 Hz, 2H). ^{13}C NMR (101 MHz, Methanol-d_4) δ 162.60, 158.31, 152.19, 144.97, 142.02, 140.52, 137.00, 128.03, 127.12, 125.89, 122.35, 120.11, 118.04, 110.30, 66.24, 63.12, 53.13, 43.32, 39.00, 7.14, 3.92. HPLC purity: 100%. HRMS (ESI) ([M+H]$^+$) Calcd. for $C_{25}H_{31}N_6O_3S$: 495.2178, found: 495.24.

N-(3-((5-bromo-4-((4-sulfamoylbenzyl)amino)pyrimidin-2-yl)amino)phenyl)pyrrolidine-1-carboxamide (13): 383 mg, 5% yield. ^{1}H NMR (500 MHz, Methanol-d_4) δ 7.95 (d, J = 2.2 Hz, 1H), 7.80 (dd, J = 8.4, 2.2 Hz, 2H), 7.71 (d, J = 2.4 Hz, 1H), 7.49–7.43 (m, 2H), 7.08 (dt, J = 4.6, 1.8 Hz, 2H), 6.95 (td, J = 4.3, 1.8 Hz, 1H), 4.77 (d, J = 2.0 Hz, 2H), 3.42 (dt, J = 6.8, 3.5 Hz, 4H), 1.94 (h, J = 2.5 Hz, 4H). ^{13}C NMR (101 MHz, Methanol-d_4) δ 158.61, 156.19, 155.36, 153.60, 144.23, 141.95, 140.23, 139.55, 128.02, 127.27, 125.75, 114.94, 114.62, 112.77, 92.26, 45.57, 43.56, 25.01. HPLC purity: 92.6%. HRMS (ESI) ([M+H]$^+$) Calcd. for $C_{22}H_{25}BrN_7O_3S$: 546.0923, found: 546.0914.

N^4-(2-(1H-imidazol-4-yl)ethyl)-5-cyclopropyl-N^2-(3-(morpholinomethyl)phenyl)pyrimidine-2,4-diamine (14): 73.0 mg, 24% yield. ^{1}H NMR (400 MHz, DMSO-d_6) δ 11.82 (s, 1H), 8.85 (s, 1H), 7.81 (s, 1H), 7.64–7.54 (m, 3H), 7.11 (t, J = 7.8 Hz, 1H), 6.90–6.81 (m, 2H), 6.77 (d, J = 7.5 Hz, 1H), 3.69 (q, J = 6.7 Hz, 2H), 3.54 (t, J = 4.6 Hz, 4H), 3.30–3.20 (m, 1H), 3.17 (d, J = 3.9 Hz, 1H), 2.85 (t, J = 7.2 Hz, 2H), 2.29 (d, J = 4.8 Hz, 4H), 1.44 (q, J = 4.8, 2.9 Hz, 1H), 0.79 (dt, J = 8.3, 3.1 Hz, 2H), 0.51–0.38 (m, 2H). ^{13}C NMR (151 MHz, Acetonitrile-d_3) δ 160.24, 156.35, 150.71, 139.02, 136.45, 132.53, 126.05, 119.42, 116.81, 115.42, 114.90, 108.19, 64.35, 60.97, 51.28, 38.46, 24.40, 5.12, 1.85. HPLC purity: 100%. HRMS (ESI) ([M+H]$^+$) Calcd. for $C_{23}H_{30}N_7O$: 420.2512, found: 420.2506.

N-(3-((4-((3-(cyclobutanecarboxamido)propyl)amino)pyrimidin-2-yl)amino)phenyl)pyrrolidine-1-carboxamide (17): 19.0 mg, 10% yield. ^{1}H NMR (400 MHz, Chloroform-d) δ 7.94 (s, 1H), 7.82 (s, 1H), 7.24 (s, 1H), 7.22–7.03 (m, 3H), 6.95 (d, J = 8.2 Hz, 1H), 6.13 (s, 2H), 5.80 (d, J = 6.5 Hz, 1H), 5.56 (s, 1H), 3.41 (m, 6H), 3.26 (m, 2H), 2.95–2.78 (m, 1H), 2.19 (d, J = 9.8 Hz, 2H), 2.07–1.89 (m, 9H), 1.68 (d, J = 6.7 Hz, 1H). ^{13}C NMR (101 MHz, DMSO-d_6) δ 174.29, 162.95, 160.25, 154.80, 154.49, 141.70, 140.83, 128.16, 113.36, 113.15, 111.41, 98.08, 55.31, 46.08, 39.17, 36.78, 29.55, 25.47, 25.11, 18.22. HPLC purity: 100%. HRMS (ESI) ([M+H]$^+$) Calcd. for $C_{23}H_{32}N_7O_2$: 438.2617, found: 438.2617.

N-(3-((5-bromo-4-((3-(cyclobutanecarboxamido)propyl)amino)pyrimidin-2-yl)amino)phenyl)pyrrolidine-1-carboxamide (18): 335 mg, 13% yield. ^{1}H NMR (400 MHz, DMSO-d_6) δ 9.07 (s, 1H), 7.97 (s, 1H), 7.87 (t, J = 2.1 Hz, 1H), 7.62 (t, J = 5.4 Hz, 1H), 7.25 (d, J = 8.1 Hz, 1H), 7.06 (t, J = 8.0 Hz, 1H), 7.00–6.91 (m, 2H), 3.42 (q, J = 6.6 Hz, 2H), 3.33 (d, J = 6.4 Hz, 4H), 3.07 (q, J = 6.5 Hz, 2H), 2.93 (p, J = 8.4 Hz, 1H), 2.14–2.02 (m, 4H), 1.96 (q, J = 9.8 Hz, 2H), 1.90–1.79 (m, 4H), 1.78–1.60 (m, 3H). ^{13}C NMR (101 MHz, Methanol-d_4) δ 176.54, 158.67, 158.61, 155.60, 155.03, 140.53, 139.71, 128.13, 114.73, 114.19, 112.40, 92.61, 45.63, 39.47, 37.91, 36.26, 28.86, 25.06, 24.84, 17.58. HPLC purity: 98.1%. HRMS (ESI) ([M+H]$^+$) Calcd. for $C_{23}H_{31}BrN_7O_2$: 516.1723, found: 516.20.

N-(3-((5-cyclopropyl-4-((4-sulfamoylbenzyl)amino)pyrimidin-2-yl)amino)phenyl)pyrrolidine-1-carboxamide (21): 16.0 mg, 8% yield. ^{1}H NMR (400 MHz, Methanol-d_4) δ 7.80 (d, J = 8.3 Hz, 2H), 7.70 (t, J = 2.1 Hz, 1H), 7.47–7.41 (m, 3H), 7.22 (t, J = 8.0 Hz, 1H), 7.15 (dt, J = 8.0, 1.5 Hz, 1H), 6.97 (dt, J = 8.0, 1.6 Hz, 1H), 4.82 (s, 2H), 3.46–3.41 (m, 4H), 1.98–1.92 (m, 4H), 1.57 (td, J = 7.9, 4.0 Hz, 1H), 1.02–0.97 (m, 2H), 0.61–0.56 (m, 2H). ^{13}C NMR (101 MHz, Methanol-d_4) δ 163.32, 155.39, 152.73, 142.84, 142.38, 140.50, 139.89, 136.96, 128.85, 127.60, 125.88, 117.51, 117.11, 115.24, 112.53, 45.66, 43.99, 25.01, 23.61, 6.92, 4.27. HPLC purity: 100%. HRMS (ESI) ([M+H]$^+$) Calcd. for $C_{25}H_{30}N_7O_3S$: 508.2131, found: 508.23.

N-(3-((4-((3-(cyclobutanecarboxamido)propyl)amino)-5-cyclopropylpyrimidin-2-yl)amino)-phenyl)pyrrolidine-1-carboxamide (22): 16.0 mg, 5% yield. ^{1}H NMR (400 MHz, Methanol-d_4) δ 7.81 (t, J = 2.1 Hz, 1H), 7.55 (d, J = 1.1 Hz, 1H), 7.25 (ddd, J = 8.1, 2.2, 1.1 Hz, 1H), 7.15 (t, J = 8.1 Hz, 1H), 6.97 (ddd, J = 8.0, 2.1, 1.0 Hz, 1H), 3.58 (t, J = 6.6 Hz, 2H), 3.47–3.42 (m, 5H), 3.24 (t, J = 6.7 Hz, 2H), 2.96 (pd, J = 8.6, 1.0 Hz, 1H), 2.24–2.14 (m, 2H), 2.10–2.01 (m, 2H), 1.98–1.93 (m, 5H), 1.84–1.75 (m, 3H), 1.46 (ttd, J = 8.1, 5.2, 1.1 Hz, 1H), 0.92–0.87 (m, 2H), 0.49–0.44 (m, 2H). ^{13}C NMR (101 MHz, Methanol-d_4) δ 176.49, 162.67, 158.29, 155.62, 151.52, 140.97, 139.70, 128.11, 114.28, 113.88, 112.08, 110.40, 45.61, 39.47, 39.00, 37.37, 36.13, 29.14, 25.06, 24.83, 17.57, 7.07, 3.81. HPLC purity: 100%. HRMS (ESI) ([M+H]$^+$) Calcd. for $C_{26}H_{36}N_7O_2$: 478.2930, found: 478.33.

4-(((5-bromo-2-((3-methyl-1-(2,2,2-trifluoroethyl)-1H-pyrazol-4-yl)amino)pyrimidin-4-yl)-amino)methyl)benzenesulfonamide (GSK8612): 379 mg, 73% yield. ^{1}H NMR (400 MHz, DMSO-d_6) δ 8.43 (s, 1H), 7.98 (s, 1H), 7.73 (d, J = 8.0 Hz, 3H), 7.62–7.53 (m, 1H), 7.41 (s, 2H), 7.27 (s, 2H), 4.90 (q, J = 9.1 Hz, 2H), 4.61 (s, 2H), 2.08 (s, 3H). ^{13}C NMR (151 MHz, Acetonitrile-d_3) δ 156.82, 156.44, 154.25, 142.15, 139.72, 139.67, 125.39, 123.87, 123.25 (q, J = 281 Hz), 121.58, 119.20, 49.92 (q, J = 34.0 Hz), 41.30, 8.17. HPLC purity: 100%. HRMS (ESI) ([M+H]$^+$) Calcd. for $C_{17}H_{18}BrF_3N_7O_2S$: 520.0378, found: 520.0378.

General Procedure for the Synthesis of Compounds 12, 15, 16, 19, and 20: Procedure C. To a solution of *6, 9, 10, 13,* or *GSK8612* (1 eq) in methanol (20 mL) were added 5% Pd/C (0.5 eq) and triethylamine (TEA, 3 eq). The resulting mixture was stirred under H$_2$ (hydrogen) atmosphere at r.t. for 16 h. Next the reaction mixture was filtered, and the filtrate was concentrated in vacuo. The crude product was purified via preparative HPLC (2–7 min, 30–55% acetonitrile, 30 mL/min; column: SunFire C18, 19 mm X 100 mm, 5 µm) to give *12, 15, 16, 19, and 20* (*amount, purity, yield*).

4-(((2-((3-methyl-1-(2,2,2-trifluoroethyl)-1h-pyrazol-4-yl)amino)pyrimidin-4-yl)amino)methyl)benzenesulfonamide (12): 108 mg, 36% yield. ^{1}H NMR (400 MHz, DMSO-d_6) δ 8.18 (s, 1H), 7.87 (s, 1H), 7.77 (dd, J = 8.9, 6.9 Hz, 3H), 7.66 (s, 1H), 7.46 (d, J = 8.0 Hz, 2H), 7.30 (s, 2H), 5.92 (s, 1H), 4.90 (q, J = 9.1 Hz, 2H), 4.57 (s, 2H), 2.11 (s, 3H). ^{13}C NMR (151 MHz, Acetonitrile-d_3) δ 161.02, 157.98, 153.76, 142.49, 139.69, 139.23, 125.44, 125.24, 123.88, 123.79, 121.45 (q, J = 279 Hz), 121.16, 119.67, 94.31, 49.96 (q, J = 34.4 Hz), 41.30, 8.11. HPLC purity: 96.6%. HRMS (ESI) ([M+H]$^+$) Calcd. for $C_{17}H_{19}F_3N_7O_2S$: 442.1273, found: 442.1270.

N^4-(2-(1H-imidazol-5-yl)ethyl)-N^2-(3-methyl-1-(2,2,2-trifluoroethyl)-1H-pyrazol-4-yl)pyrimidine-2,4-diamine (15): 86.0 mg, 10% yield. ^{1}H NMR (400 MHz, DMSO-d_6) δ 11.81 (s, 1H), 8.15 (d, J = 35.4 Hz, 2H), 7.73 (s, 1H), 7.53 (s, 1H), 7.18 (s, 1H), 6.83 (s, 1H), 5.85 (d, J = 5.8 Hz, 1H), 4.95 (q, J = 9.2 Hz, 2H), 3.51 (s, 2H), 2.75 (t, J = 7.5 Hz, 2H), 2.16 (s, 3H). ^{13}C NMR (151 MHz, Acetonitrile-d_3) δ 161.05, 157.72, 153.16, 138.57, 132.48, 122.48, 121.55 (q, J = 280 Hz), 120.74, 119.80, 116.90, 114.19, 49.77 (q, J = 32.4 Hz), 38.55, 24.75, 8.19. HPLC purity: 100%. HRMS (ESI) ([M+H]$^+$) Calcd. for $C_{15}H_{18}F_3N_8$: 367.1607, found: 367.1596.

N-(3-((4-((4-sulfamoylbenzyl)amino)pyrimidin-2-yl)amino)phenyl)pyrrolidine-1-carboxamide (16): 23.0 mg, 8% yield. ^{1}H NMR (400 MHz, DMSO-d_6) δ 8.83 (s, 1H), 7.94 (s, 1H), 7.92–7.79 (m, 3H), 7.75 (d, J = 7.9 Hz, 3H), 7.49 (d, J = 8.0 Hz, 2H), 7.27 (s, 2H), 7.19 (s, 1H), 6.99 (d, J = 7.8 Hz, 1H), 6.93 (s, 1H), 5.98 (s, 1H), 4.64 (s, 2H), 3.17 (m, 4H), 1.82 (m, 4H). ^{13}C NMR (101 MHz, DMSO-d_6) δ 162.86, 160.14, 155.30, 154.46, 144.67, 142.92, 141.44, 140.84, 128.18, 127.94, 126.07, 113.46, 113.27, 111.51, 97.85, 46.09, 40.86, 25.46. HPLC purity: 95.0%. HRMS (ESI) ([M+H]$^+$) Calcd. for $C_{22}H_{26}N_7O_3S$: 468.1818, found: 468.1814.

4-(((2-((3-(morpholinomethyl)phenyl)amino)pyrimidin-4-yl)amino)methyl)benzenesulfonamide (19): 18.8 mg, 38% yield. ^{1}H NMR (400 MHz, Methanol-d_4) δ 7.84 (d, J = 8.4 Hz, 2H), 7.77 (d, J = 6.0 Hz, 1H), 7.59 (t, J = 2.0 Hz, 1H), 7.52–7.47 (m, 2H), 7.36 (d, J = 8.2 Hz, 1H), 7.14 (t, J = 7.8 Hz, 1H), 6.90 (dt, J = 7.5, 1.4 Hz, 1H), 6.01 (d, J = 6.0 Hz, 1H), 4.70 (s, 2H), 3.61 (t, J = 4.7 Hz, 4H), 3.35 (s, 2H), 2.36 (t, J = 4.5 Hz, 4H). ^{13}C NMR (101 MHz, Methanol-d_4) δ 163.16, 159.74, 154.25, 144.48, 142.16, 140.34, 137.04, 128.07, 127.30, 125.95, 122.68, 120.45, 118.38, 97.18, 66.23, 63.11, 53.14, 43.26. HPLC purity: 100%. HRMS (ESI) ([M+H]$^+$) Calcd. for $C_{22}H_{27}N_6O_3S$: 455.1865, found: 453.20.

N^4-(2-(1H-imidazol-5-yl)ethyl)-N^2-(3-(morpholinomethyl)phenyl)pyrimidine-2,4-diamine (20): 21.0 mg, 19% yield. ^{1}H NMR (400 MHz, DMSO-d_6) δ 11.81 (s, 1H), 8.92 (s, 1H), 7.80 (d, J = 16.9 Hz, 2H), 7.61 (s, 1H), 7.54 (s, 1H), 7.24 (s, 1H), 7.12 (t, J = 7.8 Hz, 1H), 6.79 (d, J = 10.4 Hz, 2H), 5.92 (d, J = 5.8 Hz, 1H), 3.54 (m, 6H), 3.31 (s, 2H), 2.79 (m, 2H), 2.29 (s, 4H). ^{13}C NMR (101 MHz, Methanol-d_4) δ 163.14, 159.75, 153.70, 140.60, 137.24, 134.91, 134.58, 128.07, 122.50, 120.29, 118.18, 116.44, 97.18, 66.28, 63.20, 53.24, 40.31, 26.50. HPLC purity: 100%. HRMS (ESI) ([M+H]$^+$) Calcd. for $C_{20}H_{26}N_7O$: 380.2199, found: 378.24.

Biological Evaluation. Enzymatic Assays. Eurofins kinase enzymatic radiometric assays were carried out at the K_m = ATP at a single concentration (1 μM) in duplicate for each kinase in Table 1. Eurofins kinase enzymatic radiometric assays were carried out at the K_m = ATP in dose–response (9-pt curve in duplicate) for each kinase with an IC$_{50}$ value listed in Table 3. Details about the substrate used, protein constructs, controls, and assay protocol for each kinase assay can be found at the Eurofins website: https://www.eurofinsdiscoveryservices.com.

Library-wide NanoBRET Assays. Human embryonic kidney (HEK293) cells (hypotriploid, female, fetal) were purchased from ATCC and grown in Dulbecco's Modified Eagle's medium (DMEM, Gibco) supplemented with 10% (v/v) fetal bovine serum (FBS, Corning). Cells were incubated in 5% CO$_2$ at 37°C and passaged every 72 hours with trypsin. They were not allowed to reach confluency.

Constructs for NanoBRET measurements of DRAK1 (DRAK1-NLuc), MARK3 (NLuc-MARK3), MARK4 (NLuc-MARK4), and TBK1 (NLuc-TBK1) included in Table 2 were kindly provided by Promega. NanoBRET assays were executed as described previously.[17] Preferred NLuc orientations are indicated in parentheses after each construct. Assays were carried out in dose–response as described by the manufacturer using 0.5 μM of tracer K-9 for DRAK1 and MARK3 and 0.5 μM of tracer K-5 for MARK4 and TBK1. Respective tracer titration curves that we generated for DRAK1, MARK3, and MARK4 can be found at https://darkkinome.org/data.[33] Tracer titration curves for MARK3, MARK4, and TBK1 can also be found on the Promega website.

Kinome Screening. The *scan*MAX assay platform was used to assess the selectivity of each pyrimidine analog at 1 μM at Eurofins DiscoverX Corporation. As described previously, this commercial assay platform screens against 403 wild-type human kinases and provides percent inhibition values.[19] These inhibition values are captured in Table 1.

Specific NanoBRET Assay Follow-up. NanoBRET assays for the 6 kinases in Table 4 were carried out in dose–response in singlicate by Carna Biosciences. Assays were carried out according to the manufacturer's protocol.

Kinetic Solubility and Permeability (PAMPA). Kinetic solubility analysis was carried out from 10 mM DMSO stocks of compounds in phosphate buffered saline solution (PBS) at pH 7.4 by Analiza, Inc. Following 24h incubation in a Millipore solubility filter plate, samples were vacuum filtered, and the filtrates collected for analysis. Filtrates were injected into the nitrogen detector for quantification via Total Chemiluminescent Nitrogen Determination (CLND). Filtrates were quantified with respect to a calibration curve generated using standards that span the dynamic range of the instrument. Calculated solubility values are corrected for background nitrogen present in the DMSO and the media.

PAMPA analysis was carried out by Analiza, Inc using a Corning Gentest Pre-coated PAMPA plate. DMSO stocks of compound diluted in PBS at pH 7.4 were added to the Donor compartment of the plate, PBS at pH 7.4 was added to the Acceptor compartment, and the plate was left to incubate for 5h. Both the Donor and Acceptor compartments were collected and analyzed by CLND. Donor and Acceptor samples were quantified using the calibration curve generated using standards that span the dynamic range of the instrument. Measured concentrations are corrected for background nitrogen present in the DMSO and the media. Concentration values from the Donor and Acceptor compartment are used in the calculation of the effective permeability of the compound. Solubility of the compound is determined experimentally rather than assuming full solubility.

Statistics. Standard error of the mean (SEM) was calculated for NanoBRET assays executed more than once. Calculated SEM is included alongside IC$_{50}$ values in Table 2.

AUTHOR INFORMATION

Corresponding Author

*E-mail: alison.axtman@unc.edu.

Author Contributions

All authors have given approval to the final version of the manuscript.

Notes

The authors declare no competing financial interest.

ABBREVIATIONS

DIPEA, N, N-diisopropylethylamine; DMSO, dimethyl sulfoxide; HCl, hydrochloric acid; HPLC, high-performance liquid chromatography; IC$_{50}$, half maximal inhibitory concentration; LC–MS, liquid chromatography–mass spectrometry; K$_m$, Michaelis constant; LINCS, Library of Integrated Network-Based Cellular Signatures; NanoBRET, bioluminescence resonance energy transfer using Nanoluciferase; Nluc, Nanoluciferase; NMR, nuclear magnetic resonance; PAMPA, parallel artificial membrane permeability assay; Pd/C, palladium on carbon; v/v, volume for volume; w/w, weight for weight.

REFERENCES

(1) Meeta, S.; Nadeem, S. A review on biological importance of pyrimidines in the new era. *Int J Pharm Pharm Sci* **2016**, *8*, 8–21.

(2) Roskoski, R., Jr. Properties of FDA-approved small molecule protein kinase inhibitors: A 2020 update. *Pharmacol Res* **2020**, *152*, 104609.

(3) Richters, A.; Basu, D.; Engel, J.; Ercanoglu, M. S.; Balke-Want, H.; Tesch, R.; Thomas, R. K.; Rauh, D. Identification and Further Development of Potent TBK1 Inhibitors. *ACS Chem Biol* **2015**, *10*, 289–298.

(4) Llona-Minguez, S.; Baiget, J.; Mackay, S. P. Small-molecule inhibitors of IκB kinase (IKK) and IKK-related kinases. *Pharm Pat Anal* **2013**, *2*, 481–98.

(5) Perrior, T. R.; Newton, G. K.; Stewart, M. R.; Aquil, R. Pyrimidine compounds as inhibitors of protein kinases IKK epsilon and/or TBK-1, processes for their preparation, and pharmaceutical compositions containing them. International Patent Application WO/2012010826-A1, 2012; Domainex Limited.

(6) Muvaffak, A.; Pan, Q.; Yan, H.; Fernandez, R.; Lim, J.; Dolinski, B.; Nguyen, T. T.; Strack, P.; Wu, S.; Chung, R.; Zhang, W.; Hulton, C.; Ripley, S.; Hirsch, H.; Nagashima, K.; Wong, K.-K.; Jánne, P. A.; Seidel-Dugan, C.; Zawel, L.; Kirschmeier, P. T.; Middleton, R. E.; Morris, E. J.; Wang, Y. Evaluating TBK1 as a therapeutic target in cancers with activated IRF3. *Mol Cancer Res* **2014**, *12*, 1055–1066.

(7) Hutti, J. E.; Porter, M. A.; Cheely, A. W.; Cantley, L. C.; Wang, X.; Kireev, D.; Baldwin, A. S.; Janzen, W. P. Development of a High-Throughput Assay for Identifying Inhibitors of TBK1 and IKKε. *PloS One* **2012**, *7*, e41494.

(8) Crew, A. P.; Raina, K.; Dong, H.; Qian, Y.; Wang, J.; Vigil, D.; Serebrenik, Y. V.; Hamman, B. D.; Morgan, A.; Ferraro, C.; Siu, K.; Neklesa, T. K.; Winkler, J. D.; Coleman, K. G.; Crews, C. M. Identification and Characterization of Von Hippel-Lindau-Recruiting Proteolysis Targeting Chimeras (PROTACs) of TANK-Binding Kinase 1. *J Med Chem* **2018**, *61*, 583–598.

(9) Oakes, J. A.; Davies, M. C.; Collins, M. O. TBK1: a new player in ALS linking autophagy and neuroinflammation. *Mol Brain* **2017**, *10*, 5.

(10) Freischmidt, A.; Wieland, T.; Richter, B.; Ruf, W.; Schaeffer, V.; Muller, K.; Marroquin, N.; Nordin, F.; Hubers, A.; Weydt, P.; Pinto, S.; Press, R.; Millecamps, S.; Molko, N.; Bernard, E.; Desnuelle, C.; Soriani, M. H.; Dorst, J.; Graf, E.; Nordstrom, U.; Feiler, M. S.; Putz, S.; Boeckers, T. M.; Meyer, T.; Winkler, A. S.; Winkelman, J.; de Carvalho, M.; Thal, D. R.; Otto, M.; Brannstrom, T.; Volk, A. E.; Kursula, P.; Danzer, K. M.; Lichtner, P.; Dikic, I.; Meitinger, T.; Ludolph, A. C.; Strom, T. M.; Andersen, P. M.; Weishaupt, J. H. Haploinsufficiency of TBK1 causes familial ALS and fronto-temporal dementia. *Nat Neurosci* **2015**, *18*, 631–636.

(11) Hegde, R. N.; Chiki, A.; Petricca, L.; Martufi, P.; Arbez, N.; Mouchiroud, L.; Auwerx, J.; Landles, C.; Bates, G. P.; Singh-Bains, M. K.; Dragunow, M.; Curtis, M. A.; Faull, R. L.; Ross, C. A.; Caricasole, A.; Lashuel, H. A. TBK1 phosphorylates mutant Huntingtin and suppresses its aggregation and toxicity in Huntington's disease models. *EMBO J* **2020**, *39*, e104671.

(12) Verheijen, J.; van der Zee, J.; Gijselinck, I.; Van den Bossche, T.; Dillen, L.; Heeman, B.; Gómez-Tortosa, E.; Lladó, A.; Sanchez-Valle, R.; Graff, C.; Pastor, P.; Pastor, M. A.; Benussi, L.; Ghidoni, R.; Binetti, G.; Clarimon, J.; de Mendonça, A.; Gelpi, E.; Tsolaki, M.; Diehl-Schmid, J.; Nacmias, B.; Almeida, M. R.; Borroni, B.; Matej, R.; Ruiz, A.; Engelborghs, S.; Vandenberghe, R.; De Deyn, P. P.; Cruts, M.; Van Broeckhoven, C.; Sleegers, K. Common and rare TBK1 variants in early-onset Alzheimer disease in a European cohort. *Neurobiol Aging* **2018**, *62*, 245.e1–245.e7.

(13) Rodgers, G.; Austin, C.; Anderson, J.; Pawlyk, A.; Colvis, C.; Margolis, R.; Baker, J. Glimmers in illuminating the druggable genome. *Nat Rev Drug Discov* **2018**, *17*, 301–302.

(14) Krahn, A. I.; Wells, C.; Drewry, D. H.; Beitel, L. K.; Durcan, T. M.; Axtman, A. D. Defining the neural kinome: strategies and opportunities for small molecule drug discovery to target neurodegenerative diseases. *ACS Chem Neurosci* **2020**, *11*, 1871–1886.

(15) Annadurai, N.; Agrawal, K.; Džubák, P.; Hajdúch, M.; Das, V. Microtubule affinity-regulating kinases are potential druggable targets for Alzheimer's disease. *Cell Mol Life Sci* **2017**, *74*, 4159–4169.

(16) Katz, J. D.; Haidle, A.; Childers, K. K.; Zabierek, A. A.; Jewell, J. P.; Hou, Y.; Altman, M. D.; Szewczak, A.; Chen, D.; Harsch, A.; Hayashi, M.; Warren, L.; Hutton, M.; Nuthall, H.; Su, H. P.; Munshi, S.; Stanton, M. G.; Davies, I. W.; Munoz, B.; Northrup, A. Structure guided design of a series of selective pyrrolopyrimidinone MARK inhibitors. *Bioorg Med Chem Lett* **2017**, *27*, 114–120.

(17) Wells, C.; Couñago, R. M.; Limas, J. C.; Almeida, T. L.; Cook, J. G.; Drewry, D. H.; Elkins, J. M.; Gileadi, O.; Kapadia, N. R.; Lorente-Macias, A.; Pickett, J. E.; Riemen, A.; Ruela-de-Sousa, R. R.; Willson, T. M.; Zhang, C.; Zuercher, W. J.; Zutshi, R.; Axtman, A. D. SGC-AAK1-1: A Chemical Probe Targeting AAK1 and BMP2K. *ACS Med Chem Lett* **2019**, *11*, 340–345.

(18) Agajanian, M. J.; Walker, M. P.; Axtman, A. D.; Ruela-de-Sousa, R. R.; Serafin, D. S.; Rabinowitz, A. D.; Graham, D. M.; Ryan, M. B.; Tamir, T.; Nakamichi, Y.; Gammons, M. V.; Bennett, J. M.; Counago, R. M.; Drewry, D. H.; Elkins, J. M.; Gileadi, C.; Gildadi, O.; Godoi, P. H.; Kapadia, N.; Muller, S.; Santiago, A. S.; Sorrell, F. J.; Wells, C. I.; Fedorov, O.; Willson, T. M.; Zuercher, W. J.; Major, M. B. WNT activates the AAK1 kinase to promote clathrin-mediated endocytosis of LRP6 and establish a negative feedback loop. *Cell Rep* **2019**, *26*, 79–83.

(19) Davis, M. I.; Hunt, J. P.; Herrgard, S.; Ciceri, P.; Wodicka, L. M.; Pallares, G.; Hocker, M.; Treiber, D. K.; Zarrinkar, P. P. Comprehensive analysis of kinase inhibitor selectivity. *Nat Biotechnol* **2011**, *29*, 1046–1051.

(20) Clark, K.; Peggie, M.; Plater, L.; Sorcek, Ronald J.; Young, Erick R. R.; Madwed, Jeffrey B.; Hough, J.; McIver, Edward G.; Cohen, P. Novel cross-talk within the IKK family controls innate immunity. *Biochem J* **2011**, *434*, 93–104.

(21) McIver, E. G.; Bryans, J.; Birchall, K.; Chugh, J.; Drake, T.; Lewis, S. J.; Osborne, J.; Smiljanic-Hurley, E.; Tsang, W.; Kamal, A.; Levy, A.; Newman, M.; Taylor, D.; Arthur, J. S. C.; Clark, K.; Cohen, P. Synthesis and structure–activity relationships of a novel series of pyrimidines as potent inhibitors of TBK1/IKKε kinases. *Bioorg Med Chem Lett* **2012**, *22*, 7169–7173.

(22) Petherick, K. J.; Conway, O. J.; Mpamhanga, C.; Osborne, S. A.; Kamal, A.; Saxty, B.; Ganley, I. G. Pharmacological inhibition of ULK1 kinase blocks mammalian target of rapamycin (mTOR)-dependent autophagy. *J Biol Chem* **2015**, *290*, 11376–11383.

(23) Feldman, R. I.; Wu, J. M.; Polokoff, M. A.; Kochanny, M. J.; Dinter, H.; Zhu, D.; Biroc, S. L.; Alicke, B.; Bryant, J.; Yuan, S.; Buckman, B. O.; Lentz, D.; Ferrer, M.; Whitlow, M.; Adler, M.; Finster, S.; Chang, Z.; Arnaiz, D. O. Novel small molecule inhibitors of 3-phosphoinositide-dependent kinase-1. *J Biol Chem* **2005**, *280*, 19867–19874.

(24) Stathias, V.; Turner, J.; Koleti, A.; Vidovic, D.; Cooper, D.; Fazel-Najafabadi, M.; Pilarczyk, M.; Terryn, R.; Chung, C.; Umeano, A.; Clarke, D. J. B.; Lachmann, A.; Evangelista, J. E.; Ma'ayan, A.; Medvedovic, M.; Schürer, S. C. LINCS Data Portal 2.0: next generation access point for perturbation-response signatures. *Nucleic Acids Res* **2019**, *48*, D431–D439.

(25) Thomson, D. W.; Poeckel, D.; Zinn, N.; Rau, C.; Strohmer, K.; Wagner, A. J.; Graves, A. P.; Perrin, J.; Bantscheff, M.; Duempelfeld, B.; Kasparcova, V.; Ramanjulu, J. M.; Pesiridis, G. S.; Muelbaier, M.; Bergamini, G. Discovery of GSK8612, a Highly Selective and Potent TBK1 Inhibitor. *ACS Med Chem Lett* **2019**, *10*, 780–785.

(26) Faisal, M.; Kim, J. H.; Yoo, K. H.; Roh, E. J.; Hong, S. S.; Lee, S. H. Development and Therapeutic Potential of NUAKs Inhibitors. *J Med Chem* **2021**, *64*, 2–25.

(27) Drewes, G.; Ebneth, A.; Preuss, U.; Mandelkow, E.-M.; Mandelkow, E. MARK, a Novel Family of Protein Kinases That Phosphorylate Microtubule-Associated Proteins and Trigger Microtubule Disruption. *Cell* **1997**, *89*, 297–308.

(28) Lasagna-Reeves, C. A.; de Haro, M.; Hao, S.; Park, J.; Rousseaux, M. W.; Al-Ramahi, I.; Jafar-Nejad, P.; Vilanova-Velez, L.; See, L.; De Maio, A.; Nitschke, L.; Wu, Z.; Troncoso, J. C.; Westbrook, T. F.; Tang, J.; Botas, J.; Zoghbi, H. Y. Reduction of Nuak1 Decreases Tau and Reverses Phenotypes in a Tauopathy Mouse Model. *Neuron* **2016**, *92*, 407–418.

(29) Shi, B.; Conner, S. D.; Liu, J. Dysfunction of endocytic kinase AAK1 in ALS. *Int J Mol Sci* **2014**, *15*, 22918–22932.

(30) Vasta, J. D.; Corona, C. R.; Wilkinson, J.; Zimprich, C. A.; Hartnett, J. R.; Ingold, M. R.; Zimmerman, K.; Machleidt, T.; Kirkland, T. A.; Huwiler, K. G.; Ohana, R. F.; Slater, M.; Otto, P.; Cong, M.; Wells, C. I.; Berger, B. T.; Hanke, T.; Glas, C.; Ding, K.; Drewry, D. H.; Huber, K. V. M.; Willson, T. M.; Knapp, S.; Muller, S.; Meisenheimer, P. L.; Fan, F.; Wood, K. V.; Robers, M. B. Quantitative, Wide-Spectrum Kinase Profiling in Live Cells for Assessing the Effect of Cellular ATP on Target Engagement. *Cell Chem Biol* **2018**, *25*, 206–214.

(31) Wells, C. I.; Al-Ali, H.; Andrews, D. M.; Asquith, C. R. M.; Axtman, A. D.; Dikic, I.; Ebner, D.; Ettmayer, P.; Fischer, C.; Frederiksen, M.; Futrell, R. E.; Gray, N. S.; Hatch, S. B.; Knapp, S.; Lücking, U.; Michaelides, M.; Mills, C. E.; Müller, S.; Owen, D.; Picado, A.; Saikatendu, K. S.; Schröder, M.; Stolz, A.; Tellechea, M.; Turunen, B. J.; Vilar, S.; Wang, J.; Zuercher, W. J.; Willson, T. M.; Drewry, D. H. The Kinase Chemogenomic Set (KCGS): An Open Science Resource for Kinase Vulnerability Identification. *Int J Mol Sci* **2021**, *22*, 566.

(32) Drewry, D. H.; Wells, C. I.; Andrews, D. M.; Angell, R.; Al-Ali, H.; Axtman, A. D.; Capuzzi, S. J.; Elkins, J. M.; Ettmayer, P.; Frederiksen, M.; Gileadi, O.; Gray, N.; Hooper, A.; Knapp, S.; Laufer, S.; Luecking, U.; Michaelides, M.; Muller, S.; Muratov, E.; Denny, R. A.; Saikatendu, K. S.; Treiber, D. K.; Zuercher, W. J.; Willson, T. M. Progress towards a public chemogenomic set for protein kinases and a call for contributions. *PloS One* **2017**, *12*, e0181585.

(33) Berginski, M. E.; Moret, N.; Liu, C.; Goldfarb, D.; Sorger, Peter K.; Gomez, S. M. The Dark Kinase Knowledgebase: an online compendium of knowledge and experimental results of understudied kinases. *Nucleic Acids Res* **2021**, *49*, D529–D535.

(34) Fensome, A.; Ambler, C. M.; Arnold, E.; Banker, M. E.; Clark, J. D.; Dowty, M. E.; Efremov, I. V.; Flick, A.; Gerstenberger, B. S.; Gifford, R. S.; Gopalsamy, A.; Hegen, M.; Jussif, J.; Limburg, D. C.; Lin, T. H.; Pierce, B. S.; Sharma, R.; Trujillo, J. I.; Vajdos, F. F.; Vincent, F.; Wan, Z.-K.; Xing, L.; Yang, X.; Yang, X. Design and optimization of a series of 4-(3-azabicyclo[3.1.0]hexan-3-yl)pyrimidin-2-amines: Dual inhibitors of TYK2 and JAK1. *Bioorg Med Chem* **2020**, *28*, 115481.

(35) Fensome, A.; Ambler, C. M.; Arnold, E.; Banker, M. E.; Brown, M. F.; Chrencik, J.; Clark, J. D.; Dowty, M. E.; Efremov, I. V.; Flick, A.; Gerstenberger, B. S.; Gopalsamy, A.; Hayward, M. M.; Hegen, M.; Hollingshead, B. D.; Jussif, J.; Knafels, J. D.; Limburg, D. C.; Lin, D.; Lin, T. H.; Pierce, B. S.; Saiah, E.; Sharma, R.; Symanowicz, P. T.; Telliez, J.-B.; Trujillo, J. I.; Vajdos, F. F.; Vincent, F.; Wan, Z.-K.; Xing, L.; Yang, X.; Yang, X.; Zhang, L. Dual Inhibition of TYK2 and JAK1 for the Treatment of Autoimmune Diseases: Discovery of ((S)-2,2-Difluorocyclopropyl)((1R,5S)-3-(2-((1-methyl-1H-pyrazol-4-yl)amino)pyrimidin-4-yl)-3,8-diazabicyclo[3.2.1]octan-8-yl)methanone (PF-06700841). *J Med Chem* **2018**, *61*, 8597–8612.

(36) Metz, K. S.; Deoudes, E. M.; Berginski, M. E.; Jimenez-Ruiz, I.; Aksoy, B. A.; Hammerbacher, J.; Gomez, S. M.; Phanstiel, D. H. Coral: Clear and Customizable Visualization of Human Kinome Data. *Cell Syst* **2018**, *7*, 347–350.e1.